Mississippi State University
Scholars Junction

Theses and Dissertations | Theses and Dissertations

5-1-2020

Exploring the immunosuppressive properties of various agents in the experimental autoimmune encephalomyelitis models of multiple sclerosis

James Matthew Nichols

Follow this and additional works at: https://scholarsjunction.msstate.edu/td

Recommended Citation
Nichols, James Matthew, "Exploring the immunosuppressive properties of various agents in the experimental autoimmune encephalomyelitis models of multiple sclerosis" (2020). *Theses and Dissertations*. 2172.
https://scholarsjunction.msstate.edu/td/2172

This Dissertation - Open Access is brought to you for free and open access by the Theses and Dissertations at Scholars Junction. It has been accepted for inclusion in Theses and Dissertations by an authorized administrator of Scholars Junction. For more information, please contact scholcomm@msstate.libanswers.com.

Exploring the immunosuppressive properties of various agents in the experimental autoimmune encephalomyelitis models of multiple sclerosis

By

James Matthew Nichols

A Dissertation
Submitted to the Faculty of
Mississippi State University
in Partial Fulfillment of the Requirements
for the Degree of Doctor of Philosophy
in Veterinary Medical Sciences
in the College of Veterinary Medicine

Mississippi State, Mississippi
May 2020

Copyright by

James Matthew Nichols

2020

Exploring the immunosuppressive properties of various agents in the experimental autoimmune encephalomyelitis models of multiple sclerosis

By

James Matthew Nichols

Approved:

_____
Barbara L.F. Kaplan
(Major Professor)

_____
Matthew Ross
(Committee Member)

_____
Jeffrey Eells
(Committee Member)

_____
Stephen Pruett
(Committee Member)

_____
Timothy Morgan
(Committee Member)

_____
Larry Hanson
(Graduate Coordinator)

_____
Kent H. Hoblet
Dean
College of Veterinary Medicine

Name: James Matthew Nichols

Date of Degree: May 1, 2020

Institution: Mississippi State University

Major Field: Veterinary Medical Sciences

Major Professor: Barbara L.F. Kaplan, Ph.D.

Title of Study: Exploring the immunosuppressive properties of various agents in the experimental autoimmune encephalomyelitis models of multiple sclerosis

Pages in Study: 130

Candidate for Degree of Doctor of Philosophy

One of the major focuses for our lab involves examining the immunosuppressive properties of various agents and receptors in the experimental autoimmune encephalomyelitis (EAE) model of multiple sclerosis (MS). This dissertation encompasses an investigation of cannabidiol in the EAE model, the endocannabinoid CB_1 receptor in the EAE model, staphylococcal superantigens (SAgs) as immunosuppressive agents, and various aspects of the EAE model. The first chapter covers the existing literature pertinent to these studies, the second and third chapters cover the material, methods, and results from the studies, and the fourth chapter is a discussion of how those results fit into the existing body of literature. A fifth chapter has also been included which covers two additional studies designed to develop alternative EAE models for our lab; however, both studies turned out differently than expected. One of the most interesting developments from this final chapter was the discovery of an age

dependent difference in the memory T cell response of older mice, which allows for more robust disease to be induced when cells from 6 month old mice are used in the passive EAE (P-EAE) model as opposed to mice 10 weeks of age.

DEDICATION

I would like to dedicate this dissertation to my wife Christina, my son Ronald, and my daughter Emilee. Christina and Ronald have been very patient and supportive through the years and I would not be where I am without them. Emilee is due to arrive in April 2020.

ACKNOWLEDGEMENTS

I would like to acknowledge Dr. Graham Rosser for his assistance with formatting of images in this dissertation and Dr. Brittany Szafran for her diligent management of our breading colony. I would also like to acknowledge Dr. Barbara Kaplan for her amazing mentorship over the years. Dr. Kaplan's willingness to let me investigate my curiosities, her knowledge, and her skills were invaluable to my development as a researcher.

TABLE OF CONTENTS

LIST OF TABLES

LIST OF FIGURES

CHAPTER I

SPECIFIC AIMS AND LITERATURE REVIEW

1.1 Specific Aims

One of the major challenges still left to be overcome in MS research involves the development of effective treatment options for patients with MS. Many current treatments for MS have undesirable side effects and few of them prevent the long term progression of MS [1, 2]. The purpose of the studies outlined in this dissertation was to explore the effects of various compounds, including cannabinoids and staphylococcal SAgs, on the EAE model of MS, and to examine variations of the EAE model to better understand how the pathogenesis of MS might be altered. We hypothesized that through the use of cannabidiol (CBD), *Cnr1*$^{-/-}$ mice, and SAgs, and through the exploration of variations of the EAE model, we would find novel methods of modulating the EAE model of MS.

1.1.1 Specific Aim 1: Explore the effects of CBD on the EAE model

CBD is a phytocannabinoid which has been shown to be immunosuppressive in a number of disease models including the EAE; however, its effect on the peripheral immune response in the EAE model has yet to be fully explored [3-5]. The aim of these studies was to examine the effect of oral CBD on peripheral inflammatory and neuroinflammatory responses in the EAE model, with a specific focus on IFN-γ and IL-

17A producing T cells, regulatory T cells (Tregs) and myeloid derived suppressor cells (MDSC) in the peripheral immune response at various time points. Here we used flow cytometry, immunohistochemistry, and ELISAs to examine numerous inflammatory and anti-inflammatory endpoints in both the peripheral and neuroimmune responses.

1.1.2 Specific Aim 2: Exploring the immunosuppressive properties of *Staphylococcus aureus* SAgs

In previous studies, *S. aureus* SAgs have been shown to be immunosuppressive in humans and cattle through the induction of regulatory cells, but the whether or not SAgs can stimulate regulatory cell types in the murine immune system remains unknown [6-8]. To determine if *S. aureus* SAgs possess ability to induce regulatory cells in mice, we cultured splenocytes from C57BL/6 mice with various SAgs, and measured the response of Tregs and MDSCs using flow cytometry.

1.1.3 Specific Aim 3: Explore the role of the CB_1 receptor in the immune response of the EAE model.

CB_1 receptors have previously been shown to reduce clinical disease in the EAE model through their neuroprotective and anti-spasmodic effects, yet the effects of the CB_1 receptor remain to be fully explored in the peripheral immune responses of this model [9, 10]. In these studies we induced EAE in *Cnr1*$^{-/-}$ and WT littermates, and used flow cytometry, ELISAs of serum and supernatants from ex vivo restimulated cells, and a new histological scoring system developed by our lab to explore differences between *Cnr1*$^{-/-}$ and WT mice. We also sought to confirm the results found in our ex vivo restimulations with in vitro stimulations of splenocytes using anti-CD3/anti-CD28

antibodies and staphylococcal enterotoxin M (SEM) to specifically stimulate IFN-γ production in T cells.

1.1.4 Specific Aim 4: Explore variations of the EAE model

There are several challenges associated with our EAE model which result in a milder disease state compared to those previously reported by other labs. In light of this our lab has been exploring the use of isoflurane to enhance our EAE model and the use of other EAE models, like the P-EAE model, which will provide more robust disease and allow us to explore the EAE model in a different way. Additionally, we have been able to use the P-EAE model to further examine CBD's effects on neuroinflammation and we have discovered some age dependent differences in the P-EAE.

1.2 Literature review

1.2.1 Multiple sclerosis

MS is a progressive neurodegenerative autoimmune disorder of unknown etiology that has been estimated to affect more than 2 million people around the world, with more women being affected than men [11-13]. Current research suggests that there are likely several components at play in the initiation of this disease, including environmental, genetic, and immunologic factors [14, 15]. Although no one environmental factor can fully explain the etiology of MS, a study examining the current body of literature on environmental risk factors for MS determined that infection with the Epstein - Barr virus, smoking, and infectious mononucleosis had the strongest evidence for increasing the risk of contracting MS out of all the risk factors examined. The mechanism by which these factors increase the risk for MS has yet to be shown. A

correlation was also found between increased distance from the equator and the number of cases of MS, which has been supported by the assertion that decreased levels of Vitamin D may contribute to the incidence of MS [15-17].

Much like the environmental risk factors, studies of the genetics behind MS have revealed no one genetic factor that can explain the etiology of this disease; however, an analysis of the genetic risk factors that contribute to MS by The International Multiple Sclerosis Genetics Consortium and the Wellcome Trust Case Control Consortium showed that mutations in the human leukocyte antigen (HLA) genes coding for MHC class II have a higher level of association with MS than any of the other single nucleotide polymorphism (SNP) examined. This study also found that a significant number of these SNPs are located in genes that affect T cell maturation, thus providing strong evidence that dysregulation of the adaptive immune response is a key factor in the initiation of MS [18].

Despite the widespread nature of MS, the current therapeutics options for MS patients still do not provide complete relief of clinical disease, and are insufficient for controlling the progressive phase of MS [1, 2]. In light of this, our lab has been working on identifying new treatment methods for MS by using the EAE model. Highlighted in the first four chapters of this dissertation are the results from an exploration of the cannabinoid system as a target for treatment of MS, and the use of *S. aureus* superantigens as potential immunosuppressive agents. Additionally, Chapter 5 outlines the progress of we made in using the EAE model with isoflurane to enhance disease and the P-EAE model.

1.2.2 Clinical MS

Clinical symptoms of MS generally start in middle aged adults, and people who develop this disease become progressively more disabled as the immune system continues to attack the myelin sheaths of axons in the central nervous system (CNS) [14, 19]. MS often includes a wide range of debilitating symptoms including cognitive impairment, motor deficits, depression, epilepsy, focal cortical deficits, loss of vision, tremors, loss of coordination and balance, diplopia, oscillopsia, vertigo, impaired swallowing, impaired speech, emotional liability, weakness, stiffness, spasms, bladder dysfunction, erectile impotence, constipation, pain, fatigue, exercise intolerance, and temperature sensitivity [15]. MS can be categorized into one of three different types: relapsing-remitting MS (RRMS), primary progressive MS (PPMS), or secondary progressive MS (SPMS). RRMS begins with an event known as the clinically isolated syndrome (CIS), which is simply the first episode of neurologic dysfunction the patient experiences. Approximately 85% of the individuals who experience CIS will continue to have more episodes of neurologic dysfunction with periods of remission, and at this point they are considered to have RRMS. RRMS is the most common form of MS [15, 19]. SPMS occurs 10 to 20 years after the patient is initially diagnosed with RRMS and consists of a period of time where disease progression is continual due to a decrease in brain volume and loss of functional axons. PPMS is similar to SPMS, except there is not a RRMS phase preceding it [19]. Interestingly, studies examining incidence rates in MS patients showed that RRMS has a higher sex bias towards women than PPMS, however the reason for this bias is still unknown [12, 13].

1.2.3 Pathogenesis of MS

Initially Th1 cells were thought to be the driving force behind MS, but most of the current literature provides evidence that Th17 cells might be a more important component in disease initiation than Th1 cells. This idea was first suggested by an EAE study in which adoptive transfer of Th17 cells was shown to be more pathogenic than adoptive transfer of Th1 cells. This study also showed that mice lacking IL-23, an important factor in the proliferation of Th17 cells, developed less severe clinical disease, had fewer Th17 cell migrate into the CNS, and had a similar number of Th1 cells migrate into the CNS as compared to wild type mice. These results suggest IL-23 and Th17 cells play an important role in EAE pathogenesis, but are not critical for infiltration of Th1 cells into the CNS [20]. This finding sparked a search for this newly discovered pathogenic T cell in MS patients, and it was determined that Th17 cells are present in higher numbers in the CNS during active MS than in either disease remission or healthy individuals [21, 22].

In MS, autoreactive T cells enter the CNS and drive a neuroinflammatory response by secreting a host of cytokines and chemokines that recruit other immune cells to the CNS. In early MS, lesions in the CNS are predominated by macrophages and $CD8^+$ T cells, and to a lesser extent $CD4^+$ T cells, B cells, and plasma cells. These $CD8^+$ T cells appear to be derived from a small number of progenitor cells, and the number of $CD8^+$ T cells found in white and gray matter lesions correlates closely with axonal damage [19, 23]. This differs from the murine EAE model in that lesions primarily contain macrophages and $CD4^+$ T cells [19, 24]. In active lesions, macrophages and microglia are primarily responsible for the breakdown of myelin sheaths and

oligodendrocytes within the CNS, which is thought to be the cause of many of the symptoms seen in RRMS; however, they are also capable of reactivating autoreactive T cells. Fortunately, myelin sheaths have some ability to regrow with time, so the patient recovers much of their neurologic function when they go into remission. Nevertheless, there is a far more insidious process that underlies the inflammation of a relapse, and that is axonal degeneration. Gradual loss of neurons to axonal degeneration occurs as a consequence of the demyelination process and is generally believed to be responsible for the occurrence of SPMS and PPMS later in the patient's life [19, 25, 26]. As MS transitions into chronic inflammation, the number of infiltrating cells decreases, and in SPMS, tertiary lymphoid structures that resemble B cells follicles can form in the meninges of the CNS. These structures contain B cells, T cells, plasma cells and dendritic cells, and are believed to be capable of generating inflammatory responses within the CNS [19, 27].

An interesting dichotomy that forms in MS and EAE is the apparent conflict seen between the proinflammatory and the anti-inflammatory branches of the immune system. One example of this is seen in how macrophages and microglia respond during neuroinflammation. As described above, microglia and macrophages are responsible for activation of T cells and demyelination; however, once macrophages and microglia phagocytize myelin they transition to a more immunosuppressive state. This change in response to myelin is thought to contribute to remission in RRMS [25, 26]. Similarly, B cells have both a pro-inflammatory role and an anti-inflammatory role in MS and EAE. On the one hand, B cells contribute to inflammation through the production of antibodies and their presence in tertiary lymphoid structures, but B cells producing the anti-

inflammatory cytokine IL-10 have been shown to have a suppressive role in EAE and are elevated in MS patients [28]. The apparent duality of these various cell types may at first seem counterintuitive, but in the context of clinical MS they might actually make sense. If the initiation of a relapse is triggered by one cell type that causes a ripple effect through the rest of the immune system, and all other cell types eventually convert to an anti-inflammatory phenotype to block the overwhelming autoimmune response, it could explain why there is a relapsing-remitting pattern to MS. Interestingly, the Tregs of MS patients appear to be an exception to this rule. Despite some disagreement on whether or not the number of Tregs is increased in the cerebral spinal fluid (CSF), several studies report that Tregs from MS patients have decreased functionality, leading some to speculate that MS may be, at least in part, due to a defect in the Treg system [29-31].

1.2.4 EAE and P-EAE

Our lab uses two different methods of inducing EAE. The method we use most frequently is initiated by immunizing C57BL/6 mice with Complete Freund's Adjuvant (CFA) containing Heat Killed Mycobacterium tuberculosis (HKMT), and myelin oligodendrocyte glycoprotein (MOG) peptide. This causes the proliferation of Th1 and Th17 cells specific to MOG peptide, which is found on the myelin sheaths of axons in the CNS. As part of this MOG specific response cells begin trafficking across the blood brain barrier (BBB) and targeting oligodendrocytes, which are the myelinating cells of the CNS [32]. In addition to inflammatory cells, suppressor cells such as MDSCs and Tregs also become activated, and have a suppressor role in the immune response through various mechanisms. (Figure 1.1)[33, 34]. This method EAE induction is often

referred to as active EAE (A-EAE), however throughout this dissertation we will simply refer to this method as EAE.

The second type of EAE induction that our lab uses is the P-EAE model. We induce P-EAE by first initiating EAE in 2D2 transgenic C57BL/6 mice, which have a T cell receptor (TCR) specific for MOG_{35-55} peptide on the majority of their $CD4^+$ T cells. After immunization, cells from the lymph nodes and spleens of the 2D2 transgenic mice are restimulated *ex vivo* with MOG_{35-55} and transferred to WT mice to confer EAE to the recipient mice. This method of induction is very useful for examining the later stages of the immune responses in the absence of the overwhelming response to CFA and HKMT that is present in active EAE.

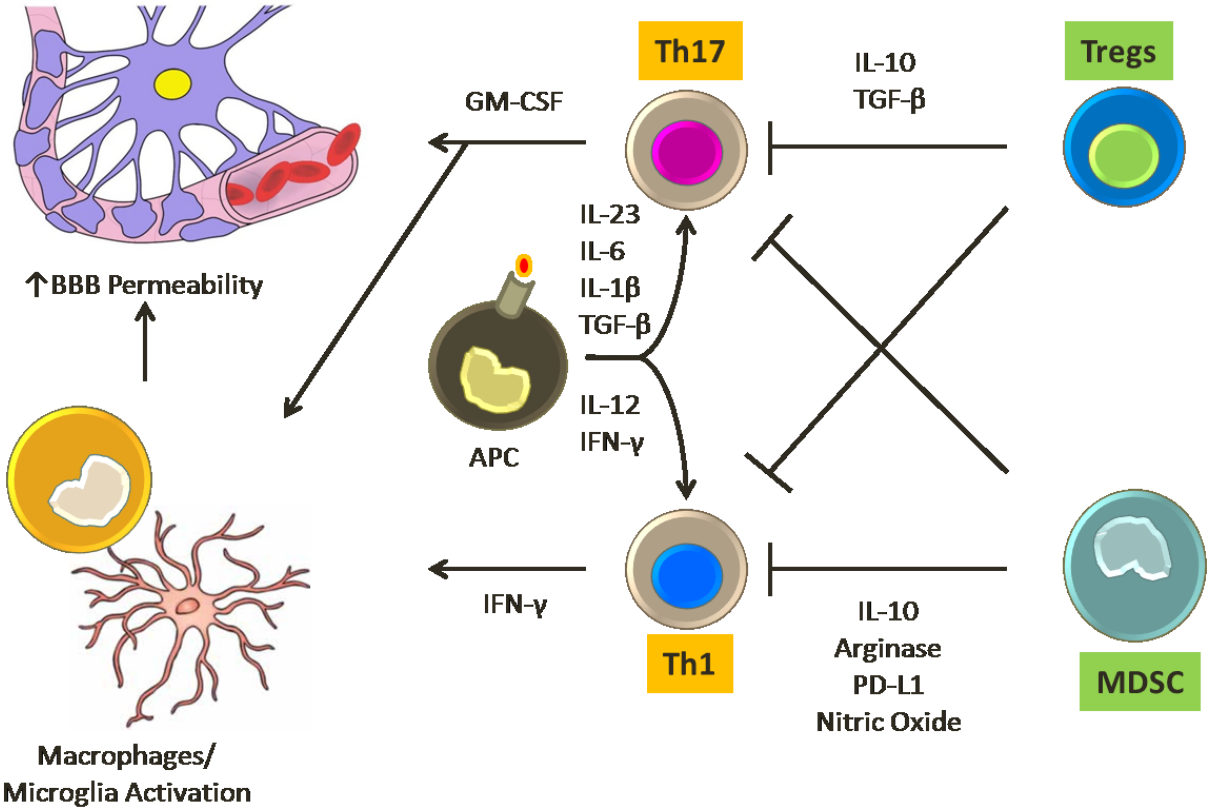

Figure 1.1 Breakdown of the BBB during EAE initiation

Presentation of MOG_{35-55} peptide to naïve T cells in the presence of IL-23, IL-6, TGF-β and IL-1β, or IL-12 and IFN-γ generates pathogenic MOG specific Th17 and Th1 cells respectively [32]. These cells then use various mechanisms to increase BBB permeability, including the production of GM-CSF by Th17 cells and production of IFN-γ by Th1 cells. GM-CSF and IFN-γ both have the ability to activate microglia and macrophages, while GM-CSF reduces the expression of claudin-5 and zonula occludens-1, which play an important role in the function of the tight junctions of the BBB [35, 36]. Additionally, suppressor cells, such as Tregs and MDSCs, become activated through the immunization process, and these cells have been shown to suppress effector T cells through various mechanisms [33, 34].

1.2.5 Cannabidiol

CBD is a phytocannabinoid found in plants of the Cannabis sp. and is similar in structure to the psychoactive phytocannabinoid Δ9-tetrahydrocannabinol (THC) (Figure

1.2). However, unlike THC, CBD possesses low affinity for CB_1 (Ki ≥ 4.35μM) and CB_2 (Ki ≥ 2.86μM) receptors, so it does not produce the psychoactive properties associated with the activation of the CB_1 receptor in the CNS. On the other hand, some evidence shows that CBD does have the ability to antagonize the CB_1 and CB_2 receptor at lower concentrations in a non-competitive manner, so some of its immunosuppressive actions may still be mediated by the cannabinoid receptors [3, 37, 38]. Several other putative targets of CBD have also been suggested, which include the Adenosine A2A receptor, GPR55 orphan receptor, peroxisome proliferator-activated receptor γ (PPARγ), opioid receptors, calcium channels, and metabolic enzymes of the Cytochrome P450 and Glutathione pathways [37]. After oral and intraperitoneal (i.p.) dosing in mice, CBD has been shown to readily distribute into the plasma and CNS, but CBD concentrations drop below detectable levels by 24hr after oral and i.p. administration [39].

One of the properties of the phytocannabinoids which has drawn a great deal of interest from the scientific community is their immunosuppressive capabilities. CBD has shown promising anti-inflammatory capabilities in animal models including: EAE, collagen-induced arthritis (rheumatoid arthritis model), carrageenan induced edema, croton oil-induced hypermotility (inflammatory bowel disease model), and pneumococcal meningitis [3]. However, it should be noted that there have been a few reports showing that CBD may actually be pro-inflammatory under certain conditions. More specifically, CBD was shown to increase IL-2 and IFN-γ production by sub-optimally stimulated splenocytes from C57BL/6 mice, which corresponded to increased translocation of nuclear factor of activated T cells (NFAT)[40]. Another study also showed that CBD increased the lipopolysaccharide (LPS) driven inflammatory response

in the lungs of C57BL/6 mice, and increased the mRNA for several proinflammatory cytokines within the lungs[41]. Although it remains unclear why CBD may be proinflammatory under some conditions, these studies do show that there is still much to learn about the use of cannabinoids as immunosuppressive agents.

While the number of explorations into CBD's ability to combat clinical disease and neuroinflammation in the EAE model are currently limited, the results have been promising so far. A study by Kozela et al. in 2011 showed that activation of microglia and invasion of T cells into the parenchyma of the spinal cord were greatly reduced when mice were treated at the first sign of disease for 3 consecutive days with i.p. injections of CBD [5]. Then in 2013 a study using the Theiler's murine encephalomyelitis virus (TMEV) model of MS showed that i.p. injections of CBD at the initiation of disease significantly decreased leukocyte invasion into the CNS, vascular cell-adhesion molecule-1 (VCAM-1) expression at the BBB, cytokine and chemokine expression, and microglial activation [4]. In addition to these studies, clinical trials of the drug Sativex, an oral mixture of THC and CBD, have shown efficacy in treating spasticity and neuropathic pain in MS patients. However, clinical trials of oral CBD alone in MS are currently lacking, and clinical trials of Sativex failed to prevent relapses from occurring [37]. Given the potential benefits seen with CBD in other disease models, it is imperative that its ability to treat MS be explored more completely. Some of the work covered in the following chapters shows a potential link between CBD and inhibition of IFN-γ production by T cells, and the subsequent suppression of the neuroimmune response in the EAE model. These results are consistent with data from Kaplan et al. which show the ability of CBD to suppress *in vitro* production of IFN-γ and IL-2 in

splenic T cells when stimulated with phorbol 12-myristate-13-acetate and ionomycin (PMA/Io) [42, 43].

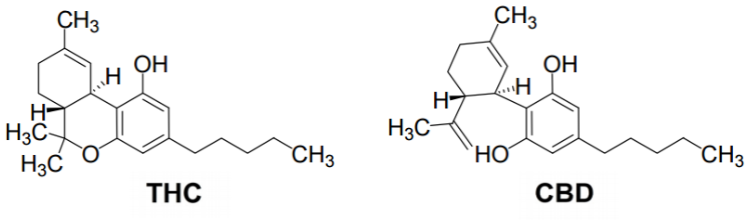

Figure 1.2 Structure of THC vs CBD

THC is a tricyclic compound with a planar conformation, but CBD is a bicyclic compound with free rotation around the C-C bond between the two rings which results in a non-planar conformation.

1.2.6 Cannabinoid receptors

The cannabinoid receptors, CB_1 and CB_2, are G-protein coupled receptors of the subtype Gi/o. Activation of these receptors influences several intracellular pathways, including the production of cyclic AMP (cAMP) by adenylyl cyclase and activation of mitogen-activated protein kinases (MAPK) [44]. The ability of the cannabinoid receptors to act through these various pathways can cause a wide range of effects including but not limited to: hyperpolarization of neurons, inhibition of neurotransmitter release, changes in neuronal structure, modulation of intracellular calcium levels, modulation of nitric oxide (NO) production, modulation of cytokine production, and increased migration of various immune cells. With this wide range of potential responses, it is obvious why

the use of cannabinoids as treatment options is such a complex area of research [44, 45].

CB_1 and CB_2 receptors have the potential to be both neuroprotective and anti-inflammatory in MS, as has been shown using EAE models [9, 10]; however, it is unclear to what extent these two receptors are involved in regulation of the neuroimmune response. EAE models are commonly used to study the pathophysiology of MS, and although they do not provide a perfect replica of the clinical progression in humans they have been critical for advancing MS therapies [19]. Previous studies of the CB_1 receptor have suggested that it is primarily responsible for the neuroprotective and antispasmodic affects seen with CB_1/CB_2 antagonists in ABH mice with EAE, while the CB_2 receptor is primarily responsible for immunosuppressive effect of these compounds [9, 10, 46]. These results coincide with the fact that the CB_1 and CB_2 receptors reside predominately in the brain and peripheral immune system respectively, but do not account for the effects of the CB_1 receptor in the peripheral immune system or CB_2 receptor in the CNS [47-50].

With phytocannabinoids, such as the THC:CBD mixture Sativex, showing more and more promise in clinical trials with MS patients, it becomes more important to fully elucidate the mechanisms of these compounds and the receptors through which they act [51-55]. In the studies outlined in this dissertation we use C57BL/6 *Cnr1*$^{-/-}$ and wild type (WT) littermates to explore the effects of the CB_1 receptor in the peripheral immune response of EAE. This work represents an important step into understanding the how CB_1 receptors influence IFN-γ production during inflammatory responses, and provides

more insight into how therapies designed to target CB_1 receptors might alter peripheral immune responses.

1.2.7 *Staphylococcus aureus* superantigens

S. aureus is a Gram positive facultative aerobe, and despite the fact that it is a commensal organism in humans, under the right conditions it is capable of causing serious disease [56]. One mechanism by which *S. aureus* causes disease is through the release of SAgs, which cause a potent immune response by nonspecifically crosslinking major histocompatibility complex (MHC) class II molecules on antigen presenting cells (APC) to Vβ domain of TCRs. This crosslinking results in a nonspecific proliferative T cell response, activation of the APC, and the release of pro-inflammatory cytokines. [56, 57] Since superantigens interact with the Vβ domain of TCRs, it was traditionally thought that T cell stimulation occurs in both the $CD4^+$ and $CD8^+$ cell lines; however, there is some evidence that shows *in vivo* T cell stimulation by SAgs is more specifically directed towards the $CD4^+$ T cells [57]. Analysis of the binding of SAgs to HLA-DR molecules has revealed that there are two main sites on the MHC class II molecules to which SAgs bind. SAgs can either bind with low affinity to the α chain of MHC class II or with high affinity in a zinc dependent manor to the β chain of MHC class II [57]. As a result of the immune response to SAgs, individuals may experience a wide range of clinical signs, with one of the most severe being toxic shock syndrome [58, 59].

In more recent years there has been an increase in evidence suggesting that SAgs may also have an immunosuppressive role in cattle and humans, both of which possess *S. aureus* as a commensal organism [6-8]. In humans SAgs are able to increase the number of functional $CD25^+FoxP3^+$ inducible Tregs (iTreg) in the

peripheral blood mononuclear cell (PBMC) population. The conversion of $CD25^-$ T cells to iTregs was shown to be dependent on the presence of APCs and the activation of T cells through the Vβ domain of the TCR [6]. In cattle, immunization with *S. aureus* causes the upregulation of $CD8^+$ T cells expressing the activation molecules ACT2 and ACT3, which in turn suppress the response $CD4^+$ T cells to both lectins and antigens [7, 60]. ACT3 is analogous to CD26 in humans, which has also been shown to be increased in $CD8^+$ T cells that can suppress $CD4^+$ T cells in humans [61]; however, it remains unclear whether ACT3 molecules are directly responsible for the suppression of $CD4^+$ T cells or if they are simply a sign that the $CD8^+$ T cells have become activated.

The goal of the work done involving *S. aureus* SAgs in this dissertation was to characterize the murine regulatory T cell response to various staphylococcus SAgs, including several staphylococcal enterotoxins (SEs) and toxic shock syndrome toxin-1 (TSST-1). This work was done in collaboration with Dr. Keun Seo at Mississippi State University as part of a species comparison between humans, cattle, dogs, and mice. As part of this comparison, we also investigated the effects of various SAgs on the MDSC populations, since one study found that mice chronically infected with *S. aureus* developed a strong MDSC response in addition to a less robust Treg response [62].

CHAPTER II

MATERIALS AND METHODS

2.1 Reagents

CBD was provided by the National Institute on Drug Abuse. MOG_{35-55} peptide (MEVGWYRSPFSRVVHLYRNGK) was obtained from Biosynthesis (Lewisville, TX). HKMT was purchased from Difco/BD Biosciences (Detroit, MI). CFA was obtained from Sigma (St. Louis, MO). *S. aureus* SAgs were provided by Dr. Keun Seo of Mississippi State University, College of Veterinary Medicine.

2.2 Animals

Experiments were approved by Mississippi State University Institutional Animal Care and Use Committee (IACUC). WT female C57BL/6 mice obtained from Envigo (Indianapolis, IN) at 8 weeks of age, ≥8 week old WT and *Cnr1*$^{-/-}$ C57BL/6 littermates bred at Mississippi State University College of Veterinary Medicine, 2D2 TCR transgenic mice obtained from Jackson Laboratories at 8 weeks of age, and FoxP3^{GFP} transgenic mice obtained from Jackson Laboratories at 8 weeks of age were used in the experiments outlined in this dissertation. Mice were housed five to a cage at most in a temperature (22°C±1°C), humidity (40-60%), and light (12h light: 12h dark) controlled room. Food and water were provided *ad libitum.* As EAE progressed, access to water

was ensured with use of long sipper tubes and food pellets were placed on the floor of the cage after day 7 for EAE and from day 1 for P-EAE.

2.3 EAE induction and clinical assessment

C57BL/6 mice were immunized with 100 µl of CFA containing either 100 µg of MOG_{35-55} peptide (MEVGWYRSPFSRVVHLYRNGK) with 0.5 mg of HKMT or 20 µg of MOG_{35-55} peptide with 0.1 mg HKMT to induce EAE and Mild EAE, respectively. Control mice were injected with saline. To perform the injections, mice were anesthetized with 3% isoflurane, and immunizations were given subcutaneously over the shoulders and hips (25µl at each site), after which the mice were allowed to recover in a portion of the cage cleared of bedding. For all studies involving CBD, starting 24 hr after the injections were administered, mice were dosed each morning with either 75mg/kg of CBD in 100 µl of corn oil (CO) or 100 µl of CO for 5 days via oral gavage. This dose of CBD has been used in previous studies and results in serum concentrations of CBD similar to that found in humans [41]. Throughout this dissertation, EAE is often referred to as "active EAE" to differentiate it from P-EAE induction discussed in Chapter 5; however, it should be noted that if the term "EAE" is used it specifically refers to active EAE.

Clinical scores were recorded for each experiment using the following clinical scale: 0 – Healthy; 0.5 – Flaccid tail; 1 – Hind limb paresis; 1.5 – waddling gait; 2 – Unable to prevent being placed in dorsal recumbency; 2.5 – Hind limb dragging; 3 – Single hind limb paralysis; 3.5 – Single hind limb paralysis with other hind limb dragging; 4 – Complete hind limb paralysis; 5 – Moribund/involvement of forelimbs. Mice were

never allowed to progress past the clinical score of 4 for animal welfare purposes. (Modified from Rao et al.) [63].

2.4 Cell cultures

2.4.1 *Ex vivo* restimulation with MOG peptide

Ex vivo restimulations of leukocytes from secondary lymphoid organs of EAE mice is a method that our lab uses to examine the MOG_{35-55} specific peripheral immune response, which can be measured using flow cytometry of cells and ELISAs of supernatants. For all *ex vivo* restimulations, cells were isolated from the secondary lymphoid tissues by mechanical disruption of individual spleens and lymph nodes in 1X RPMI, followed by filtration using a 70 µm filter to obtain a single cell suspension. For the CBD study, prior to restimulation, a portion of these isolates were set aside to stain for the presence of Tregs and MDSCs as described below. In the CBD study, 1 x 10^6 cells were seeded into 96 well U-bottom plates in 200 µl of 1X RPMI supplemented with 5% bovine calf serum (BCS; HyClone, Logan, UT), 1% penicillin/streptomycin (Pen/Strep; Gibco, Gaithersburg, MD), and 50 µM 2-mercaptoethanol (2-ME, Gibco) and restimulated with 100 µg/ml of MOG_{35-55} peptide for 48 hr at 37°C; however it was later determined that seeding 20 x10^6 cells into 4ml of complete media in a 6 well plate with 50 µg/ml of MOG peptide was more effective at restimulating cells, so for the *Cnr1*$^{-/-}$ vs WT studies this set up was used. At 44 hr, supernatants were collected for ELISAs, and cells were resuspended in 1x RPMI containing 5µg/ml of Brefeldin A (BioLegend, San Diego, CA) for the last 4 hr. Cells were then stained for extracellular markers (CD4

and CD8) and intracellular cytokine production (IFN-γ and IL-17A) and analyzed using flow cytometry.

2.4.2 Isolation of mononuclear cells from the spinal cords

To examine the infiltration of various T cells into the CNS, we isolated leukocytes for analysis by flow cytometry. To isolate cells from the spinal cord of each mouse, the spinal column was first removed and PBS was injected into the caudal aspect of the spinal canal. This caused extrusion of the spinal cord from the cranial spinal canal, which makes the spinal cord easier to process for the mononuclear cell isolation. The spinal cord of each mouse was then cut into small pieces and digested with 1mg/ml collagenase type 4 (Worthington) and 20 µg/ml DNase I for 45 min at 37°C with agitation. To isolate mononuclear cells the digestion solution was then pressed through a 70 µm filter and resuspended in 30% Percoll. The 30% Percoll was then underlain with 70% Percoll to form a gradient and centrifuged at 500 x g on low speed with no brake for 20 min. The mononuclear cells were then gently removed from the buffy coat layer, and washed in PBS twice before proceeding to staining and flow cytometry. To ensure enough cells were obtained for analysis, cells from two mice were pooled before staining for flow cytometry.

2.4.3 *S. aureus* SAg stimulation of suppressor cells

Splenocytes were isolated by mechanically disrupting the splenic capsule in RPMI, and bone marrow cells were isolated by rinsing the inside of the femurs from each mouse with sterile PBS. Cells were then centrifuged into a pellet at 500 x g for 5

min, and resuspended in RPMI containing 10% BCS, 1% Pen/Strep, and 50μM 2-ME. Throughout these experiments the culture conditions varied by plate type, number of cells, types of cells, duration of culture, and SAgs type in an attempt to optimize the stimulation conditions for Treg and MDSC induction. Cultures were done in either 6 well or 96 well plates for durations ranging from 1 to 5 days with shorter cultures typically being used for MDSCs as compared to Tregs, and the SAgs used were SEC, SEG, SEI, SEM, SEN, SEO, and TSST. Additionally, in some cultures TGF-β and IL-2 were used in an attempt to further induce Treg proliferation.

2.5 *In vitro* anti-CD3/anti-CD28 and *Staphylococcus* superantigen stimulation

To generate a T cells specific response from splenocytes that could be compared to the MOG_{35-55} specific responses from *ex vivo* restimulations, we chose to use anti-CD3/anti-CD28 antibodies and SEM. 48 well plates were pre-coated with 200μl of anti-CD3 antibody (BioLegend Clone 145-2C11) diluted in sterile PBS at 1μg/ml (1:1000) or 0.5 μg/ml (1:2000) for 1hr at 37°C prior to culture. Next, the wells were rinsed 3x PBS, and anti-CD28 antibody (BioLegend Clone 37.51) was added to the wells immediately prior to seeding $1x10^6$ splenocytes isolated from male and female WT or *Cnr1*$^{-/-}$ mice in 1ml of RPMI supplemented with 5% bovine calf serum, 1% penicillin/streptomycin, and 50 μM 2-ME. The final concentrations of anti-CD28 antibody were 1μg/ml (1:1000) or 0.5 μg/ml (1:2000). Other wells were treated with either 1μg of SEM, 5μg of SEM, or received no treatment (NT). SEM was chosen for these experiments based on preliminary experiments which showed consistent stimulation of T cells from C57BL/6 mice. These cultures were then incubated at 37°C for 2 or 3 days, and stained for flow

cytometry as described below. Supernatant from these cultures were taken for IFN-γ ELISA to determine total production of IFN-γ within the stimulated cultures.

2.6 Extracellular and intracellular staining

2.6.1 *IL-17A and IFN-γ producing T cells*

After treatment with Brefeldin A, cells were centrifuged at 500 x g for 5 min and the media was removed. The cells were then rinsed by suspending them in 200 µl of 1X PBS, centrifuging at 500 x g for 5 min, and PBS was removed. To measure viability, Fixable Viability Dyes (FVD) were used. For early studies (EAE/CBD study) we used 0.5 µl Pacific Blue Zombie FVD (BioLegend, San Diego, CA) in 200 µl of PBS, but later studies (*Cnr1*$^{-/-}$ vs WT EAE study) used 0.1µl of Near IR (NIR) FVD (BioLegend) in 50 µl of PBS. In each case, the FVD was added to each well and allowed to incubate for 30 min at 4°C. The cells were centrifuged again at 500 x g for 5 min and the FVD solution was removed. Then the cells were rinsed 2x with PBS. To prevent non-specific Ab binding, cells were incubated at room temperature (RT) for 15 min in 50 µl of flow cytometry buffer (FC buffer, 1X Hank's Buffered Saline Solution with 1% bovine serum albumin, pH 7.4) containing 0.5 µl of Fc Block (purified mouse CD16/CD32, BD Biosciences, Billerica, MA). Without removing the Fc Block from the wells, 50 µl of FC buffer containing 0.3 µl of extracellular antibodies was added to each well and allowed to incubate at RT for 30 min. For stains performed during the EAE/CBD study these extracellular antibodies consisted of CD4-FITC (BioLegend Clone Gk1.5) and CD8α-PE/Cy7 (BioLegend Clone 53-6.7); however during the *Cnr1*$^{-/-}$ vs WT EAE study these antibodies included CD4-PE (BioLegend Clone RM4-4), CD8α-PE/Cy7 (BioLegend

Clone 53-6.7), and CD3-FITC (BD Bioscience Clone 145-2C11). The plate was then centrifuged at 500 x g for 5 min, the supernatants containing the antibodies were removed, and a rinse step was performed with FC buffer.

To stain for intracellular cytokines in the EAE/CBD study, 200 µl of fixation/permeabilization solution (eBioscience/ThermoFisher, San Diego, CA) was added to each well in preparation for intracellular staining, allowed to incubate for 30 min at RT, and removed by centrifuging the plate and dumping off the supernatants. 50 µl of 1X permeabilization solution (eBioscience) containing 0.5 µl of intracellular IL-17A-APC (BioLegend Clone TC11-18H10.1) and 0.5 µl IFN-γ-PE (BioLegend Clone XMG1.2) was added to each well, and allowed to incubate at RT for 1 hr. The antibodies were then removed as before and the cells were resuspended in 200µl of FC buffer for analysis by flow cytometry. This approach was later modified for the *Cnr1*$^{-/-}$ vs WT EAE study. During these later studies, after the rinse step with FC buffer, the cells were fixed by incubating them in BD Cytofix solution (BD Bioscience) for 15min, and then rinsing them once with FC buffer and once with BD permwash buffer (BD Bioscience).Then the cells were resuspended in BD Permwash buffer containing 0.5 µl of IFN-γ-APC (BioLegend Clone XMG1.2) and allowed to incubate overnight at 4°C. After incubation the cells were rinsed with FC buffer and resuspended in 300 µl of FC buffer.

2.6.2 *Tregs*

Identification of Tregs from wild type mice

Cells isolated from SAg stimulate cultures were first stained with Zombie Green FVD as described above, while cells isolated directly from secondary lymphoid organs for our CBD/EAE studies were directly suspended in 200 µl of FC buffer, and centrifuged at 500 x g for 5 min to rinse the cells before blocking. As before, cells were treated with Fc Block, and then extracellular antibodies were added and allowed to incubate for 30 min at room temperature. 50 µl of FC buffer containing 0.3µl of CD4-PE/Cy7 (BioLegend Clone GK1.5) and CD25-FITC (BioLegend Clone PC61) was added for the CBD studies, and 0.3µl of CD4-PE/Cy7 (BioLegend Clone GK1.5) and CD25-PE (eBioscience Clone PC61.5) was used for the SAg regulatory T cell studies. The antibodies were then removed and cells were washed with FC buffer. For intracellular staining, cells were incubated with 200 µl of fixation/permeabilization solution for 30 min at RT. Next the fixation/permeabilization solution was removed, the cells were incubated with 50 µl of 1X permeabilization solution containing 0.5 µl FoxP3-APC (eBioscience Clone FJK-16s) for 1 hr at RT or overnight at 4°C, and then suspended in 200 µl of FC buffer for analysis by flow cytometry.

Identification of Tregs from FoxP3^{GFP} mice

The extracellular staining protocol for the identification of Tregs from FoxP3^{GFP} mice was the same as for the WT mice; however, since GFP fluorescence is detected in the same channel as the Zombie Green FVD signal, Sytox Red dead cell stain (ThermoFisher) was used in these mice. After the extracellular staining was completed, Sytox in FCM buffer (1:100) was added to each sample and the samples were analyzed by flow cytometry.

2.6.3 *MDSC*

Cells isolated from SAg stimulate cultures were first stained with Zombie Green FVD as described above, while cells isolated directly from secondary lymphoid organs during the CBD/EAE studies were directly suspended in 200 µl of FC buffer, and centrifuged at 500 x g for 5 min to rinse the cells before blocking. As before, cells were treated with Fc Block, and then extracellular antibodies were added and allowed to incubate for 30 min at RT. 50 µl of FC buffer containing 0.3µl of CD11b-APC (BioLegend Clone M1/70), Ly6G-PE/Cy7 (BioLegend Clone 1A8) and Ly6C-PE (BioLegend Clone HK1.4) was added. The antibodies were then removed and cells were washed with FC buffer. The MDSCs were fixed using BD Cytofix and then resuspended in 200 µl of FC buffer for analysis by flow cytometry.

2.6.4 *Spinal cord infiltrates*

The cells isolated from spinal cords were rinsed two times with PBS, as described above, and then incubated for 30 min at 4°C in 50 µl of PBS containing 0.1 µl NIR FVD. The cells were then rinsed twice with PBS and incubated for 15 min in 50 µl of FC buffer containing 0.5 µl of Fc Block. Without removing the Fc Block from the wells, 50 µl of FC buffer containing 0.3 µl of CD45-Brilliant Violet 605 (BV605;Biolegend Clone 30-F11), CD4-FITC (BioLegend Clone Gk1.5), CD3-Pacific Blue (BioLegend Clone 17A2), CD8α-PE/Cy7 (BioLegend Clone 53-6.7), and CD25-PE (eBioscience Clone PC61.5) was added to each well and allowed to incubate at RT for 30 min. After this incubation the cells were rinsed with FCM and 50 µl of fixation/permeabilization solution

was added and allowed to incubate for 30 min at RT. Intracellular staining for FoxP3 was performed as described in the previous section.

2.7 Flow cytometry

Cells stained with intracellular and extracellular florescent antibodies were analyzed using an ACEA Novocyte flow cytometer (ACEA Biosciences, San Diego, CA) or BD FACS Calibur flow cytometer.

2.7.1 *IL-17A and IFN-γ producing T cells*

To determine the percentage of Th1, Th17, Tc1, and Tc17 cells from the MOG_{35-55} *ex vivo restimulated* cultures, dead cells were initially excluded from analysis by selecting cells that were not stained by Pacific Blue FVD. Doublets were then eliminated based on side scatter characteristics (SSC-A/H) and forward scatter characteristics (FSC-A/H). Lymphocytes were selected based on their FSC and SSC, and $CD4^+$ and $CD8^+$ positive populations were selected. Once the $CD4^+$ and $CD8^+$ lymphocytes had been identified, gates were set up to determine the percentage of these cells that contained intracellular IL-17A and IFN-γ (Figure 2.1).

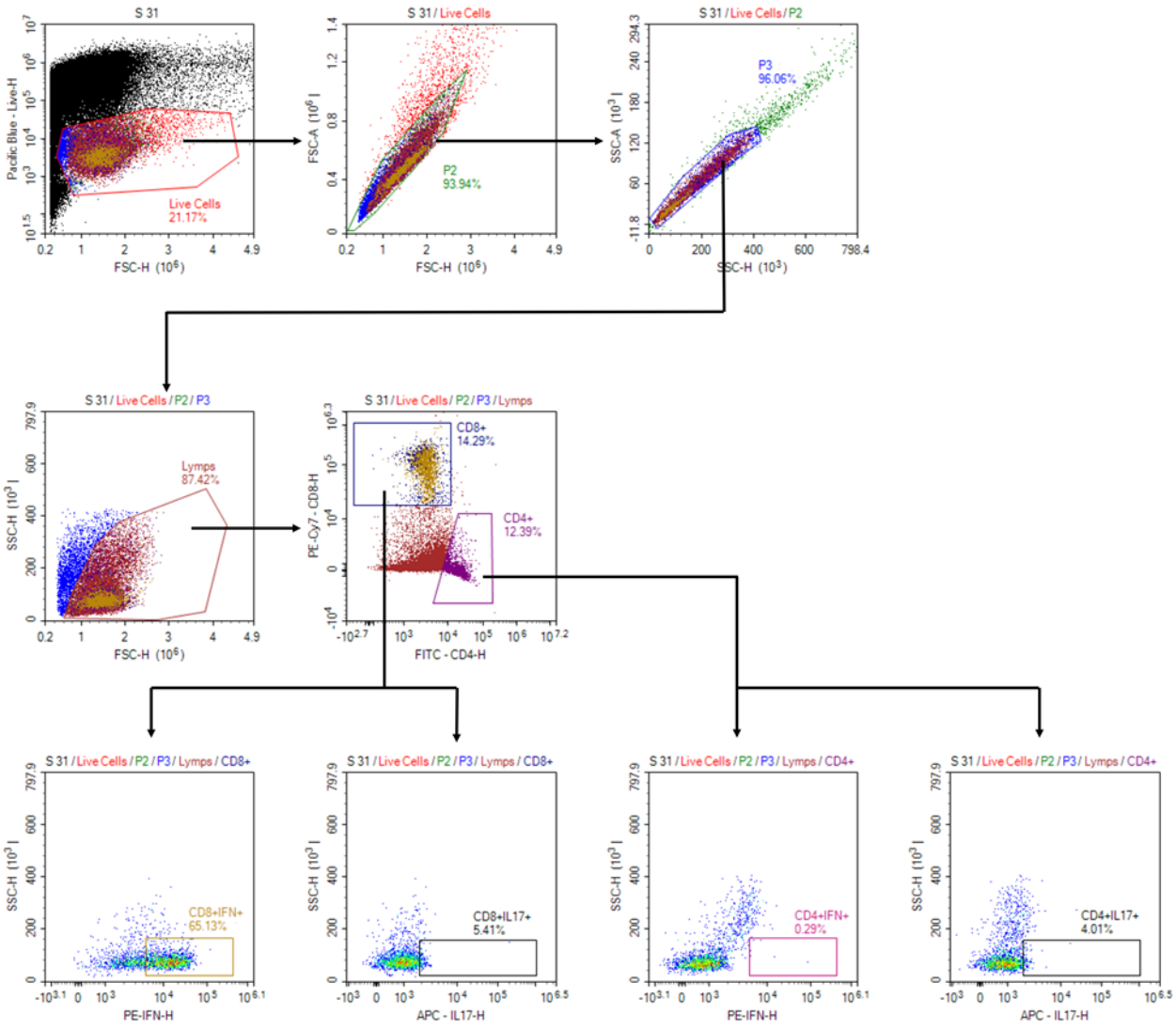

Figure 2.1 Gating strategy for identifying Tc1, Tc17, Th1, and Th17cells in the CBD EAE study.

Live cells were first selected based on lack of staining with Pacific Blue FVD dye, and these cells were then passed through two singlet gates to eliminate any doublets. Lymphocytes were then selected based on FSC and SSC characteristics and from this population cells were subdivided into $CD8^{+}IFN\text{-}\gamma^{+}$, $CD8^{+}IL\text{-}17A^{+}$, $CD4^{+}IFN\text{-}\gamma^{+}$, $CD4^{+}IL\text{-}17A^{+}$ lymphocytes population.

2.7.2 Tregs

2.7.2.1 *Cannabidiol study*

To identify Tregs from the spleens and lymph nodes of mice from the CBD study, lymphocytes were first selected using FSC and SSC gating, and doublets were then eliminated based on SSC-A/H and FSC-A/H characteristics. Then $CD4^+$ cells were selected by expression of CD4. Once $CD4^+$ Cells were identified, the percentage of double positive $CD25^+Foxp3^+$ cells within the $CD4^+$ population was determined (Figure 2.2).

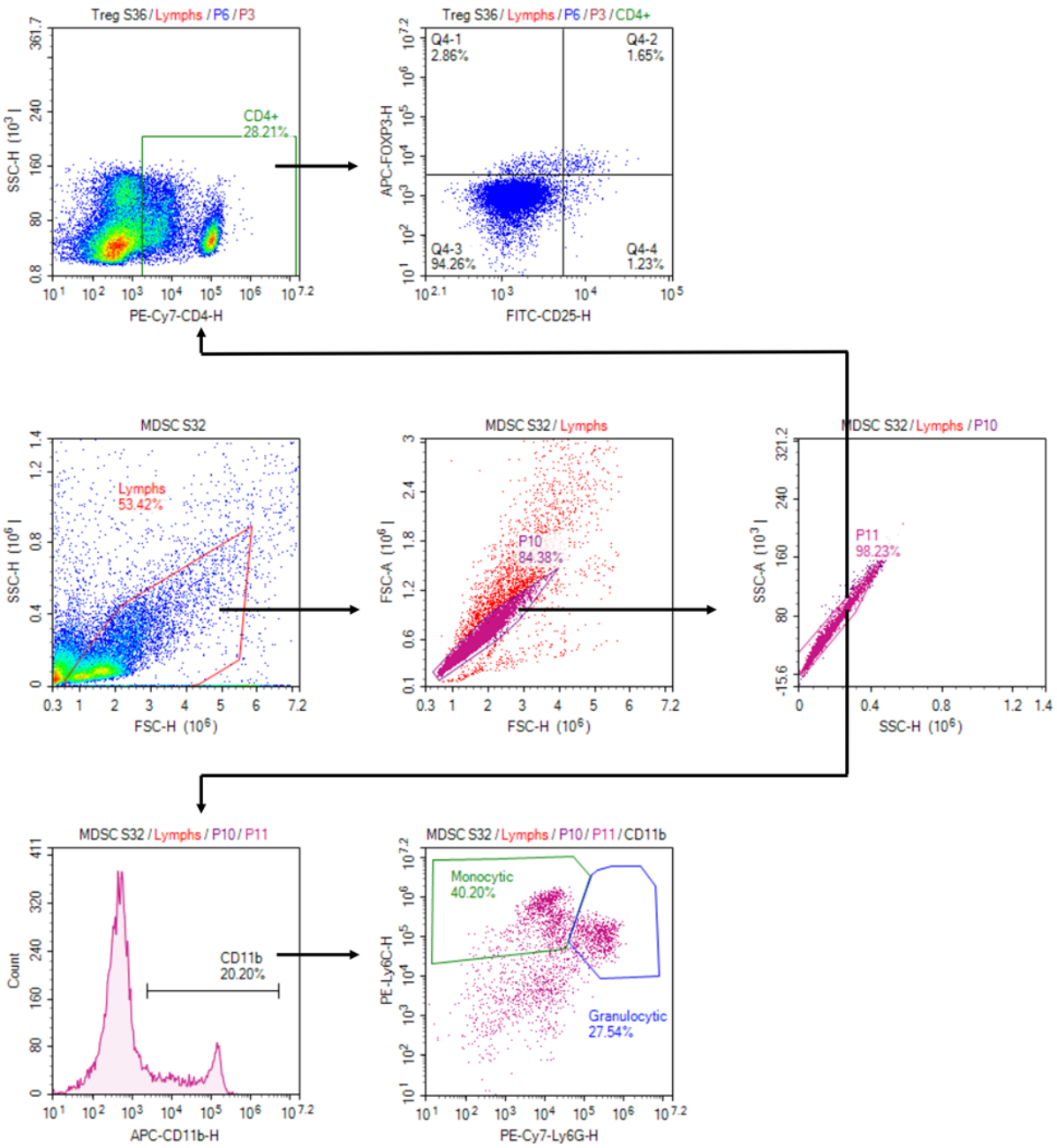

Figure 2.2 Gating strategy for identifying MDSCs and Tregs in the CBD EAE study.

To identify regulatory cells from the spleens of mice in the EAE CBD study, lymphocytes first identified based on FSC and SSC characteristics, and then passed through two singlet gates to eliminate any doublet formation. From this population Tregs were identified as $CD4^{+}CD25^{+}FoxP3^{+}$ lymphocytes, granulocytic MDSCs were identified as $CD11b^{+}Ly6C^{lo}Ly6G^{+}$ lymphocytes and monocytic MDSCs were identified as $CD11b^{+}Ly6C^{+}Ly6G^{-}$ lymphocytes.

2.7.2.2 *SAg study*

When live/dead staining was used in an experiment, dead cells were first excluded from analysis, and then analyzed using FSC vs SSC gating was used to identify lymphocytes. If no live/dead staining was used, the cells were first analyzed with FSC vs SSC gating. Lymphocytes were selected using FSC and SSC gating, and $CD4^+$ cells were selected based on expression of CD4. From this population the percentage of double positive $CD25^+Foxp3^+$ cells was identified (Figure 2.3).

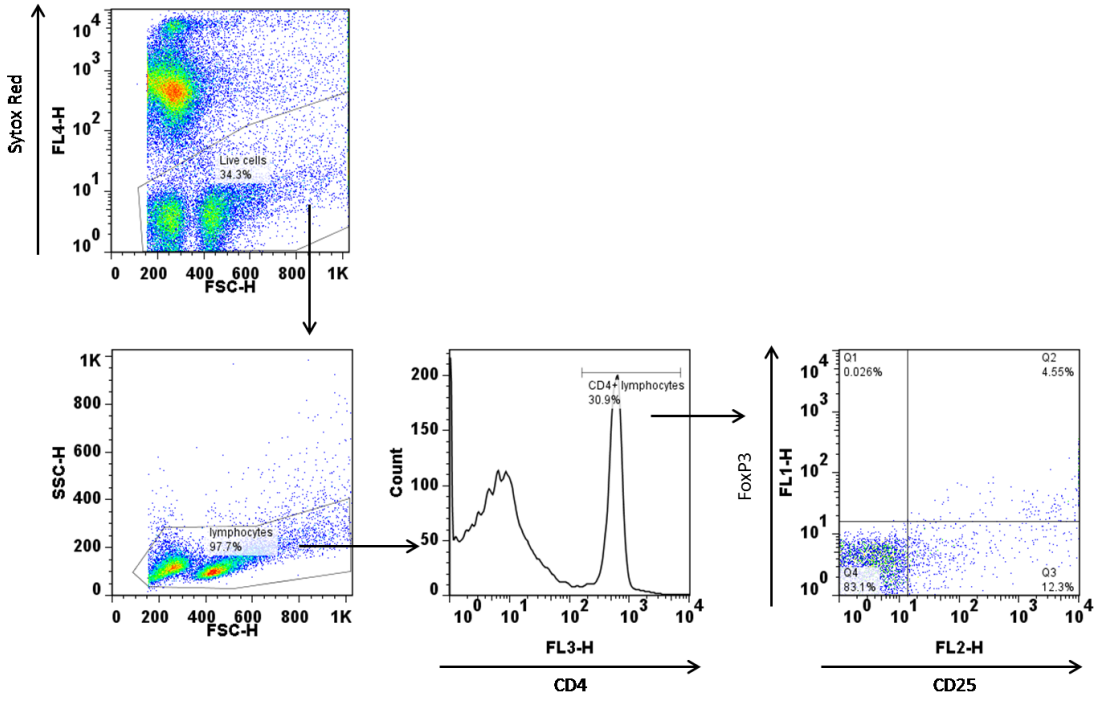

Figure 2.3 Gating strategy for Tregs in SAg studies with $FoxP3^{GFP}$ mice

Live cells were first identified based on Sytox Red staining, and then lymphocytes were identified based on FSC and SSC characteristics. Tregs from this population of live lymphocytes were then identified as $CD4^+CD25^+FoxP3^+$ cells.

2.7.3 *MDSCs*

2.7.3.1 Cannabidiol study

To identify MDSCs isolated from the spleens of mice in the CBD study, lymphocytes were first selected using FSC and SSC gating, and MDSC were identified based on their expression of CD11b, Ly6C, and Ly6G extracellular markers. Monocytic MDSCs and granulocytic MDSCs were differentiated based on their Ly6C and Ly6G profiles. Granulocytic MDSC were identified as $CD11b^{+}Ly6C^{+}Ly6G^{+}$ cells and monocytic MDSC were identified as $CD11b^{+}Ly6C^{+}Ly6G^{-}$ (Figure 2.2).

2.7.3.2 SAg study

During our studies with *S. aureus* Sags, live cells were first identified using Zombie Green FVD. From this population we identified granulocytic MDSC as $CD11b^{+}Ly6C^{+}Ly6G^{+}$ cells and monocytic MDSC as $CD11b^{+}Ly6C^{+}Ly6G^{-}$ (Figure 2.4).

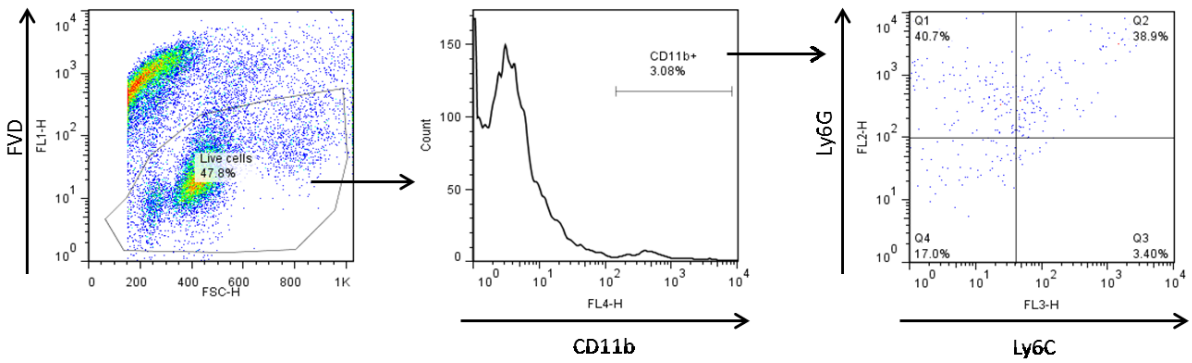

Figure 2.4 Gating strategy for MDSCs in *S. aureus* SAg studies

Within the live cell population, which were identified based on Zombie Green FVD uptake, granulocytic MDSC were identified as $CD11b^{+}Ly6C^{lo}Ly6G^{+}$ cells and monocytic MDSC were identified as $CD11b^{+}Ly6C^{+}Ly6G^{-}$ cells.

2.7.4 Spinal cord infiltrates

As before, dead cells were excluded from analysis by selecting cells that were not stained by NIR FVD, doublets were excluded by their SSC-A/H and FSC-A/H characteristics, and lymphocytes were selected based on FSC and SSC gating. $CD45^+CD3^+$ cells were then selected and subdivided base on their expression of $CD4^+$ and $CD8^+$. Further gating of $CD3^+CD4^+$ T cells was performed to determine the number of Tregs within the spinal cords based on their expression of CD25 and FoxP3.

2.8 ELISA

Immulon 4 HBX flat bottom plates were coated with purified mouse IL-17A (BioLegend Clone TC11-18H10.1) or IFN-γ (BioLegend Clone AN-18) antibodies by adding 100 µl of coating buffer (4.2g of $NaHCO_3$ in 500mls of DI water) containing the desired antibody at a 1:500 dilution, and incubating the plate overnight at 4°C. The next day the plates were washed three times with PBS containing 0.05% Tween 20 (PBST). PBS containing 3% BSA (3% BSA-PBS) was placed in the plate for at least 1 hr at RT to block non-specific binding, and then the plate was washed three times with PBST. 100 µl of recombinant IL-17A (BioLegend) and IFN-γ (BioLegend) standards were then pipetted into their respective wells at increasing concentrations (7.8-4000 pg/ml or 7.8-8000pg/ml), and 50µl of supernatants obtained from the 48 hr cultures were pipetted into each plate to measure the concentration of IL-17A and IFN-γ in each supernatant. 1:10 dilutions of all supernatants were prepared in the same manner to detect higher ranges of these cytokines. 100 µl of 3% BSA-PBS was used as a blank control. The plates containing the standards and supernatants were then incubated for 1 hr at RT,

and subsequently washed three times with PBST. 100 µl of biotinylated IL-17A (BioLegend) or biotinylated IFN-γ (BioLegend) antibodies in 3% BSA-PBS at a 1:500 dilution were added to their respective plates and incubated for 1 hr at RT. The plates were next washed three times with PBST. 100 µl of HRP-Avidin (BioLegend) in 3% BSA-PBS at a dilution of 1:500 was added to each well and incubated for 1 hr at RT, and then the plates were rinsed three times with PBST. 100 µl of TMB substrate (BioLegend) was added to each well and incubated until color development was detected in the lowest standard, then the reaction was stopped with 100 µl of 2N H2SO4, and optical density (OD) was measured at 450nm.

2.9 Processing of brains and spinal cords for histology

After the mice were euthanized, to make manipulation of the cranium and spinal column easier, the spinal column was severed at the base of the skull just caudal to the first cervical vertebra (C1), and the brain and spinal column were processed separately.

2.9.1 Brain

To remove the brain from the cranial cavity, the calvarium was removed, the brain was elevated out of the cranial cavity, and sharp dissection of the cranial nerves was performed to disconnect the brain from the skull. The brain was then cut along the sagittal plane using a razor blade and the right half of the brain was placed in 10% neutral buffered formalin (NBF) for fixation. Once fixation was complete, the brains were embedded in paraffin wax blocks so that sections of the tissue could be cut for histologic analysis.

2.9.2 Spinal column

After the spinal column was separated from the skull, the excess tissue and ribs were trimmed, and the caudal end of the spinal cord was cut at the level of the L6 vertebra. Next, the entire spinal column was placed in 10% NBF for fixation. The fixed spinal columns were rinsed in PBS to remove the 10% NBF, and were placed in a 10% EDTA solution at pH 7.4 for decalcification. 10% EDTA was made by diluting 0.5M EDTA, pH 8 (ThermoFisher) with distilled water, and adjusting the solution to pH 7.4 with acetic acid. The spinal columns were left in this solution for 15 days and the solution was refreshed every 5 days. Once decalcification was complete, the spinal column was cut at the T7 vertebra to isolate the lumbar intumescence. This method of dissection left the spinal column between T7 and L6. The T7-L6 region was then either cut at intervals of approximately 0.3cm or 0.5cm depending on the study. The segments were then embedded in a cranial to caudal orientation within paraffin wax blocks so the tissue could be cut for histologic analysis.

2.10 Immunohistochemistry and histologic analysis

2.10.1 CBD study

5-µm sections of brains and spinal cords from each time point were initially stained with hematoxylin and eosin (H&E) to determine the level of cellular invasion. Based on the results seen from this initial analysis, it was determined that brains from the day 18 mice in the SAL/CO, EAE/CO and EAE/CBD groups would be stained for

CD3 to determine which regions contained T cells, and spinal cords would be used for quantification of T cell numbers and lesion size.

2.10.1.1 CD3 staining

5-µm sections from brains and spinal cords of the day 18 mice from SAL/CO, EAE/CO and EAE/CBD groups were used for CD3 staining. Sections were first deparafinized and rehydrated by placing them in the following solutions for 2 min each: xylene, 100% ethanol, 95% ethanol, and DI water. Antigen retrieval was performed in a steamer by treating the slides for 20 min with Target Retrieval Solution (TRS; Dako, Santa Clara, CA) which is a modified citrate buffer with a pH 6.1. After retrieval, slides were air dried for 10 mins, rinsed with phosphate buffered saline (PBS), and covered with 3% H_2O_2 for 30 min to block endogenous peroxidases. H_2O_2 was removed by washing the slides three times in PBS. A PBS solution containing 1% bovine serum albumin (BSA) and 4% goat serum (Vector Laboratories, Burlingame, CA) was then added to each slide and incubated for 1 hr to block non-specific binding of the primary antibodies. The blocking solution was removed and polyclonal rabbit anti-human CD3 antibody in PBS/1% BSA/0.1% Triton X-100 (Tx) (1:2500; Dako) was added to each slide and incubated overnight at 4°C. The following day, slides were rinsed three times with PBS and treated with a biotinylated goat anti-rabbit secondary antibody diluted in PBS/1% BSA/0.1% Tx (1:100; Vector Laboratories,) for 2 hr at RT. Slides were then rinsed with distilled water three times, and incubated in a solution containing avidin D and biotinylated horseradish peroxidase H (Vectastain Elite ABC Kit; Vector Laboratories) in PBS for 2 hr. Sections were then rinsed three times with distilled water

and incubated with diaminobenzidine (DAB; Dako) for approximately 5 min. The reaction with DAB was stopped by dipping the slides in distilled water, and the slides were dipped in hematoxylin to make visualization of histologic structures easier. Each slide was then dipped in 0.3% ammonia water to lighten the hematoxylin stain. For dehydration, slides were dipped in each of the following solutions for 1 min: distilled water, 75% ethanol, 100% ethanol, and xylene. A cover slip was placed on the slide with permount and allowed to dry.

2.10.1.2 CD4 and CD8 double stain

Due to the extremely dim staining that resulted from CD4 immunofluorescent staining, it was decided that the best route to achieve a double stain would be to stain the CD4 first as an immunoperoxidase stain, and then follow up with a CD8 immunofluorescent stain. Much like the CD3 stain, slides for the double stain underwent deparafinization, antigen retrieval and blocking with 3% H_2O_2; however, it is important to note that 1% Tx was added to the antigen retrieval solution to help uncover the antigens. Following the blocking step, a biotinylated monoclonal rat CD4 antibody in PBS/1% BSA/1% Tx (1:40; ThermoFisher Clone 4SM95) was added to each slide and allowed to incubate overnight at 4°C. The next day, the slides were rinsed with distilled water and incubated in a solution containing avidin D and biotinylated horseradish peroxidase H (Vectastain Elite ABC Kit; Vector Laboratories) and an unconjugated monoclonal rabbit CD8 antibody in PBS (1:50; Abcam, Cambridge, MA Clone EPR21769) for 2 hr at RT. Sections were then rinsed three times with distilled water and incubated with DAB for approximately 20 min. The reaction with DAB was stopped by

dipping the slides in distilled water, and the slides were dipped in hematoxylin to make visualization of histologic structures easier. Each slide was then dipped in 0.3% ammonia water to lighten the hematoxylin stain. Next an Alexa Fluor 488 conjugated goat anti-rabbit IgG antibody in PBS/1% BSA/0.1% Tx (1:200; ThermoFisher) was added to each slide and allowed to incubate for 2 hr. To protect the Alexa Fluor 488 from degradation during visualization, slides were coverslipped with Vectashield (Vector Laboratories).

2.10.1.3 Glial fibrillary acidic protein (GFAP)

GFAP is a marker that is commonly used to identify activation of astrocytes within the CNS. However, here we use this stain to delineate the boarder of the BBB so that we can show measure the size of lesions within the BBB. Deparafinization, antigen retrieval and blocking with 4% goat serum was performed as it was for the CD3 stain. After blocking, slides were incubated with PBS/1% BSA/0.1% Tx containing unconjugated polyclonal rabbit GFAP antibody (1:200; Millipore, Burlington, MA) overnight at 4°C in the dark. The next day, the slides were rinsed in distilled water and incubated for 2 hr with PBS/1% BSA/0.1% Tx containing Alexa Fluor 488 conjugated goat anti-rabbit IgG antibody (1:200; ThermoFisher) and 0.5µg/ml of 4′,6-Diamidine-2′-phenylindole dihydrochloride (DAPI; ThermoFisher) as a nuclear counterstain. Slides were then rinsed and coverslipped with Vectashield.

2.10.1.4 Iba-1 Staining

5μm sections of spinal cords from SAL/CO, EAE/CO, and EAE/CBD mice taken on days 10 and 18 of the study were used for Iba-1 staining. Sections for the Iba-1 staining were first deparafinized and rehydrated by placing them through xylene, 100% ethanol, 95% ethanol, DI water at 2 mins each. Antigen retrieval was performed by placing the slides in TRS for 30mins in a steamer. The slides were then allowed to cool for 10mins and rinsed in PBS. Non-specific binding was blocked by placing the sections in PBS containing 1% BSA and 4% goat serum for 1hr at RT. The blocking solution was then removed and polyclonal rabbit Iba-1 antibodies (anti-AIF-1; Millipore) were placed on the sections in PBS/1% BSA/0.1% Tx. These slides were then incubated overnight at 4°C. The next day the slides were rinsed in distilled water to remove excess antibodies, and incubated for 2 hr in PBS/1% BSA/0.1% Tx containing Alexa Fluor 488 conjugated goat anti-rabbit IgG antibody (1:200). Slides were rinsed and coverslipped with Vectashield before imaging.

2.10.1.5 Imaging and quantification

Images were captured using a Lumenera Digital Camera equipped with Infinity Analyze Software, and analyzed using the ImageJ software. To analyze the number of $CD3^+$, $CD4^+$, and $CD8^+$ T cells present within the spinal cord a total of four lesions from two sections of lumbosacral intumescence of each mouse were analyzed at 400 x magnifications. The number of each cell type was averaged across the four lesions to get the average number of cells for lesions within the lumbosacral region of each mouse. To determine lesion size for each mouse, 40x magnification images of 2

sections from the same region were analyzed using the GFAP/DAPI stain, which allowed us to determine the size of the lesion within the parenchyma of the spinal cord and exclude the portion of the lesions within the meninges.

2.10.2 *Cnr1*$^{-/-}$ vs WT study

2.10.2.1 Histologic scoring

Spinal cords were processed and each 0.5 cm section was embedded in a cranial to caudal orientation within paraffin wax blocks to ensure 0.5 cm spacing between subsequent sections (Figure 2.1 A&C).

In order to analyze neuroinflammation within the spinal cord a new scoring system was developed to account for variations in lesion size, location along the spinal cord, and location within a section. H&E stains of the first 5 sections of spinal cord from each histologic preparation were used to generate histologic scores for each mouse. Each section was first divided into four regions (Figure 2.1B) and then each region was given a score based on the number of infiltrating cells within the largest lesion found in that region. The possible scores given to each region were: 0 = no cells; 1 = 10 to 100 cells; 2 = 100 to 200 cells; 3 = 200+ cells. Microscopic images were captured using a Lumenera Digital Camera and Infinity Analyze Software. Scoring and lesion area calculations were done with ImageJ software.

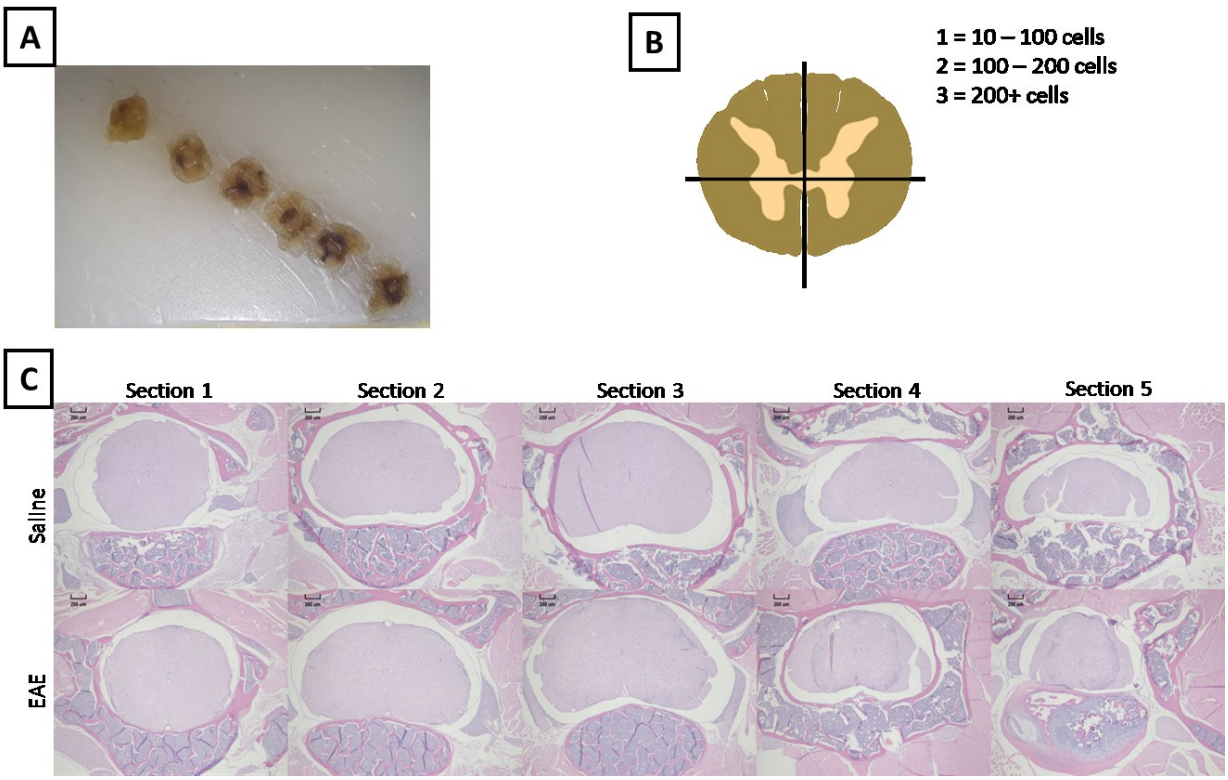

Figure 2.5 Histologic scoring system

The spinal column for each mouse was sectioned in to six 0.5 cm section and placed in paraffin wax blocks so that the cranial aspect of each section would be cut first (A). Then each of the quarter of the first 5 sections was given a score based on the number of cells found within each quarter of the spinal cord (B). Representative H&E images of the first 5 sections are shown (C).

2.11 Statistical analysis

Statistical analysis was done with GraphPad Prism 6 or GraphPad Prism 7 software. For clinical scoring and histological scoring the Mann-Whitney U test was used for comparisons between groups. All other comparisons were done using ANOVA or T-Test as appropriate. Transformations were performed on all percentages obtained

by flow cytometry before ANOVA was performed. Graphical representations of data show averages within each group and the error bars represent the standard deviation of each group.

CHAPTER III

RESULTS

3.1 Effects of oral CBD on the peripheral immune and neuroimmune response

The aim of these experiments was to examine the effects of oral CBD on the peripheral and neuroimmune response using the EAE model. Using this model we were able to induce disease in C57BL/6 mice, and oral CBD was administered for the first 5 days after the initiation of disease. Mice were euthanized on days 3, 10, and 18, and lymph nodes, spleens, spinal cords and brains were used to examine the effect CBD had on the EAE immune response.

3.1.1 Clinical scores

Average clinical scores recorded during the 18 day time course showed that clinical disease began on approximately day 14 for all groups except for the SAL/CO group (n=5). On day 18, the EAE/CO group (n=11) had the highest average clinical score out of all the groups, with the EAE/CBD group (n=11) having a significantly lower average clinical score than the EAE/CO group. The Mild EAE/CO group (n=5) also had a significantly lower average clinical score as compared to the EAE/CO group. There was no significant clinical difference seen between the Mild EAE/CO and Mild EAE/CBD (n=5) groups. The control group showed no signs of clinical disease (Figure 3.1).

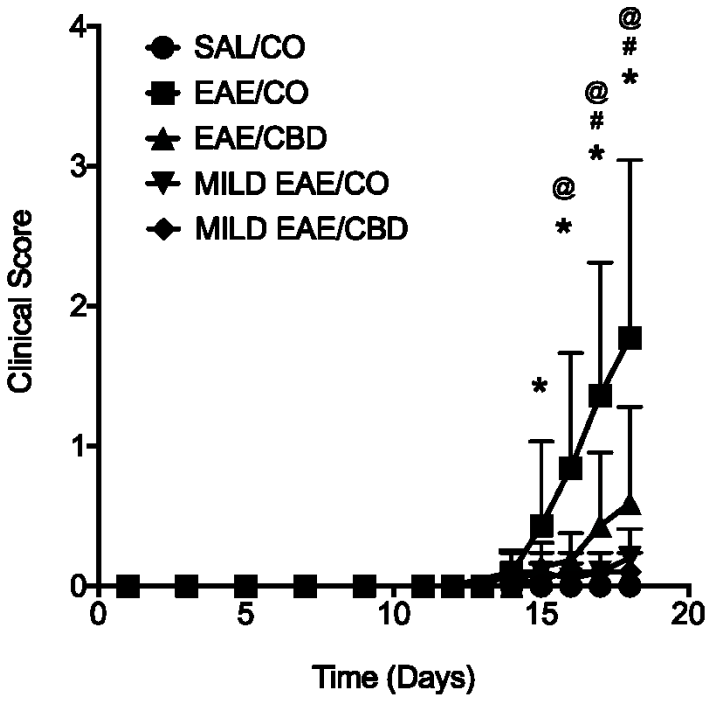

Figure 3.1 Effects of oral CBD in EAE clinical scores.

Average clinical scores recorded for each group of mice during the 18 day time course. Mice from 3 and 10 day time points were included in each group until they were euthanized. Disease incidence in day 18 groups was as follows: SAL/CO = 0% (n=5), EAE/CO = 81.82% (n=11), EAE/CBD = 63.64% (n=11), Mild EAE/CO = 60% (n=5), Mild EAE/CBD = 40% (n=5). * $p < 0.05$ differences between SAL/CO and EAE/CO; # $p < 0.05$ difference between EAE/CO and EAE/CBD; @ $p < 0.05$ difference between EAE/CO and Mild EAE/CO.

3.1.2 Effects of CBD on suppressor cell populations

Same day analysis by flow cytometry of suppressor cells isolated from the secondary lymphoid tissue showed that treatment with CBD did not significantly change the percentage of Tregs isolated from the lymph nodes and spleen, or MDSCs from the spleen (Figure 3.2). However, significant increases were seen in the percentage of MDSCs recovered from the spleens of EAE and Mild EAE mice as compared to the

SAL/CO group at several time points with the most pronounced differences being seen on day 10 (Figure 3.2C-D). Significant decreases were also seen in the percentage of Tregs recovered from the spleens and lymph nodes of the EAE/CO and Mild EAE/CO groups. On day 10, a lower percentage of Tregs was recovered from the lymph nodes of EAE/CO and Mild EAE/CO groups as compared to the SAL/CO group, and the percentage of Tregs recovered from the spleens of the EAE/CO mice was significantly decreased as compared to the SAL/CO group and the Mild EAE/CO group (Fig. 3.2A-B). Lastly, a significant decrease was found in percentage of monocytic MDSCs present in splenocytes from Mild EAE/CBD as compared to the EAE/CBD group on day 10 (Fig. 3.2D).

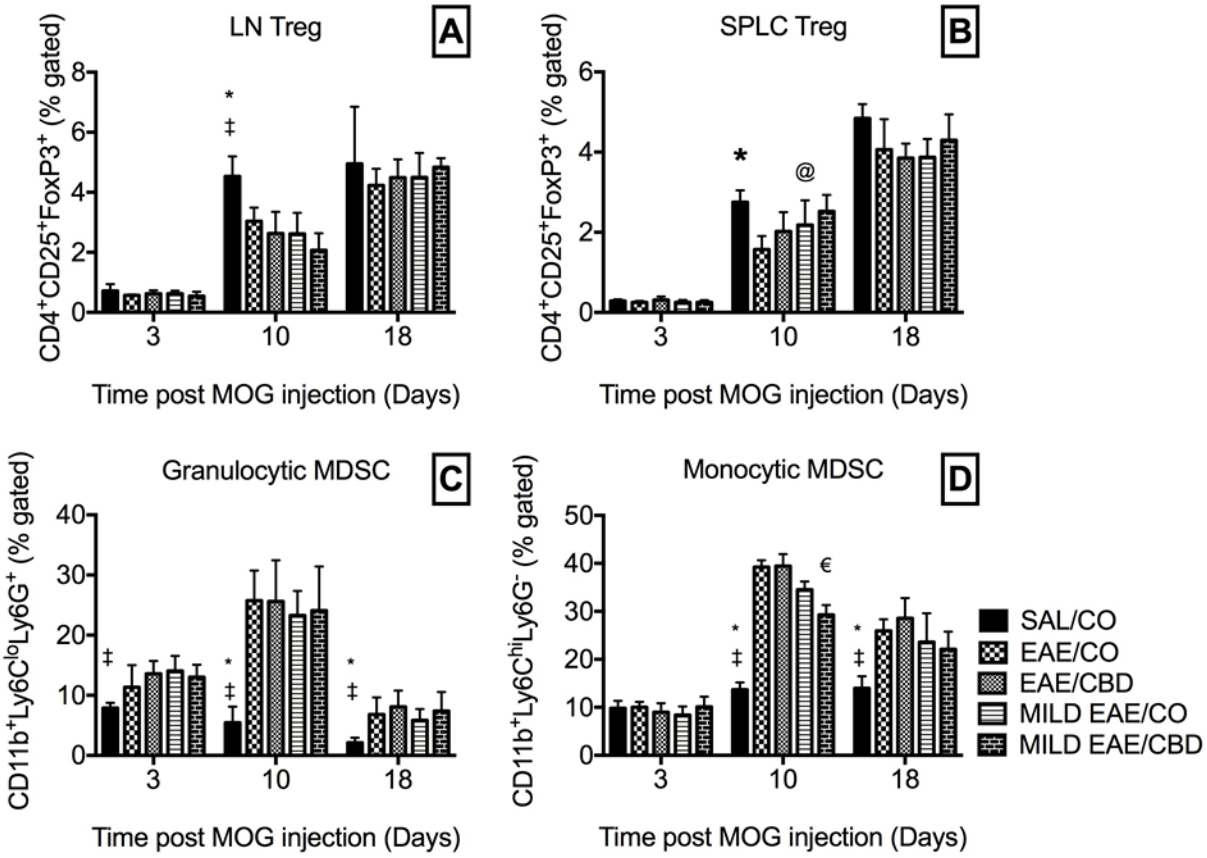

Figure 3.2 Regulatory cells from secondary lymphoid organs

Lymph nodes and spleens were taken from each mouse on the day of necropsy and made into single cell suspensions by passing them through a 70µm filter. Cellular isolates from the lymph nodes were then stained for the classic Treg markers ($CD4^+CD25^+FoxP3^+$)(A), and cellular isolates from the spleens were stained for Treg markers (B), Granulocytic MDSC markers ($CD11b^+Ly6C^{lo}Ly6G^+$)(C) or Monocytic MDSC markers ($CD11b^+Ly6C^+Ly6G^-$)(D). These cells were then analyzed using flow cytometry to determine the percentage of regulator cells for each sample. n=5 for each group of mice (SAL/CO, EAE/CO, EAE/CBD, Mild EAE/CO, and Mild EAE/CBD) on each day. * $p<0.05$ differences between SAL/CO and EAE/CO; ‡ $p<0.05$ difference between SAL/CO and Mild EAE/CO; @ $p<0.05$ difference between EAE/CO and Mild EAE/CO; € $p<0.05$ difference between EAE/CBD and Mild EAE/CBD.

3.1.3 Effects of CBD on IFN-γ and IL-17 producing T cells

3.1.3.1 *Intracellular cytokine staining*

Analysis of IFN-γ^+ and IL-17A$^+$ T cells after a 48 hr restimulation with MOG_{35-55} peptide showed significant differences in the percentage of MOG_{35-55} specific IFN-γ producing CD8$^+$ T cells isolated from the spleens of day 10 mice (Fig. 3.3C). On this day, EAE/CO had the highest percentage of IFN-γ producing CD8$^+$ T cells as compared to all other groups, with the SAL/CO, EAE/CBD, and Mild EAE/CO groups having a significantly lower percentage than the EAE/CO group. Interestingly, this pattern was also seen in the CD4$^+$ T cells from the spleen, but only the difference between EAE/CO and SAL/CO groups was significant. Lastly, the number IL-17A$^+$CD8$^+$ T cells isolated from the spleen of EAE/CO mice on day 10 was significantly increased as compared to the SAL/CO group. There were no effects of CBD on IL-17-producing T cells in the spleen.

Analysis of IFN-γ^+ and IL-17A$^+$ T cells from the lymph nodes after a 48 hr restimulation with MOG_{35-55} peptide revealed very low cytokine production at all time points tested (Fig. 3.4A-D). There were no significant changes noted in response to disease or CBD.

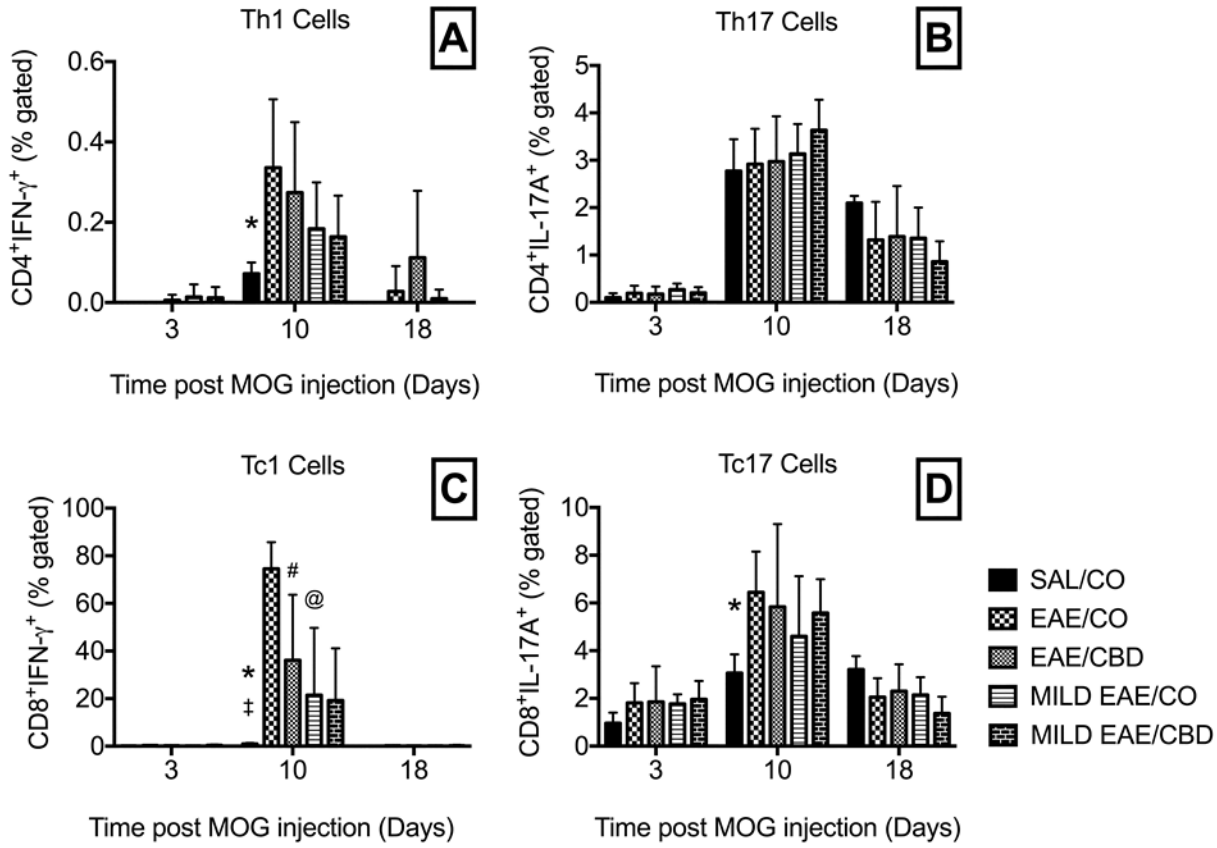

Figure 3.3 Cytokine production in T cells isolated from spleens after ex vivo restimulation.

Splenocytes were restimulated ex vivo with MOG_{35-55} peptide for 48 hr, and then treated with Brefeldin A to block the secretion of cytokines. Cells were then stained for expression of CD4, CD8, IFN-γ and IL-17A, and Flow cytometry was used to measure the percentage of IFN-γ and IL-17A producing cells within the CD4 (A & B) and CD8 (C & D) populations. n=5 for each group of mice (SAL/CO, EAE/CO, EAE/CBD, Mild EAE/CO, and Mild EAE/CBD) on each day. * $p<0.05$ differences between SAL/CO and EAE/CO; ‡ $p<0.05$ difference between SAL/CO and Mild EAE/CO; # $p<0.05$ difference between EAE/CO and EAE/CBD; @ $p<0.05$ difference between EAE/CO and Mild EAE/CO

3.1.3.2 Cytokine production in supernatants

ELISAs were performed on the supernatants following 48 hr restimulation with MOG_{35-55} peptide to determine the cumulative production of IFN-γ and IL-17A during culture. In general, the cultured cells from EAE mice produced more IFN-γ and IL-17A than Mild EAE groups, with this difference reaching significant levels within the cultured splenocytes, and cytokine production was increased earlier in the lymph nodes than in the spleen (Fig. 3.5A-D). There was also a significant increase in IFN-γ production in EAE/CBD as compared to EAE/CO in splenocytes at day 18.

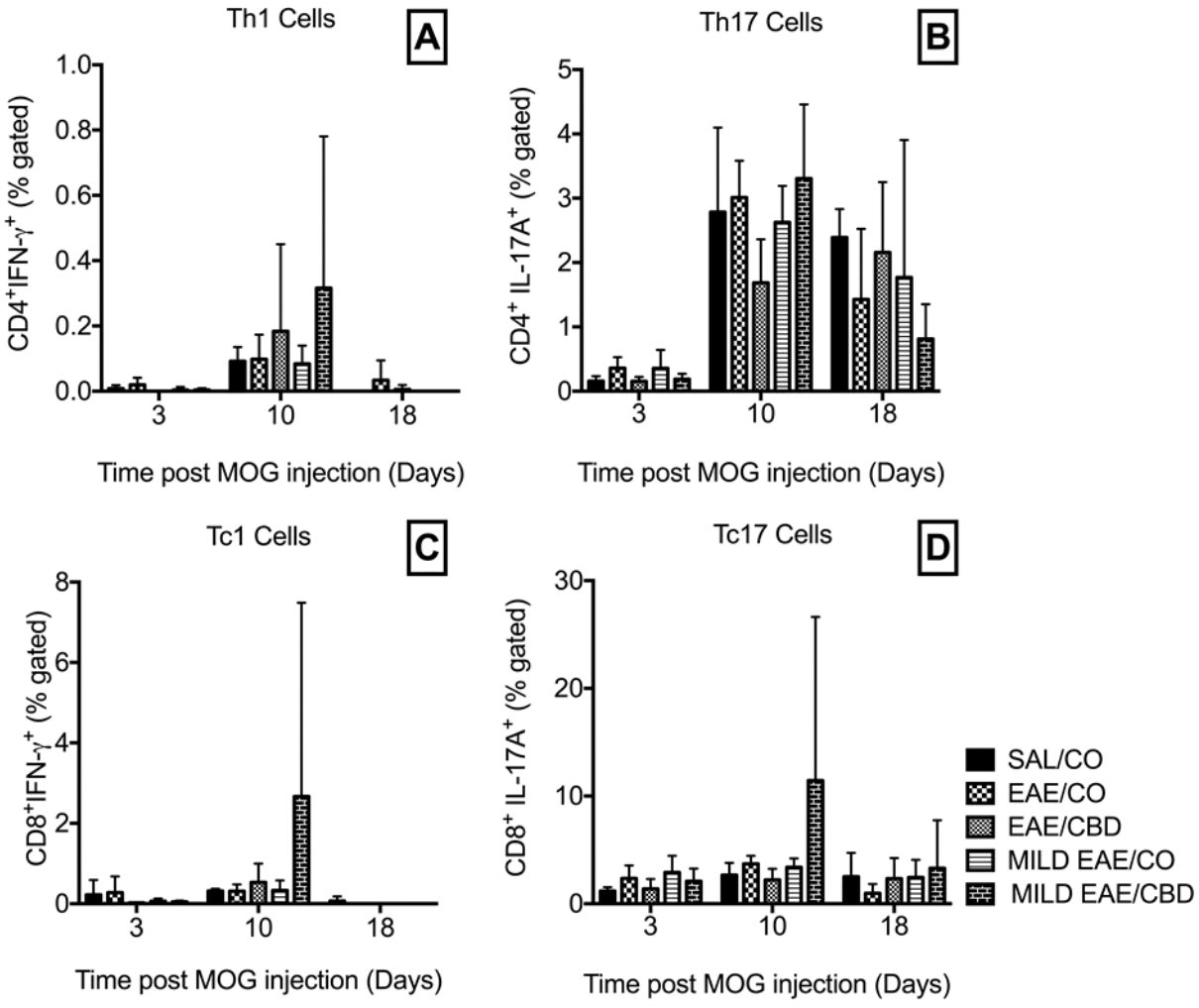

Figure 3.4 Cytokine production in T cells isolated from lymph nodes after ex vivo restimulation.

Cells isolated from lymph nodes were restimulated ex vivo with MOG_{35-55} peptide for 48 hr, and then treated with Brefeldin A to block the secretion of cytokines. Cells were then stained for expression of CD4, CD8, IFN-γ and IL-17A, and flow cytometry was used to measure the percentage of IFN-γ and IL-17A producing cells within the CD4 (A & B) and CD8 (C & D) population. n=5 for each group of mice (SAL/CO, EAE/CO, EAE/CBD, Mild EAE/CO, and Mild EAE/CBD) on each day.

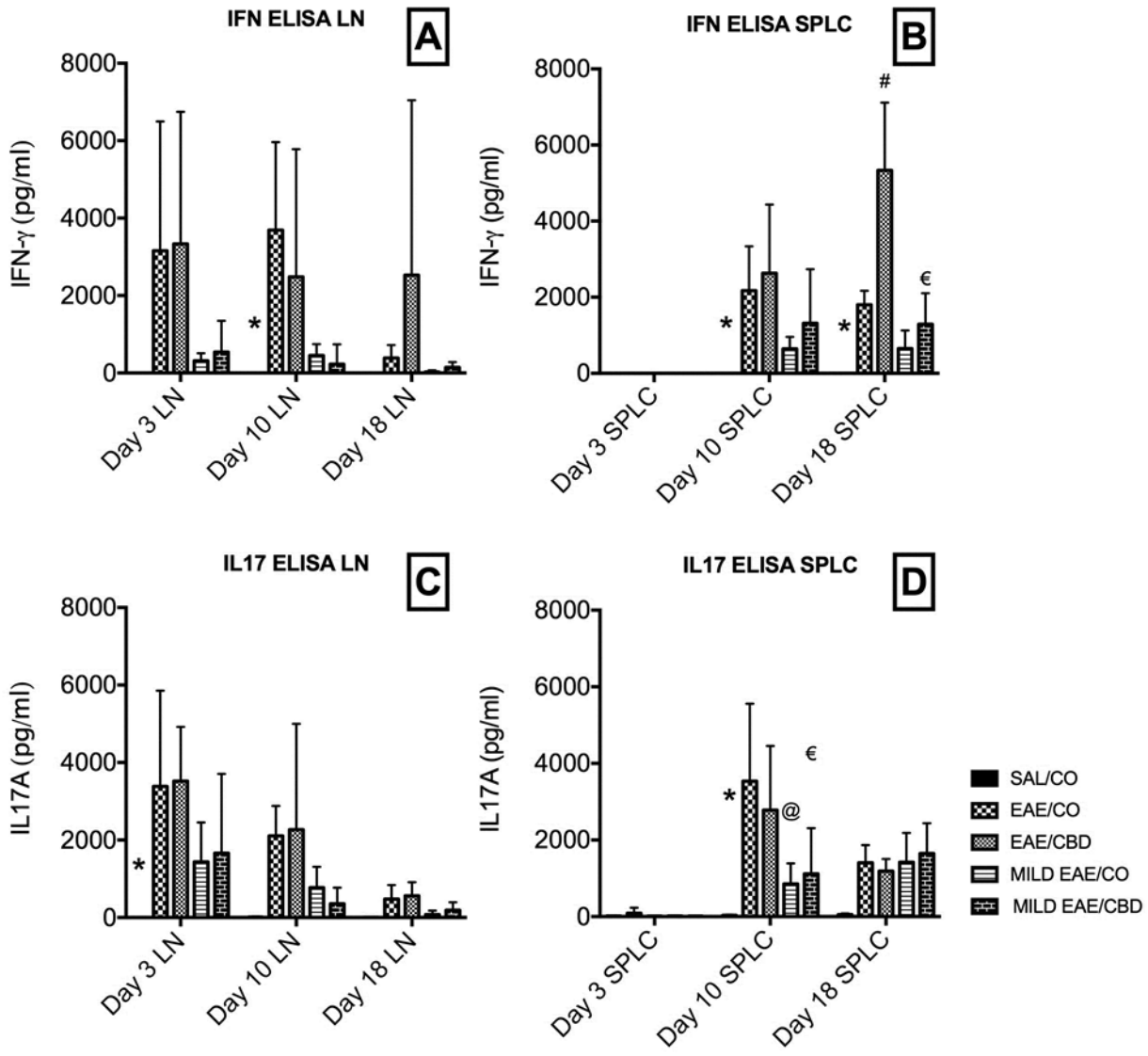

Figure 3.5 ELISA of cytokines after ex vivo restimulation

After 48 hr restimulation of lymphocytes from secondary lymphoid tissues with MOG_{35-55} peptide, the supernatants from these cultures were analyzed by ELISA for the total amount of IFN-γ (A & B) and IL-17A (C & D). n=5 for each group of mice (SAL/CO, EAE/CO, EAE/CBD, Mild EAE/CO, and Mild EAE/CBD) on each day. * $p < 0.05$ differences between SAL/CO and EAE/CO; # $p < 0.05$ difference between EAE/CO and EAE/CBD; @ $p < 0.05$ difference between EAE/CO and Mild EAE/CO; € $p < 0.05$ difference between EAE/CBD and Mild EAE/CBD.

3.1.4 Analysis of brain and spinal cord

3.1.4.1 Brain

H&E stains were performed on all mice to examine the level of cellular infiltration, and it was determined that cellular infiltrates were primarily observable at day 18. H&E stains of the brain from day 18 EAE/CO mice revealed cellular infiltrates throughout the white matter tracts of the brain, with the highest levels of infiltration being consistently seen in the white matter of the cerebellum. The infiltrating cells in the cerebellum of EAE/CO mice were evenly spread throughout the white matter tracts, and there was significant perivascular cuffing evident in these mice (Fig. 3.6B). Immunoperoxidase staining for CD3 also revealed that a significant number of the infiltrating cells within these sections were T cells (Fig. 6E and H). In contrast to this, the EAE/CBD group had fewer cellular infiltrates and T cells within the white matter tracts of the cerebellum as compared to the EAE/CO group, and the cells were localized primarily in the perivascular cuffs with CBD treatment (Fig. 6C, F, and I). No cellular infiltrates or T cells were observed in the SAL/CO group (Fig. 6A, D, and G).

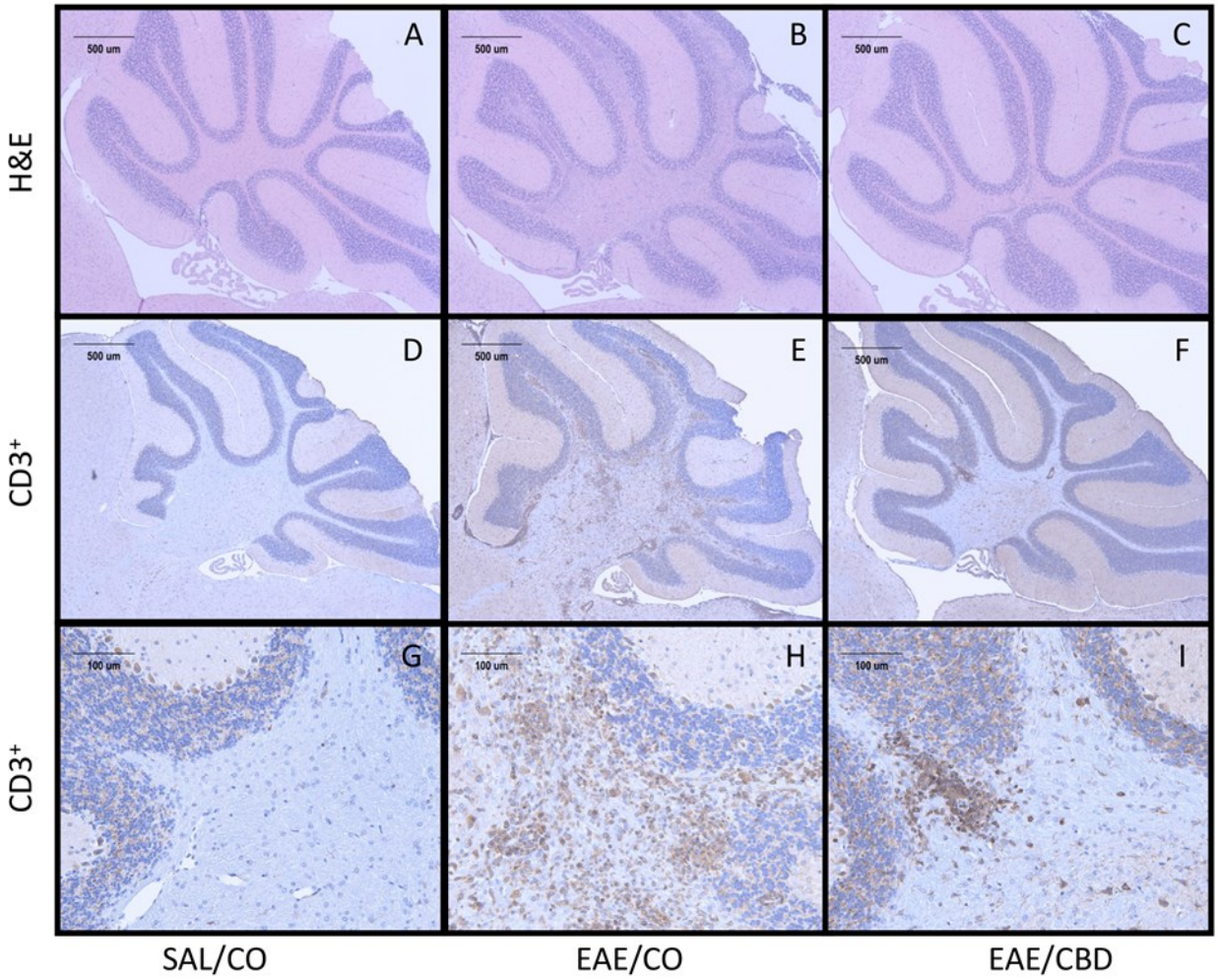

Figure 3.6 CBD reduces neuroinflammation in the cerebellum of EAE mice.

Brains from SAL/CO, EAE/CO and EAE/CBD mice on day 18 were embedded in paraffin wax blocks and 5µm longitudinal sections of the cerebellums were examined using H&E and CD3 stains. Images of H&E stains show increased cellular infiltration into the white matter tracts of the cerebellum in EAE/CO mice (n= 5) as compared to SAL/CO (n= 5) and EAE/CBD mice (n= 5) (A-C). Similarly, CD3 stains revealed a higher level of T cell infiltrates in the EAE/CO group as compared to the SAL/CO and EAE/CBD groups. CD3 stains are shown at 40x (D-F) and 200x (G-I) magnifications.

3.1.4.2 Spinal cord

H&E stains were performed on all mice to examine cellular infiltration, and it was determined that cellular infiltrates were present primarily at the day 18 time point. The most prominent feature observed in the H&E stains of lumbosacral spinal cord from day 18 EAE/CO mice was the presence of subpial and perivascular cellular infiltrates that were comprised largely of $CD3^+$ T cells (Fig. 7B, E, and H). Subpial and perivascular infiltration was also seen in the spinal cords of EAE/CBD mice, but to a lower extent (Fig. 7C, F, and I). Double staining of the spinal cord for $CD4^+$ and $CD8^+$ T cells (Figure 7 J-R) from each group showed similar patterns of infiltration compared to those seen with the CD3 stain. To maximize our ability to accurately analyze the T cell compartment, quantifications of $CD3^+$ cells were performed on the same lesions as the quantifications for $CD4^+$ and $CD8^+$ cells in the next consecutive slice taken from the paraffin blocks containing the spinal cords. No cellular infiltrates or T cells were observed in the SAL/CO group (Fig. 7A, D, G, J, M, and P). Spinal cord sections were also analyzed for lesion size using a GFAP/DAPI stain, which allowed for a more accurate measurement of lesion size within the parenchyma by eliminating the cells that were located in the meninges (Figure 8). As with the T cell stains, the GFAP/DAPI stain showed a large amount of subpial and perivascular infiltration, but this stain also highlights the boundary between meningitis and myelitis in these sections. An observation that was of particular note in all of the stains that were performed was a surprising lack of cellular infiltrates in the white matter of the nerve roots surrounding the lumbosacral spinal cord. Quantification and statistical analysis of the T cells and lesions of the spinal cords revealed a modest decrease in the number of T cells and size of the

lesions in the EAE/CBD group as compared to EAE/CO group at the day 18 time point (Figure 3.9 A-C). In contrast to this, staining of spinal cord sections from SAL/CO, EAE/CO, and EAE/CBD mice from day 10 and day 18 for Iba-1 showed that microglial activation was not affected by treatment with CBD in the day 18 mice (Figure 3.10). We also found that microglial activation was not elevated above basal levels at the day 10 time point (Figure 3.10D).

Analysis of spinal cord infiltrates by flow cytometry

Flow cytometry performed on cells isolated from the spinal cord of EAE/CO and EAE/CBD mice showed a modest reduction in the percentage of $CD3^+CD4^+$ T cells, which closely resembled the results found by histologic analysis of the spinal cord (Figure 3.9D). No difference was seen in the percentage of $CD3^+CD8^+$ or $CD3^+CD4^+CD8^+$ T cells. Further analysis of CD25 and FoxP3 expression by $CD4^+$ cells also revealed very small numbers of Tregs present within the spinal cords of both groups, and no significant difference was seen between groups (data not shown).

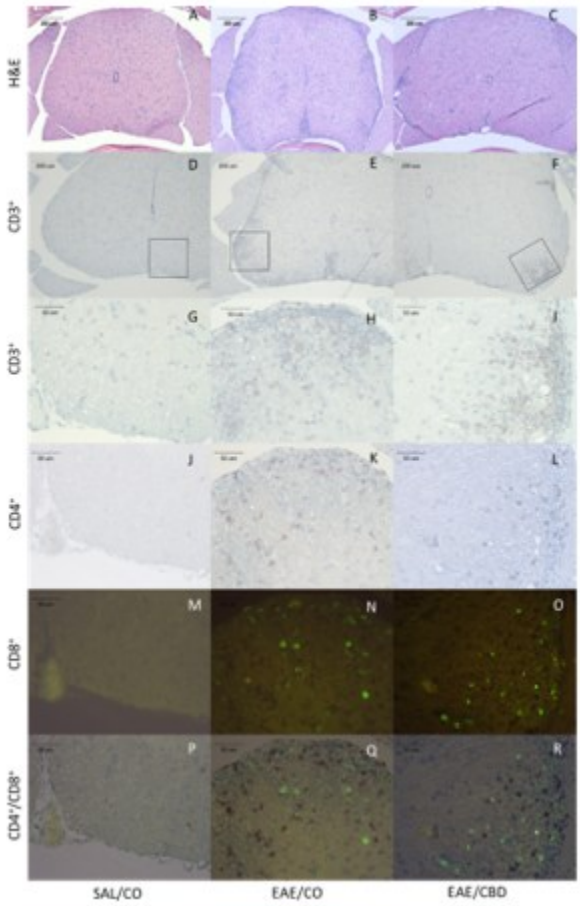

Figure 3.7 CBD reduces neuroinflammation in the spinal cord of EAE mice

Spinal columns from SAL/CO (n=5), EAE/CO (n=5) and EAE/CBD (n=5) mice on day 18 were embedded in paraffin wax blocks and 5μm sections were examined using H&E, CD3, CD4, and CD8 stains. Images of H&E stains showed increased cellular infiltration around large blood vessels and in peripheral white matter tracts of the spinal cords of EAE/CO mice as compared to SAL/CO and EAE/CBD mice (A-C). Similarly, CD3 stains revealed a higher number of T cell in these regions in the EAE/CO group as compared to the SAL/CO and EAE/CBD groups. CD3 stains are shown at 10x (D-F) and 40x (G-I) magnifications. CD4 and CD8 double staining was performed on the next slice taken from the paraffin blocks containing the spinal cords, thus allowing for intralesional comparisons to be made between the number of CD3, CD4, and CD8 positive cells. CD4 staining (J-L) revealed moderately lower numbers of $CD4^+$ T cells present within the lesions of the spinal cords, while CD8 staining (M-O) revealed no substantial difference between the number of $CD8^+$ T cells when comparing the EAE/CO and EAE/CBD groups. To overcome the dark background of the CD8 immunofluorescent stain in the combined CD4/CD8 images (P-R) the contrast of the original CD4 stains (J-L) was enhanced by 0.2% using ImageJ software.

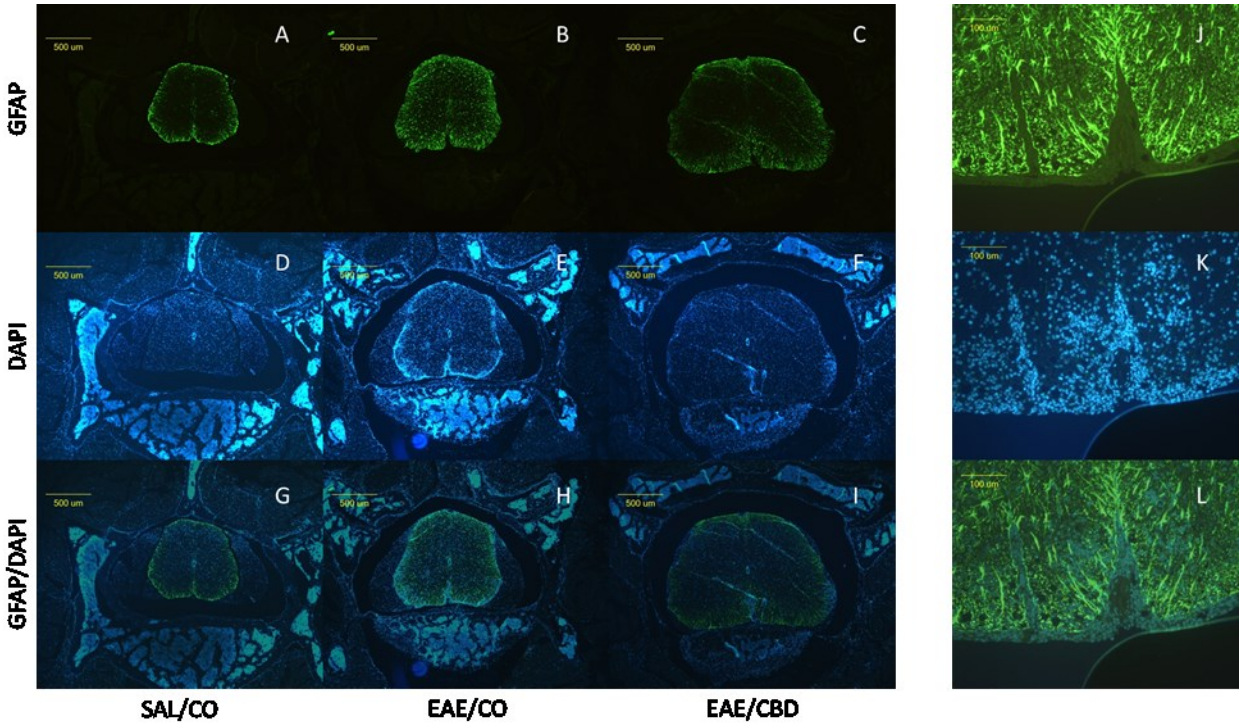

Figure 3.8 Measuring lesion size within the parenchyma of the spinal cord

From the same paraffin wax blocks that were used for T cell staining, 5µm sections of spinal columns from SAL/CO (n=5), EAE/CO (n=5) and EAE/CBD mice (n=5) on day 18 were stained for expression of GFAP to highlight astrocytes. By using an immunofluorescent GFAP Stain (A-C & J) to define the boundary of the spinal cord parenchyma created by the glial limitans, and a DAPI nuclear stain (D-F & K) to identify lesions within the spinal cord, we were able to accurately determine total lesion area within the parenchyma of spinal cord sections by overlaying images of the two stains and removing cells within the meninges from consideration. Images were taken at 40x magnification (A-I) and 200x magnification (J-L). Images J-L show the accumulation of cells outside of the glial limitans around major vessels and help to illustrate the difference between meningitis and myelitis.

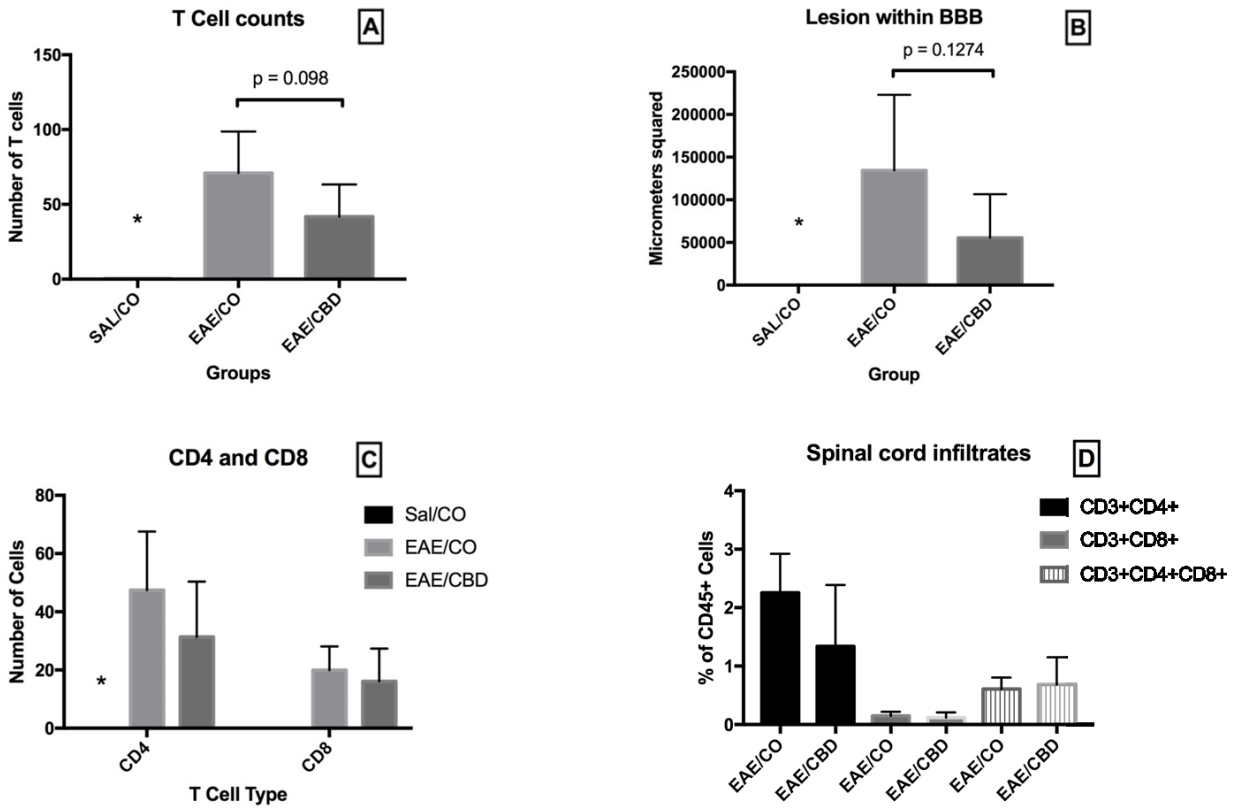

Figure 3.9 Quantification of T cells and lesion area within the spinal cord

A total of 4 lesions from the lumbosacral intumescence were analyzed for the number and type of T cells present, as well as lesion size. CD3 (A) and CD4/CD8 double staining (C) were done on consecutive slices from the paraffin blocks, which allowed for intralesional comparisons to be made for the T cell counts. Quantification of T cells was performed by counting the number of cells present within an image captured at 400x magnification for each of the four lesions, and averaging the counts for each mouse. Lesion area within the parenchyma of the spinal cord (B) was measured first outlining the area of the lesion seen in the DAPI image, then overlaying the GFAP image and adjusting the outline so that only cells within the parenchyma were considered (Figure 8). Analysis of spinal cord infiltrates by flow cytometry also revealed a moderate increase in the percentage of $CD3^{+}CD4^{+}$ T cells within the spinal cord (D). * $p < 0.05$ differences between SAL/CO and EAE/CO

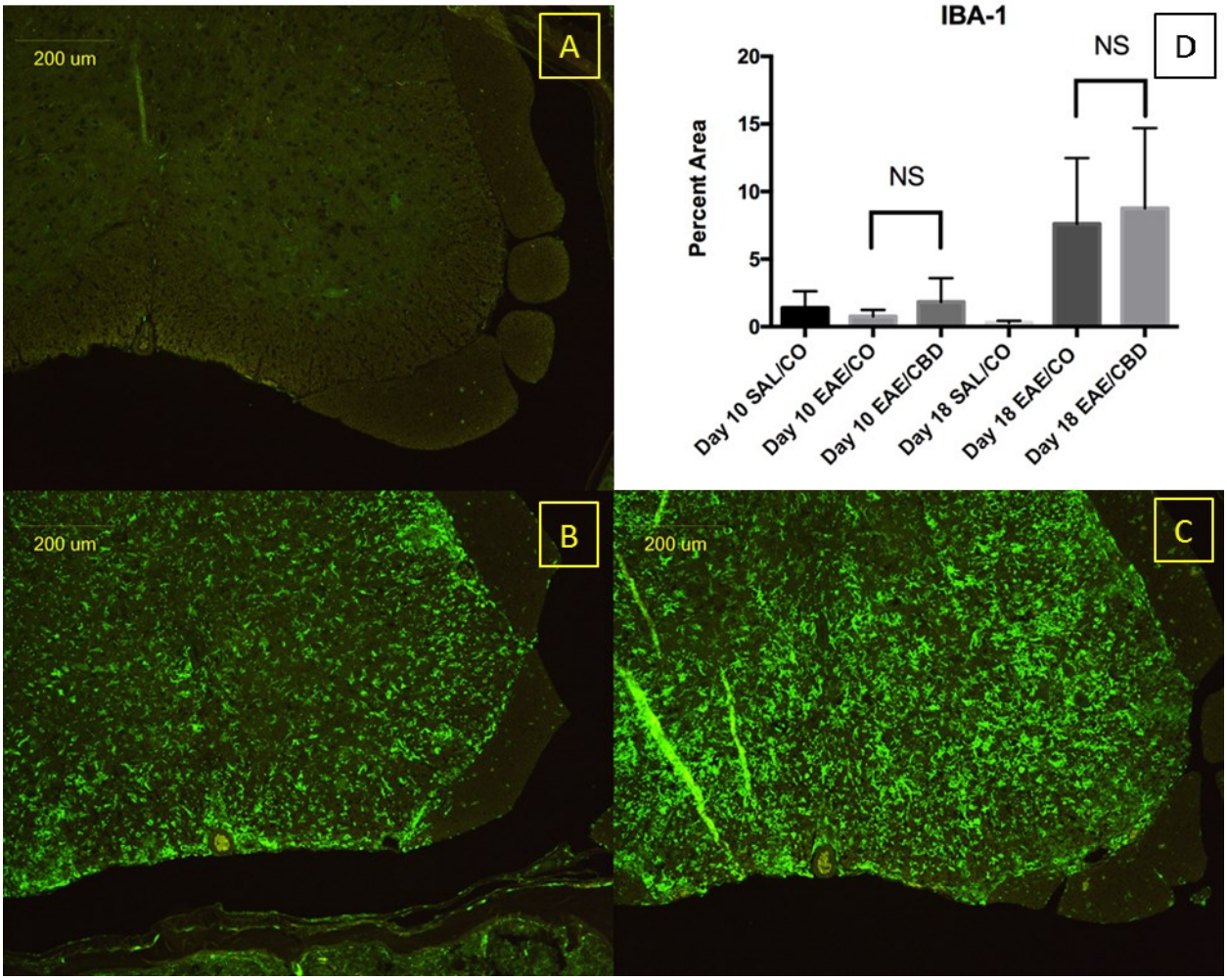

Figure 3.10 The effects of CBD on microglial activation in the EAE model

5µm sections of spinal cords from SAL/CO (n=5) (A), EAE/CO (n=5) (B) and EAE/CBD (n=5) (C) mice from days 10 and 18 were stained for the presence of Iba-1 in activated microglia. Representative images of day 18 spinal cords from each group are depicted. For each mouse two spinal cord sections were selected from the lumbosacral region of the spinal cord, and the area of each section covered by activated microglia was quantified as a percentage of the total area of the parenchyma. The two sections were then combined to get an average percentage for each mouse and statistical analysis was performed on each group (D).

3.2 Exploring *S. aureus* SAgs as immunosuppressive agents

3.2.1 The effects of *S. aureus* SAgs on murine regulatory cells.

Despite multiple attempts under various conditions, we were unable to induce FoxP3 in mouse Tregs using the *S. aureus* SAgs *in vitro* outlined in Table 3.1. However, when we measured the effects of the superantigens on MDSCs we found that under several conditions MDSCs were significantly increased by the SAgs, with granulocytic MDSCs being the most consistently increased (Table 3.2). Unfortunately, many of the SAgs varied greatly in their ability to induce this suppressor cell type as well. In later studies it was determined that despite the lack of FoxP3 induction in T cells, or consistent induction of MDSCs, splenocytes cultured with *S. aureus* SAgs were immunosuppressive through an unknown soluble factor within the supernatants of these cultures. This work is being continued by others in our lab to determine the immunosuppressive ability of these supernatants the EAE model.

Table 3.1 Stimulation of Tregs by *S. aureus* SAgs

Conditions	Duration	SAgs	Notes	Effect
6 well plate; 10E6 cells in 4mls of media; TGF-β added at 24hrs and 72hrs	4 Days	SEC (50ng/well)	Single wells were done for each condition. Statistical analysis was not done.	No increase in Treg percentages was seen with the addition of SEC
6 well plate; 10E6 cells in 4mls of media; TGF-β (20ng/well) and IL2 (7.5ng/well) added at 24hrs and 72hrs	4 Days	SEC (50ng/well)	Single wells were done for each condition. Statistical analysis was not done.	Treg percentages generally appeared to be lower with the addition of SEC
6 well plate; 13E6 cells in 4mls of media; TGF-β (20ng/well) and IL2 (20ng/well) added at 24hrs and 72hrs	4 Days	SEC (50ng/well)	FoxP3/GFP mice were used for this study. Single wells were done for each condition. Statistical analysis was not done.	Treg percentages appeared to be slightly higher with the addition of SEC; however SEC did not have much affect when TGF-β and IL2 were added
6 well plate; 9E6 cells in 4mls of media; TGF-β (20ng/well) and IL2 (20ng/well) added at 24hrs and 72hrs	4 Days	SEC (50ng/well)	FoxP3/GFP mice were used for this study. Single wells were done for each condition. Statistical analysis was not done. This was a repeat of the previous study.	Treg percentages appeared to be slightly higher with the addition of SEC; however SEC did not have much affect when TGF-β and IL2 were added

This table lists the culture conditions, duration of culture, SAg used, special notes, and significant effects noted for each condition tested during our experiments on stimulating Tregs with *S. aureus* superantigens.

Table 3.1 (continued)

Conditions	Duration	SAgs	Notes	Effect
6 well plate; 10E6 cells in 4mls of media; anti-TGF-β (4μg/well) and anti-IL2 (4μg/well) added at 24hrs and 72hrs	4 Days	SEC (50ng/well)	FoxP3/GFP mice were used for this study. Single wells were done for each condition. Statistical analysis was not done.	Treg percentages appeared to be slightly higher with the addition of SEC; and Treg percentages were reduced by anti-IL2 and anti-TGF-β both with and without SEC
6 well plate; 10E6 cells in 4mls of media; anti-TGF-β (4μg/well) and anti-IL2 (4μg/well) added at 24hrs and 72hrs	4 Days	SEC (50ng/well)	FoxP3/GFP mice were used for this study. Single wells were done for each condition. Statistical analysis was not done. This was a repeat of the previous study.	Treg percentages appeared to be slightly higher with the addition of SEC; and Treg percentages were reduced by anti-IL2 and anti-TGF-β both with and without SEC
6 well plate; 10E6 splenocytes in 4mls of media +/- 2.5E6 purified dendritic cells	4 Days	SEC (50ng/well)	Single wells were done for each condition. Statistical analysis was not done.	Adding dendritic cells did not enhance the effects of SEC on Treg percentages. SEC had slightly lower percentages of Tregs

This table lists the culture conditions, duration of culture, SAg used, special notes, and significant effects noted for each condition tested during our experiments on stimulating Tregs with *S. aureus* superantigens.

Table 3.1 (continued)

Conditions	Duration	SAgs	Notes	Effect
96 well plate; 2E6 splenocytes in 0.2mls of media +/- 1E6 purified dendritic cells or 1E6 splenocytes in 0.2mls of media + 1E6 purified dendritic cells	4 Days	SEC (2.5ng/well)	FoxP3/GFP mice were used for splenocytes, but WT mice were used to obtain dendritic cells.	SEC significantly reduced Treg percentages in 2E6 splenocytes with 1E6 dendritic cells
96 well plate; 1E6 splenocytes in 0.2mls of media + 1E6 cells bone marrow cells	5 Days	SEC (5ng/ml), SEG (5ng/ml), SEI (5ng/ml), SEM (5ng/ml), SEN (5ng/ml), SEO (5ng/ml), TSST (5ng/ml),		SEM and SEN significantly reduced the percentage of Tregs
6 well plate; 10E6 splenocytes or 5E6 splenocytes + 5E6 bone marrow cells in 4mls of media	5 Days	SEC (5ng/ml), TSST (5ng/ml)	Single wells were done for each condition. Statistical analysis was not done.	SEC did not appear to effect Treg percentages

This table lists the culture conditions, duration of culture, SAg used, special notes, and significant effects noted for each condition tested during our experiments on stimulating Tregs with *S. aureus* superantigens.

Table 3.2 Stimulation of MDSCs by *S. aureus* SAgs

Conditions	Duration	SAgs	Notes	Effects
96 well plate; 2E6 splenocytes in 0.2mls of media	1 & 2 Days	SEC (5ng/ml), SEG (5ng/ml), SEI (5ng/ml), SEM (5ng/ml), SEN (5ng/ml), SEO (5ng/ml), TSST (5ng/ml),	Since splenocytes were used, very low numbers of $CD11b^+$ cells were recovered	Day 1: SEG and SEM significantly decreased Granulocytic MDSCs
96 well plate; 2E6 splenocytes in 0.2mls of media	2 & 3 Days	SEC (5ng/ml), SEG (5ng/ml), SEI (5ng/ml), SEM (5ng/ml), SEN (5ng/ml), SEO (5ng/ml), TSST (5ng/ml),	Since splenocytes were used, very low numbers of $CD11b^+$ cells were recovered.	Day 2: SEG and SEM significantly increased the percentage of Granulocytic MDSCs Day 3: SEG, SEM, SEN and TSST significantly increased the percentage of Granulocytic MDSCS

This table lists the culture conditions, duration of culture, SAg used, special notes, and significant effects noted for each condition tested during our experiments on stimulating MDSCs with *S. aureus* superantigens

Table 3.2 (continued)

Conditions	Duration	SAgs	Notes	Effects
96 well plate; 2E6 splenocytes in 0.2mls of media	3 Day	SEC (5ng/ml), SEG (5ng/ml), SEI (5ng/ml), SEM (5ng/ml), SEN (5ng/ml), SEO (5ng/ml), TSST (5ng/ml),	Since splenocytes were used, very low numbers of $CD11b^+$ cells were recovered.	No significance found
96 well plate; 2E6 splenocytes in 0.2mls of media	3 Days	SEC (5ng/ml), SEG (5ng/ml), SEI (5ng/ml), SEM (5ng/ml), SEN (5ng/ml), SEO (5ng/ml), TSST (5ng/ml),	Since splenocytes were used, very low numbers of $CD11b^+$ cells were recovered.	SEG, SEI, SEM, SEN, TSST significantly increased the percentage of Monocytic and Granulocytic MDSCs

This table lists the culture conditions, duration of culture, SAg used, special notes, and significant effects noted for each condition tested during our experiments on stimulating MDSCs with *S. aureus* superantigens.

Table 3.2 (continued)

Conditions	Duration	SAgs	Notes	Effects
96 well plate; 1E6 splenocytes in 0.2mls of media +/- 1E6 cells bone marrow cells	5 Days	SEC (5ng/ml), SEG (5ng/ml), SEI (5ng/ml), SEM (5ng/ml), SEN (5ng/ml), SEO (5ng/ml), TSST (5ng/ml),	Use of bone marrow greatly increased the number of MDSCs recovered from cultures.	SEM, SEN and TSST significantly decreased Monocytic MDSCs, but SEI, SEM, SEN, and TSST significantly increased the Granulocytic MDSCs
6 well plate; 10E6 splenocytes or 5E6 splenocytes + 5E6 bone marrow cells in 4mls of media	5 Days	SEC (5ng/ml), TSST (5ng/ml)	Single wells were done for each condition. Statistical analysis was not done.	Although statistical analysis was not done SEC did not appear to effect MDSC percentages; TSST reduced the percentage of Granulocytic MDSCs

This table lists the culture conditions, duration of culture, SAg used, special notes, and significant effects noted for each condition tested during our experiments on stimulating MDSCs with *S. aureus* superantigens.

3.3 *Cnr1*$^{-/-}$ vs WT EAE

3.3.1 Clinical scores

By analyzing average AUC for each group of mice we found that *Cnr1*$^{-/-}$ mice with EAE (n=12) had significantly higher levels of disease over the 18 day time course as compared to their WT littermates (n= 14)(Figure 3.11A). Saline treated mice*Cnr1*$^{-/-}$ (n=13) and WT (n=13) mice had no clinical disease. Figure 3.11B shows the progression of clinical disease during the 18 day time course.

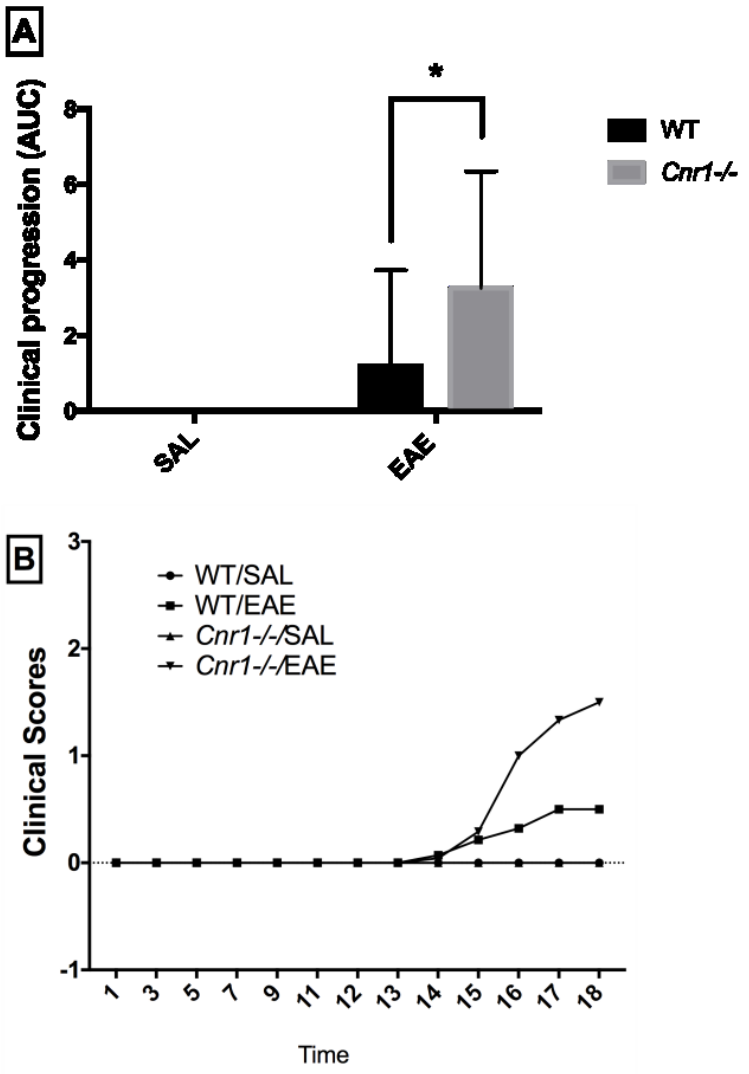

Figure 3.11 Differences in clinical EAE between *Cnr1*$^{-/-}$ and WT littermates

Clinical scores for WT/SAL (n=13), WT/EAE (n= 14) *Cnr1*$^{-/-}$/SAL (n=13) and *Cnr1*$^{-/-}$/EAE (n=12) mice were recorded over the 18 day time course of disease. Average area under the curve (AUC) was then calculated for each experimental group (A). The clinical scores were also graphed over time to show clinical progression for each group (B). Analysis of the average area under the curve for disease progression of each group showed a statistically significant difference between the *Cnr1*$^{-/-}$ /EAE mice and WT mice. * $p<0.05$

3.3.2 Histologic scoring

The histologic scores obtained from our new scoring process were totaled and analyzed for each section of spinal cord, and this analysis revealed that *Cnr1*$^{-/-}$ mice with EAE had significantly higher levels of cellular infiltration as compared to their WT littermates in sections 2-4, while the 1st and 5th spinal cord section showed only a modest difference between these two groups (Figure 3.12A). No infiltration was seen in any of the saline mice examined. To verify the validity of this new scoring system, the correlation between total histologic score and clinical score on day 18 was analyzed (Figure 3.12B). Total lesion area was also tabulated for each mouse over the 5 sections, and then correlated to the clinical score to determine if lesion area would be a more representative measurement than our histologic scoring system (Figure 3.12C). When section scores were totaled for each mouse and compared to clinical score at the day 18 time point, the histologic scores showed a high level of correlation to clinical scores ($r^2 = 0.7171$) (Figure 3.12B). A similar level of correlation was found between the total lesion area and clinical score for each mouse ($r^2 = 0.7563$) (Figure 3.12C).

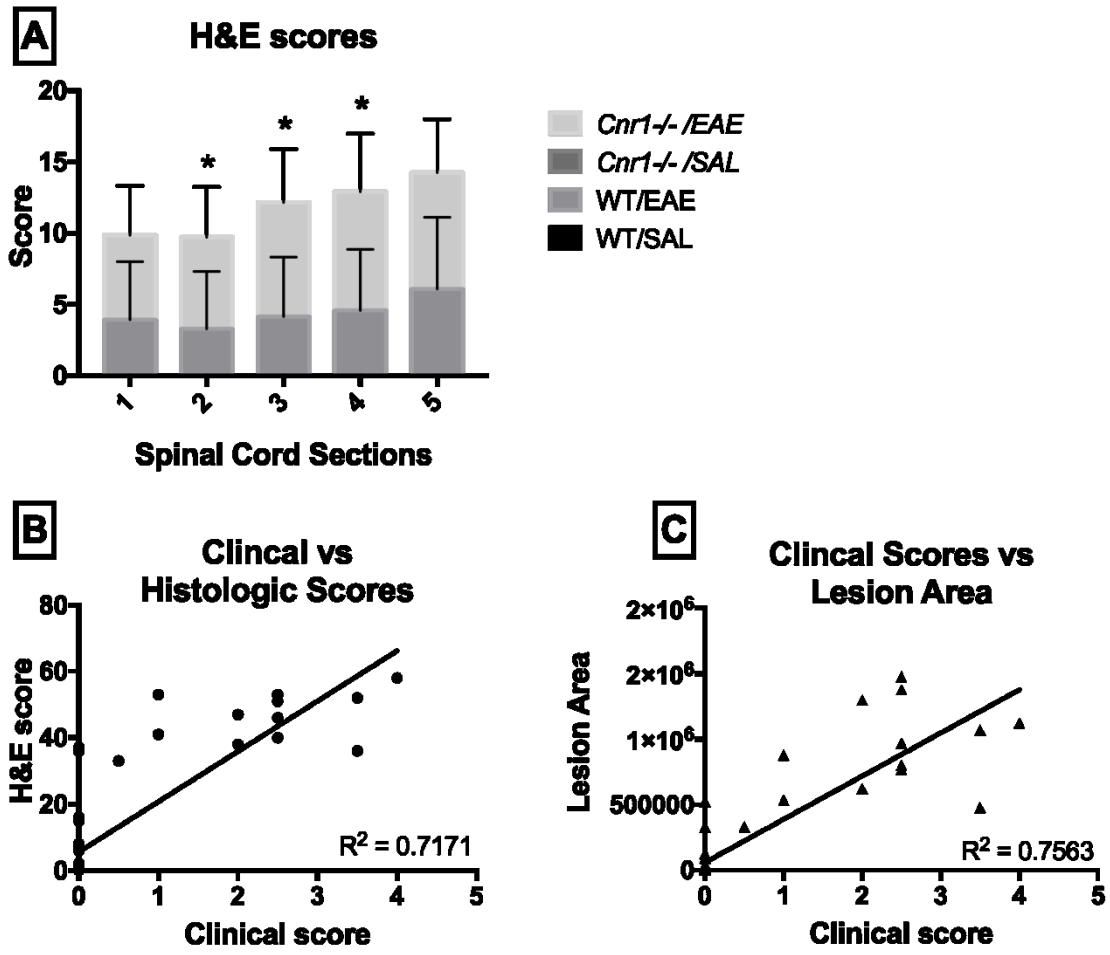

Figure 3.12 Histologic scoring

Using the histologic scoring system outlined above, histologic scores for WT/SAL (n=13), WT/EAE (n= 14) *Cnr1*$^{-/-}$/SAL (n=13) and *Cnr1*$^{-/-}$/EAE (n=12) mice were obtained and analyzed by section (A). To validate this method of scoring, the clinical scores were also correlated to the clinical scores for each mouse (B). Lesion area for each mouse was also tabulated by finding the lesion area for each of the 5 spinal cord sections and adding them together, and then this area was correlated to the clinical score for each mouse to determine if lesion area was more representative of clinical disease (C). * $p<0.05$

3.3.3 ELISAs

MOG_{35-55} ex vivo restimulation

Analysis of IFN-γ and IL-17A in serum taken on day 18 and supernatants from *ex vivo* restimulated splenocytes showed that production of IFN-γ was significantly higher in restimulated cells from *Cnr1*$^{-/-}$/EAE mice as compared to WT/EAE mice (Figure 3.13A). However, no difference was seen with serum IFN-γ, serum IL-17A, or supernatant IL-17A (Figure 3.13B-D).

Anti-CD3/anti-CD28 and SEM in vitro stimulation

To further investigate the T cell IFN-γ response of the *Cnr1*$^{-/-}$ mice, naïve splenocytes were cultured for 2 or 3 days in the presence of anti-CD3/anti-CD28 antibodies or SEM, and IFN-γ was measured in the supernatants of these cultures by ELISA. For both male and female mice, the IFN-γ response in WT splenocytes stimulated with anti-CD3/anti-CD8 antibodies was significantly higher than that from *Cnr1*$^{-/-}$ mice at two different concentrations. Interestingly, while SEM treated splenocytes showed a similar trend to the anti-CD3/anti-CD28 treated splenocytes, the differences observed between WT and *Cnr1*$^{-/-}$ mice did not reach the same level of significance seen with anti-CD3/anti-CD28 stimulation (Figure 3.14 A-D).

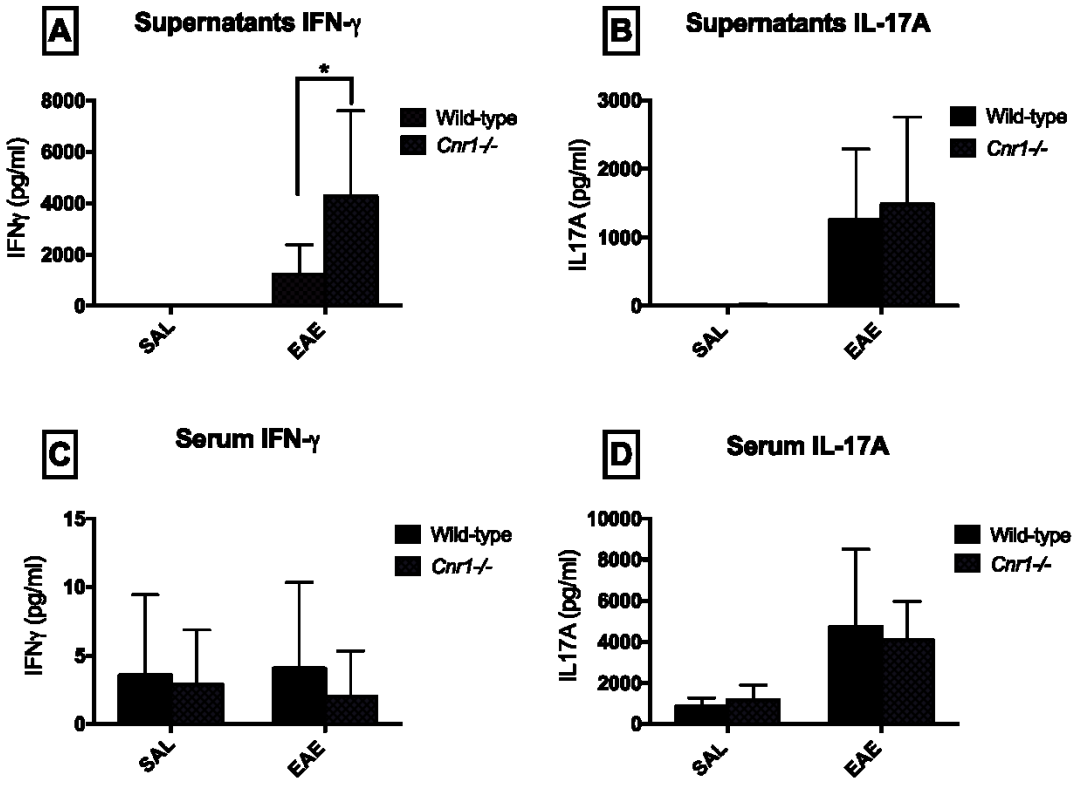

Figure 3.13 IFN-γ and IL-17A in serum and MOG_{35-55} restimulation cultures

Splenocytes were harvested from WT/SAL (n=13), WT/EAE (n= 14) *Cnr1*$^{-/-}$/SAL (n=13) and *Cnr1*$^{-/-}$/EAE (n=12) mice and restimulated with MOG_{35-55} peptide for 3 days. The supernatants from these cultures were then tested by ELISA for concentrations of IFN-γ (A) and IL-17A (B). Serum was also taken from each mouse at time of necropsy and tested by ELISA for concentrations of IFN-γ (C) and IL-17A (D). * $p<0.05$

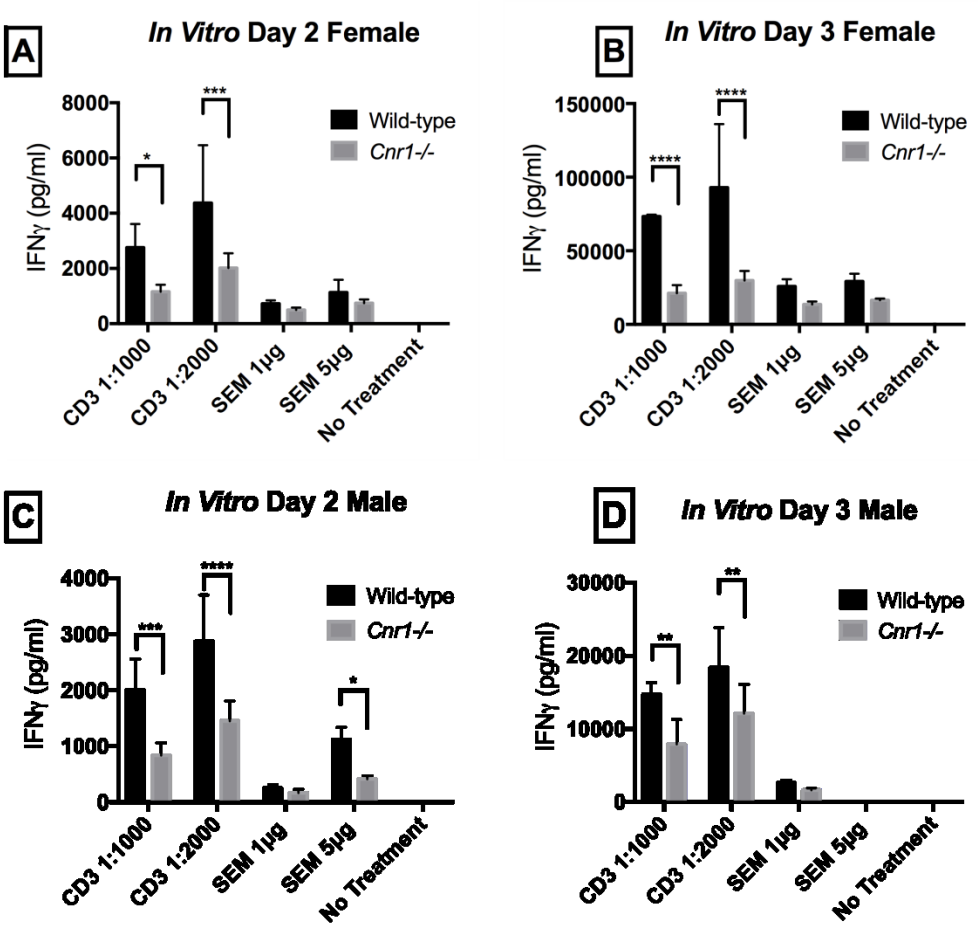

Figure 3.14 Anti-CD3/anti-CD28 and SEM stimulation of T cells

Splenocytes were harvested from female and male WT and *Cnr1*$^{-/-}$ mice and stimulated with either anti-CD3/anti-CD28 antibodies or SEM SAg for 2-3 days before IFN-γ concentration within the supernatants were analyzed by ELISA (A-D). These experiments were performed in duplicate for both female and male mice.* $p<0.05$, **$p<0.01$, ***$p<0.001$, **** $p<0.0001$

3.3.4 Flow cytometry

MOG_{35-55} ex vivo restimulation

Analysis of the percentage of IFN-γ producing cells within the *ex vivo* restimulated splenocytes from EAE mice by flow cytometry revealed no significant differences between the *Cnr1*$^{-/-}$ mice and WT littermates. However, it did show the primary source of IFN-γ to be a $CD3^{-}CD4^{-}CD8^{-}$ cell population (Figure 3.15).

Anti-CD3/anti-CD28 and SEM in vitro stimulation

Analysis of the percentage IFN-γ producing cells within the *in vitro* stimulated splenocytes by flow cytometry revealed a significantly higher percentage of $CD8^{+}IFN\text{-}\gamma^{+}$ T cells in the anti-CD3/anti-CD28 stimulated WT cells as compared to the *Cnr1*$^{-/-}$ cells. Unlike the *ex vivo* restimulation, the $CD3^{+}$ population plays a large role in IFN-γ production (Figure 3.16).

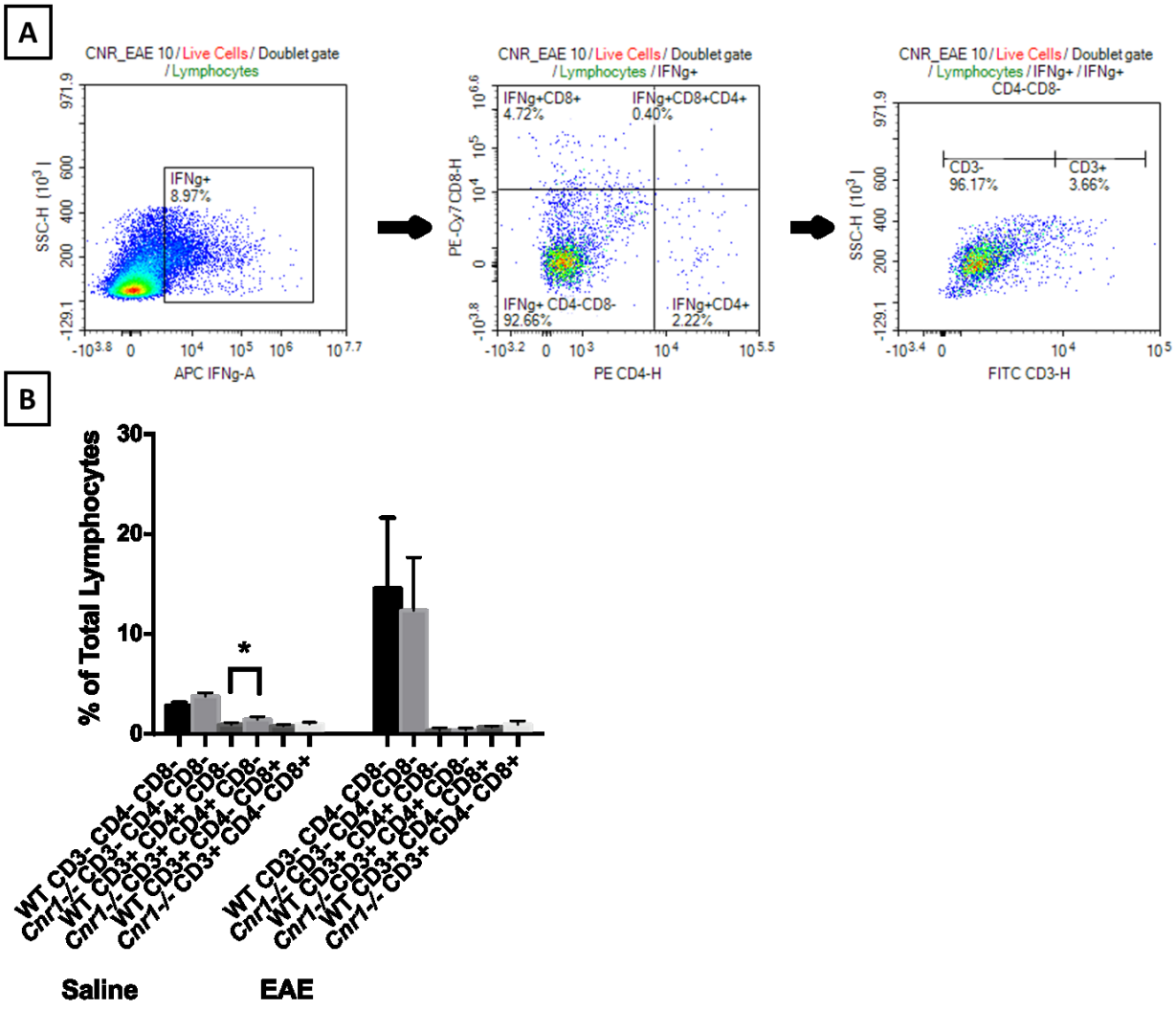

Figure 3.15 Analysis of IFN-γ production in MOG_{35-55} restimulated splenocytes by flow cytometry

For one round of EAE IFN-γ production was analyzed in the ex vivo MOG_{35-55} restimulated splenocytes of WT/SAL (n=5), WT/EAE (n= 6) *Cnr1*$^{-/-}$/SAL (n=5) and *Cnr1*$^{-/-}$ /EAE (n=5) mice by flow cytometry, and IFN-γ producing cells were subdivided based on their CD4, CD8 and CD3 expression (A). Analysis of various cell types revealed no significant differences between *Cnr1*$^{-/-}$ /EAE and WT/EAE mice. A significantly higher percentage of $CD3^+CD4^+CD8^-$ cells was seen in *Cnr1*$^{-/-}$ /Saline mice as compared to WT/Saline mice. Additionally, in these experiments $CD3^-$ cells appear to be the predominant source of IFN-γ (B). * $p<0.05$

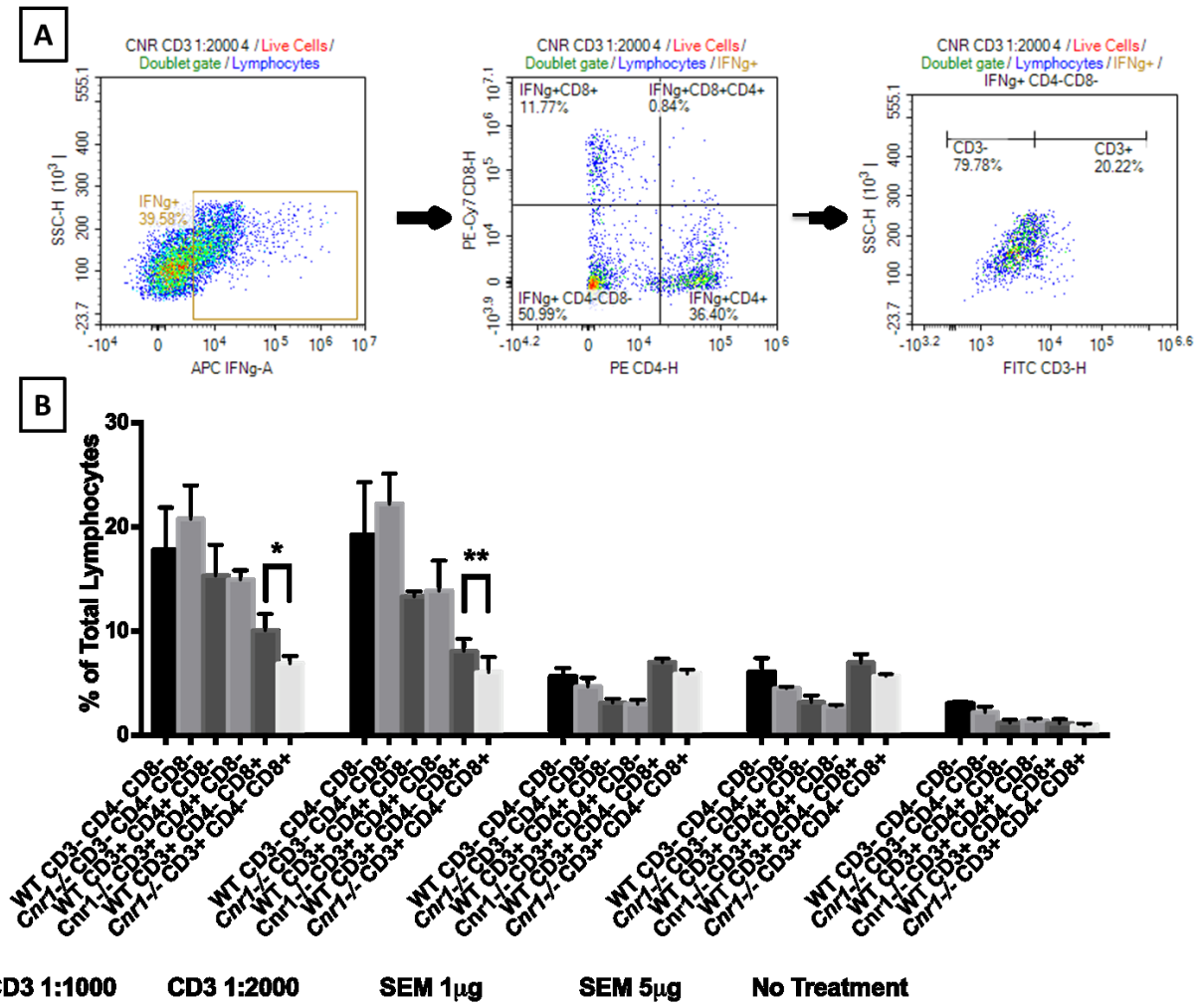

Figure 3.16 Analysis of IFN-γ production in anti-CD3/anti-CD28 and SEM stimulated splenocytes by flow cytometry

IFN-γ production was analyzed in the anti-CD3/anti-CD28 antibody or SEM stimulated splenocytes from female and male *Cnr1*$^{-/-}$ and WT mice by flow cytometry, and IFN-γ producing cells were subdivided based on their CD4, CD8 and CD3 expression (A). Analysis of various cell types revealed a significantly lower percentage of CD3^{+}CD4^{-} CD8^{+}IFN-γ^{+} cells in *Cnr1*$^{-/-}$ as compared to WT mice when splenocytes were stimulated with anti-CD3/anti-CD28 antibodies. Additionally, in these experiments CD3^{+} cells appear to be the predominant source of IFN-γ. The graph in this figure represents one of the female 3 day stimulations of the *in vitro* experiments for comparison to the *ex vivo* 3 day restimulation of the female EAE mice in figure 3.14 (B). * $p<0.05$, ** $p<0.01$

CHAPTER IV

DISCUSSION

The primary treatment for MS revolves around a two-step approach that first uses immunosuppressive drugs, such as corticosteroids, to reduce the severity of disease, and then uses immunomodulatory drugs, such as glatiramer acetate and IFN-β, to reduce the occurrence of relapses. While this method does help patients that are in the relapsing and remitting stage of disease, it does very little to stop the long term progressive stages of MS [1-3]. For this reason the search for more viable therapies is still underway, and the main focus of the research done in this dissertation has been dedicated to exploring potential therapeutics, such as CBD and *S. aureus* induced regulatory cells, and potential therapeutic targets, such as the CB_1 receptor. Unfortunately, no conclusive evidence has been collected for the use of SAgs as a therapeutic agent in MS, and as we previously mentioned we had some difficulty producing a consistent response from the suppressor cell populations while using various Sags. Therefore, the main focus of this discussion will revolve around our experiments with CBD and *Cnr1*$^{-/-}$ mice in the EAE model.

4.1 CBD in the EAE model

Recently, CBD has shown promise as a treatment for MS through its use in the EAE model and the use of Sativex in MS patients; however the number of studies

looking at CBD in the EAE model is limited, and none have examined CBD alone in MS. One study using the MOG_{35-55} peptide to induce EAE has shown that when CBD was administered i.p. for 3 days after the first signs of disease it was capable of reducing microglial activation and T cell infiltration in the CNS [5]. Similarly, a study looking at the i.p. administration of CBD in the Theiler's murine encephalomyelitis virus (TMEV) model of MS highlighted CBD's ability to reduce the expression of vascular cell-adhesion molecule-1 (VCAM-1) on vascular endothelial cells, suppress the production of chemokines and cytokines, and reduce the activation of microglia [4]. While these studies provide vital information about the effects of CBD on neuroinflammatory components of the MS models, they did not evaluate the systemic immune response associated with the CBD treatment. Furthermore, the i.p. route of administration is used less often in a clinical setting as compared to oral administration or inhalation.

For these reasons, in our CBD study we sought to examine the response of EAE to oral CBD by exploring the systemic immune system in addition to the neuroinflammatory component of the model. By administering CBD for 5 days after the initiation of disease, we provide evidence that early treatment of EAE with CBD reduced clinical disease in EAE mice, which was accompanied by a modest reduction in neuroinflammation. As part of our exploration into the effects of oral CBD on EAE we chose to examine several suppressor cell types that could potentially contribute to CBD's immunosuppressive properties. Tregs and MDSCs represent two distinct linages of suppressor cells that may have a role in the pathogenesis of MS. Tregs are of particular interest because several studies have suggested that Treg function is decreased in MS patients, leading some to speculate that dysregulation of Tregs may

lead to the CNS based autoimmunity seen in MS [29-31]. On the other hand, MDSCs have been reported to be increased in the peripheral blood of MS patients and both the secondary lymphoid tissues and CNS lesions of EAE mice [33, 64, 65].

In previous studies, CBD has been shown to be capable of inducing both Tregs and MDSCs; however, in our CBD study analysis by flow cytometry showed CBD had no effect on the percentage of either suppressor cell population in the secondary lymphoid organs, or on the percentage of Tregs present in the spinal cord. One possible explanation for the discrepancy between previous MDSC studies and the results reported here is that the previous studies used i.p. injection for CBD, while we used oral gavage to administer CBD. This is supported by results from Hegde et al. which suggest that the induction of MDSCs seen after the i.p. injection of CBD is dependent on the production of G-CSF by peritoneal mast cells [66]. Additionally, i.p. injection limits CBD modification by the metabolic enzymes of the liver, which could cause differential effects as compared to oral administration of CBD. In an earlier paper, Hegde et al. also showed that i.p. administration of CBD was capable of modest induction of Tregs in conjunction with increased MDSC in an autoimmune hepatitis model [67]. These results were more recently supported by our own *in vitro* study showing CBD's ability to induce Tregs at low level T cell stimulation [68]. In the EAE model, i.p. injections of CBD have been shown to decrease clinical severity, which correlated to an increase number of MDSCs in the peritoneal cavity. The MDSCs were placed in culture with MOG restimulated splenocytes or adoptively transferred into EAE mice the MDSCs were capable of suppressing T cell proliferation and disease respectively [69]. These results suggest that induction of suppressor cells by CBD may be an important mechanism in

CBD's ability to suppress neuroinflammation. However, despite the lack of significant enhancement of either of the suppressor cell populations in the spleen in the current study, CBD was still an effective treatment in the EAE model. This suggests that CBD may have differential effects on the immune response depending on the route of administration.

In addition to examining the suppressor cell populations, *ex vivo* restimulation of cellular isolates from the spleen and lymph nodes of each mouse with MOG_{35-55} peptide allowed us to examine the effects of oral CBD on four separate MOG-specific inflammatory T cell populations at three separate time points: $CD4^+IFN\text{-}\gamma^+$ (Th1 cells), $CD4^+IL\text{-}17A^+$ (Th17 cells), $CD8^+IFN\text{-}\gamma^+$ (Tc1 cells), and $CD8^+IL\text{-}17A^+$ (Tc17 cells). Analysis of these T cell populations by flow cytometry after restimulation revealed a significant decrease in the percentage of MOG-specific Tc1 cells by CBD in EAE on day 10. This decrease in the percentage of Tc1 cells within the spleen corresponded to a reduction in clinical disease and neuroinflammation at the day 18 time point. In previous studies IFN-γ production was shown to be reduced *in vitro* and *in vivo* with CBD treatment, and very recently this relationship has been shown in the CNS of EAE mice treated with i.p. CBD, although no work was done to identify the source of the IFN-γ within the CNS [42, 70, 71]. Here we have shown that CBD suppresses the peripheral Tc1 population and is capable of reducing clinical disease in the EAE model even when administered before the clinical signs or neuroinflammation are present. This correlation suggests that CBD could be effective in reducing the pathogenesis of MS, since $CD8^+$ T cells have been shown to be one of the predominant cell types in the CNS lesions of MS patients [23]. Furthermore, $CD8^+$ T cells have been shown to be capable of initiating

EAE, which might explain why inhibition of the Tc1 cells has such a profound effect on EAE pathogenesis [72].

Interestingly, when ELISAs were performed on the supernatants from the cultures to determine total cytokine production there was an unexpected spike in IFN-γ production by CBD in EAE mice on day 18. This increase in IFN-γ production could represent a delay in the immune response in this group of mice due to the CBD treatment, and suggests that given enough time these mice would eventually begin to develop more severe disease; however, further work must be done to determine the population of cells that are responsible for this increase in IFN-γ production. In our studies of EAE in *Cnr1*$^{-/-}$ mice we did find that one of the major contributors to IFN-γ concentrations in supernatants during *ex vivo* restimulation was actually a CD3^{-} population of cells, and taken together these results suggest that although there was suppression of the Tc1 cells in this study, IFN-γ production by another cell type might have been enhanced by CBD. Importantly, in the study by Elliott et al., a method similar to the one here was used to restimulate splenocytes from EAE mice, and it was determined that supernatants from splenocyte cultures of CBD treated mice had lower levels of IFN-γ and IL-17A, and higher levels of IL-10 as compared to EAE mice that did not receive CBD. Together our results and theirs suggest that duration or route of CBD administration may affect the long term suppression of the IFN-γ response. Further work needs to be done to determine exactly which cell types are affected by CBD.

Unlike the effects seen on the Tc1 population, no correlation was seen in the present study between CBD treatment and IL-17A producing T cells from either secondary lymphoid tissue, despite previous reports of CBD's effects on IL-17A

production [71, 73]. In particular, a study by Kozela et al. showed that *in vitro* treatment of T cells with CBD reduced IL-17A production, but did not affect IFN-γ production [73]. The contrast in cytokine production seen between their study and ours might hint at a temporal component to CBD's effects, since their study examined the *in vitro* effects of CBD only 24 hr after the MOG_{35-55} specific T cells were stimulated, and our study examined the *in vivo* effects of CBD after 48 hr of restimulation. Another explanation for the lack of effect seen with IFN-γ in the Kozela et al. paper could be that the concentration of CBD used was not high enough to affect IFN-γ levels. In a study by Kaplan et al. a range of concentrations were examined, and the results shown by this study suggest that higher concentrations provide more IFN-γ suppression [42]. Based on these inconsistencies, it is apparent that more work needs to be done to explore the temporal and dose dependent effects of CBD on cytokine production, with specific attention on IL-17 and IFN-γ, so that a more conclusive connection can be made between CBD and its effects on these two cytokines.

Despite the differences in CBD's effect on cytokine production between our studies and others, the reduction by CBD on neuroinflammation and T cells present in the white matter tracts of the brain and spinal cord of EAE mice was consistent with other studies. Specifically, our results mirror those seen by Kozela et al. who noted reduced levels of T cell infiltrates in the spinal cord with i.p. CBD treatment, and observations seen by Mecha et al. who noted reduced leukocyte infiltrates within the brain of EAE mice with i.p. CBD treatment [4, 5]. However, in this study the reduction in neuroinflammation , as measured by histological analysis and flow cytometry at the day 18 time point, did not reach the level of statistical significance expected, suggesting that

reduced leukocyte infiltration is only one of the neuroprotective mechanisms by which early CBD treatment reduces clinical disease in EAE.

One neuroinflammatory endpoint which differed in the present study as compared previous studies was microglial activation. Here we did not find any significant difference in microglial activation at the day 18 time point when mice were treated with CBD. Considering the body of evidence which has shown that CBD does inhibit microglial activation, we believe that there might have been a delay in microglia activation in the mice treated with CBD; however it likely occurred between day 10 and day 18, and was undetectable by day 18 [4, 5]. To determine if microglial activation is indeed delayed by oral CBD in the EAE model, a microglia specific investigation of days 10-18 would need to be conducted. It is also important to note that the functional capabilities of the cells within the CNS were not examined, so the possibility exists that the cells present within the CNS of CBD treated mice have more of an immunosuppressive phenotype which would contribute to the reduced clinical disease seen in EAE/CBD mice. In consideration of possible functional changes within the T cell compartment, the number of colocalization events was determined between the $CD4^+$ and $CD8^+$ T cells within each lesion to estimate possible changes in communication between the two cell types. It was determined that low numbers of colocalization existed within each lesion with no increases or decreases noted between treatment groups (results not shown).

When examining the longitudinal sections of brain tissue from day 18 mice the highest levels of infiltrates were noted in the cerebellum of EAE/CO mice, where the T cells can be seen evenly and specifically spread throughout the white matter tracts with

notable amounts of perivascular cuffing, while the gray matter of the cerebellum remains relatively untouched. Inflammation was also notably seen in the white matter of the cerebellum of EAE/CBD mice, but to a lesser extent than in the EAE/CO mice. The choroid plexus of each mouse was also examined for buildup of inflammatory cells with CBD treatment that might indicate a reduction in the ability of inflammatory cells to migrate into the CNS; however, there was no evidence of leukocyte buildup within the choroid plexus of any group at any time point (results not shown).

In the spinal cord CBD showed a similar effect where meningeal, subpial, and perivascular infiltrates were increased in the EAE/CO mice, and reduced by administration of CBD. Notably, the spinal cord sections seen in this study show an almost complete lack of infiltration in the white matter of the nerve roots even in the EAE/CO group. This observation was unexpected, since one would presume all myelinated tracts to be targeted equally when the mouse was inoculated with MOG_{35-55} peptide. One possible explanation may be that leukocytes infiltrate primarily in the perivascular spaces through the glial limitans and not through the CSF, which would limit their ability to attack the myelin of the nerve roots that run through the subarachnoid space. This is supported by the two step pathogenesis put forward by Sallutso et al. in which the initial step of pathogenesis involves the migration of $CCR6^+$ T cells across the choroid plexus which facilitate the flow of other leukocytes through the blood brain barrier at various points in the CNS [32]. Another possible explanation for this observation is that the myelin sheaths in the nerve roots are fundamentally different from the myelin sheaths of the spinal cord and brain, and do not contain high levels of MOG. This latter explanation is supported by observations made by Pagany et al. who

found that although MOG can be expressed by Schwann cells intracellularly *in vitro* and MOG mRNA can be identified by PCR analysis of the sciatic nerve, expression of MOG by Schwann cells could not be detected *in vivo* using IHC [74]. Either way, this observation raises some important questions about the pathogenesis of EAE, and provides insight into how peripheral nerves might be immunologically distinct from the CNS even before they leave the vertebral column.

4.2 Differential IFN-γ responses in *Cnr1*$^{-/-}$ and WT mice

The purpose of this study was to examine the role of the CB_1 receptor in the EAE model, with a specific focus on differences in the peripheral immune response between *Cnr1*$^{-/-}$ mice and WT littermates. This was done as a continuation of our previous work with CBD in the EAE model, since there is the potential for CBD to act indirectly through the CB_1 receptor. As we mentioned previously, CBD has very low affinity for the cannabinoid receptors; however some studies suggest that CBD can increase serum anandamide (AEA) levels through the inhibition of fatty acid amide hydrolase (FAAH) and/or fatty acid binding proteins (FABPs), and AEA is an endogenous ligand for the CB_1 and CB_2 receptors [75-77].

Our results show that *Cnr1*$^{-/-}$ C57BL/6 mice have higher levels of clinical disease as compared to their WT littermates. These results are slightly different than results previously reported. In one study, the authors found that ABH *Cnr1*$^{-/-}$ mice had similar levels of disease onset, incidence and severity, but exhibited less of an ability to recover from paralytic episodes as compared to WT mice [10]. Then in another study, CB_1 deficient mice only showed a higher level of disease when THC was used to treat the

mice. The assumption in this later study was that the CB_1 receptor didn't play a role in suppressing disease in the steady state, but was important in cannabinoid therapies [9]. The differences seen between our results and those seen in the ABH mice might be due to a strain difference in the endocannabinoid system. More specifically, since neither of the previous studies in ABH mice showed the higher level of disease severity in *Cnr1*$^{-/-}$ mice that we show here and the latter study showed differences in clinical disease only upon activation of the CB_1 receptor with THC, there may be higher levels of endocannabinoids or higher sensitivity of the CB_1 receptor to endocannabinoids in C57BL/6 mice as compared to ABH mice. A previous study using C57BL/6 mice in the EAE model also found that mice treated with SR141716, a CB_1 receptor antagonist, developed EAE more rapidly than vehicle treated mice, which resembles the differences in early EAE that we found in our studies [78]

To confirm the results of our clinical scoring, a new histologic scoring system was developed to support the findings and determine which regions within the lumbosacral spinal cord differed between *Cnr1*$^{-/-}$ mice and their WT littermates. Differences seen in sections 2, 3, and 4 are important since these sections represent the lumbosacral intumescence, the region of the spinal cord where the nerves for the hind limbs branch off. Higher histologic scores for these sections could reasonably result in an increase in dysfunction in the hind limbs and worse clinical disease. We also found that our histologic scoring system was more sensitive for detecting disease than clinical scores. This is shown in Figure 3B, where some of the mice with a clinical score of 0 received a histologic score >0. One of the major challenges associated with the EAE model is that there is no good way to correlate the commonly used clinical scoring systems with

histologic disease [10, 69, 71]. To help resolve this problem, the new scoring system is designed to specifically account for the complex distribution of lesions found in the lumbosacral region of the spinal cords of EAE mice, and simplifies the quantification of these lesions into a scoring system that can be easily analyzed using a Mann-Whittney U test or correlated to clinical disease. To validate the scoring system we generated both a total histologic score and a total lesion area for each spinal cord, and correlated these to the clinical score for each mouse. Analysis of the lesion area showed only a slight increase in the r^2 value as compared to the histologic scoring system, which shows that either method would be reasonable for confirming clinical disease. These results show that our method of histologic scoring is a relatively simple way to validate clinical scores in EAE mice. Another method commonly used for analyzing neuroinflammation in the EAE model is by flow cytometry of cells obtained from homogenizing the spinal cord [79, 80]. While this is an undeniably valid way to analyze immune infiltrates, our model does have some advantages over this method. One of the major advantages is that our scoring system allows you to analyze lesion distribution along the spinal cord, and preserves the tissues for future histologic stains. When flow cytometry is used to analyze neuroinflammation, the entire spinal cord is used, which does not show distribution over the spinal cord, and if further information is required, the entire study must be repeated. It is our hope that this method will provide researchers who utilize the EAE model with another tool to validate clinical differences seen in the model, without needing access to anything more than a microscope and the reagents for an H&E stain. Moreover, the preservation of tissues will allow researchers to revisit

previous studies with more immunohistochemical technics to collect more data without the need to perform additional studies.

In addition to our examination of neuroinflammation, we also chose to examine IFN-γ and IL-17A in the peripheral immune response. These two cytokines are commonly used endpoints in the EAE model because Th1 cells and Th17 cells have been shown to be important in the pathogenesis of EAE and MS [20-22, 71, 73, 81]. Analysis of IFN-γ and IL-17A concentrations within the supernatants of MOG_{35-55} restimulated splenocytes and serum obtained from our EAE mice showed increased levels of IFN-γ within the supernatants restimulated splenocytes from *Cnr1*$^{-/-}$ mice as compared to their WT littermates. These finding suggest that the antigen specific IFN-γ response to MOG_{35-55} is much higher in *Cnr1*$^{-/-}$/EAE mice as compared to WT/EAE mice. These results are also consistent with those found in another study which showed that treatment of EAE mice with SR141716A, a CB_1 receptor antagonist, increased IFN-γ production in MOG_{35-55} restimulated splenocytes, along with other proinflammatory cytokines such as IL-17A, IL-1β, IL-6, and TNF-α [82].

Since the restimulation method used in these EAE studies relies on the uptake of MOG_{35-55} by APCs and presentation to T cells, we decided to further test the T cell specific IFN-γ responses of *Cnr1*$^{-/-}$ and WT mice using two additional methods of T cell stimulation: anti-CD3/anti-CD28 and the *S. aureus* superantigen SEM. Anti-CD3/anti-CD28 antibodies act directly on the T cell receptor (TCR) CD3 subunit and on the CD28 co-stimulatory molecule to invoke a strong T cell specific response, which includes increases in IFN-γ production. Conversely, the stimulation of T cells with SEM, a pyrogenic toxin superantigen, is dependent on cross bridging of the TCR to MHC class

II molecules on APC [83]. Thus by including both methods we were first able to assess the ability of T cells alone to produce IFN-γ and then assess their ability to produce IFN-γ in an APC dependent manner. Interestingly, when anti-CD3/anti-CD28 antibodies were used a very robust IFN-γ response was seen in WT and *Cnr1*$^{-/-}$ mice, but the WT mice had nearly a two-fold higher level of IFN-γ in the supernatants as compared to the *Cnr1*$^{-/-}$ mice. In contrast to this, when SEM was used to stimulate the splenocytes a lower level of IFN-γ was observed as compared to the anti-CD3/anti-CD28 stimulation and although WT mice generally had higher levels of IFN-γ production compared the CB_1 deficient mice the difference was less significant than observed with anti-CD3/anti-CD28 stimulation. Since these results contradicted the results found from the *ex vivo* restimulation of splenocytes in our EAE studies, we used flow cytometry to determine the sources of IFN-γ under both conditions.

Interestingly, while the results from our flow cytometry did not show a difference in the percentage of IFN-γ producing cells between *Cnr1*$^{-/-}$ and WT mice under most conditions, with the one exception being the anti-CD3/anti-CD28 stimulated $CD3^+CD8^+$ cells, it did reveal that the major source of the IFN-γ in our EAE studies was a $CD3^-CD4^-CD8^-$ cell population and the major source of IFN-γ from the T cell specific stimulations were the $CD3^+CD4^+$ and $CD3^+CD8^+$ populations. Based on these results it is clear that IFN-γ production in the EAE model was enhanced in the peripheral immune system of *Cnr1*$^{-/-}$ mice as compared to WT mice, however the increased IFN-γ production *ex vivo* is not explained by an increase in IFN-γ production by T cells specifically. Furthermore, since our flow cytometry analysis showed this cell population to be a $CD3^-$ population, we can rule out NKT cells and γδ T cells as the source of IFN-γ. These results suggest

that NK cells or APCs could be sources of IFN-γ since they are both $CD3^-$. Given the fact that only MOG_{35-55} peptide was added to the cultures to stimulate an antigen-specific response, the data suggest the major source of IFN-γ in the *ex vivo* cultures was likely either macrophages or dendritic cells, which would suggest the inflammatory potential of these APCs are enhanced in the *Cnr1*$^{-/-}$ mice. This is supported by another study by Lou et al. in which they examined the effects of SR141716A on IFN-γ production in T cells from EAE mice and BV-2 microglia. When this group examined the effects of SR141716A on T cells from EAE mice they did so by flow cytometry, much like our present study, and while they did find a significant increase in the overall percentage of $CD4^+IFN\text{-}\gamma^+$ cells with SR141716A treatment, the total percentage of $CD4^+IFN\text{-}\gamma^+$ cells was less than 5% with the difference found between groups only being about 1% of cells [78]. These numbers are very similar to those found in the present study for percentages $CD4^+IFN\text{-}\gamma^+$ cells, despite the fact that they specifically isolated $CD4^+$ T cells and co-cultured them with BV2 microglial cells prior to flow cytometry. Additionally, when this group examined IFN-γ production by BV2 microglial cells by ELISA of supernatants from culture, they found that SR141716A treated cells had significantly more IFN-γ production as compared to those not treated with SR141716A[78]. While further studies need to be done to confirm the source of IFN-γ in our study, the similarities between microglial cells and macrophages strongly support macrophages as major source of IFN-γ within the peripheral immune response of the EAE model and that CB_1-deficient mice may have a higher level of IFN-γ production in these cells. It should also be noted that when mononuclear cells (MNC) from the spleen of EAE mice in the presence of MOG_{35-55} and MBP_{68-86} in their study, an increase in

IFN-γ production was also noted in Lou et al. however in the previous study no determination of cell types was made for this analysis [78]

4.3 Conclusions

The exploration of CBD as an immunosuppressive therapy has shown promise in models of rheumatoid arthritis (RA), inflammatory bowel disease (IBD), and MS [3-5], and the neuroprotective effects of the CB_1 receptor have been highlighted in other studies [9, 10]. However, in the studies outlined in this dissertation we sought to further the understanding of how the CB_1 receptor and CBD modulate the peripheral and subsequent neuroimmune response in the EAE model. The major contributions from these studies are as follows. 1) Our early studies with CBD in the EAE model determined that early treatment with oral CBD significantly decreased the Tc1 responses in the spleen of CBD-treated EAE mice on day 10, which correlated with modest reduction in neuroinflammation of the CBD-treated EAE mice on day 18. These data are significant since suppression of immune function endpoints were observed following oral CBD and the reduction of clinical and neurological disease seen at later time points after early treatment with CBD suggest that residual effects of CBD treatment were still present for over a week after discontinuing the treatment. 2) Our examination of IFN-γ production in *Cnr1*$^{-/-}$ and WT mice under various experimental conditions found that CB_1-deficient mice had both increased and decreased production of IFN-γ which was highly dependent on which cells were stimulated. More specifically, when T cells dominated IFN-γ production WT mice had higher levels of IFN-γ, and when the $CD3^-$ populations dominated IFN-γ production *Cnr1*$^{-/-}$ mice had higher levels of IFN-γ. These results represent an important step in understanding the complex mechanism

of the CB_1 receptor in different cells types, and under different stimulation conditions. Moreover, with the recent increase in the clinical application of cannabinoids for various diseases, including MS, these results represent a vital piece of information that may guide future clinical decisions, since they imply that inhibition of the CB_1 receptors may enhance the inflammatory responses of innate cells and depress the inflammatory response of T cells, and that the reverse may be true for stimulation of the CB_1 receptors. 3) A new method of scoring histologic disease was developed in our later studies which we hope will help standardize the methods for reporting histologic disease in future studies. In the author's opinion, this is a much needed addition to the use of EAE as a model for MS, which will not only help to confirm clinical scores obtained while using these studies, but also deepen our understanding of the pathogenesis of this complex disease.

CHAPTER V

THE EAE MODEL: ISOFLURANE AND PASSIVE EAE

Pertussis Toxin (PTX) is often used by other labs to enhance the severity of the EAE model; however PTX is also an inhibitor of G-protein coupled receptors like CB_1 and CB_2 [84]. Since the CB_1 receptors were considered to be important factors in our *Cnr1*$^{-/-}$ study, and indirectly in our CBD study through CBD's ability to modulate AEA metabolism, we decided to avoid the possible confounding factor of inhibiting these receptors with PTX. As a result we saw a milder form of EAE than what is reported by other labs, which made analysis of clinical disease more difficult [69, 85, 86]. Thus, in addition to the work outlined in the chapters above, we have also been exploring other methods of enhancing clinical disease that do not require PTX. This chapter will outline two such methods, and discuss the outcome from each method.

5.1 Effects of isoflurane on the EAE model

In our EAE model we often find increases in the peripheral immune response to MOG_{35-55} peptide even when no clinical disease is present. Based on this, we believe that one of the major obstacles for our model is centered on the infiltration of the MOG_{35-55} specific immune cells across the BBB, and thus we began looking for ways to enhance migration of cells across the BBB. The method outlined in this section was

developed based a paper which showed that high levels of isoflurane administered to cats was capable of increasing the permeability of the BBB [87]. Given this evidence we hypothesized that isoflurane could open the BBB in mice in a similar fashion to that seen in cats, and that if isoflurane were given to EAE mice in sufficient dosages at the proper time, it could be used to synchronize the infiltration of immune cells across the BBB.

5.1.1 Methods

5.1.1.1 Exposure to high levels of isoflurane

Experiments were approved by Mississippi State University Institutional Animal Care and Use Committee (IACUC). WT female C57BL/6 mice raised at Mississippi State College of Veterinary Medicine were used for these experiments. Prior to prolonged exposure to isoflurane, mice were briefly anesthetized using isoflurane and injected i.p. with Evans blue dye. 2 hr after injection, mice were placed in a clear plastic container and exposed to either 3% isoflurane or oxygen for 15mins. Body temperature was controlled using a heating pad under the plastic container, and mice were monitored during recovery to be sure there were no complications. The mice were then euthanized and the spinal cords were placed in 10% NBF for approximately 1 week.

5.1.1.2 Spinal cord processing

Fixation of the spinal column prior to removal of the spinal cord allowed us to remove the spinal cords without accidental disruption of the blood vessels, which would have generated a false positive in our images. After fixation, the spinal cords were

removed from the spinal columns by removing the dorsal lamina of each vertebra and carefully extracting the length of the spinal cord. The spinal cords were then placed in OTC and 30µm sections were cut using a cryostat. Evans blue was detected within the vessels of each section using a fluorescence microscope with a TRITC filter. Microscopic images were captured using a Lumenera Digital Camera and Infinity Analyze Software.

5.1.1.3 EAE induction and isoflurane exposure

EAE was induced and scored as described in Chapter 2 using 100 µl of CFA containing 100 µg of MOG_{35-55} peptide with 0.5 mg of HKMT. 11 days after EAE induction mice were exposed to 3% isoflurane or oxygen for 15 minutes as described in the previous section. Clinical disease was allowed to progress normally until day 18 when the mice were euthanized.

5.1.2 Results

5.1.2.1 Examination of spinal cords after exposure to isoflurane.

Upon examination of spinal cords from mice exposed to 3% isoflurane and oxygen for 15 mins, we found no evidence extravasation of Evans blue dye in either set of mice (Figure 5.1)

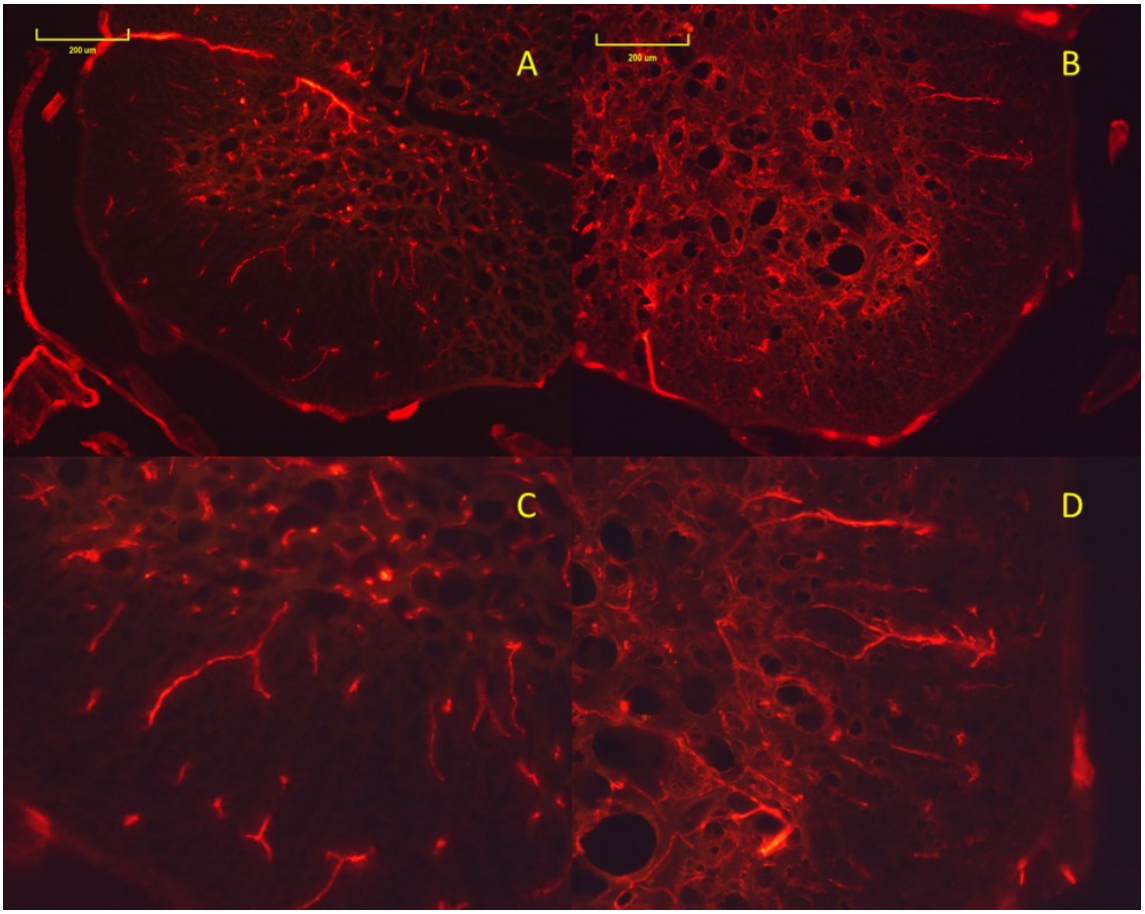

Figure 5.1 Examination of BBB integrity after exposure to isoflurane

No extravasation of Evans blue dye was noted in mice exposed to isoflurane or oxygen for 15 mins. The images in the figure are representative images of spinal cords taken at 100 x magnification for isoflurane (A) or oxygen (B) treated mice, and 200 x magnification images of isoflurane (C) or oxygen (D) treated mice.

5.1.2.2 Effects of isoflurane on EAE

Exposure to 3% isoflurane for 15mins did not enhance EAE disease progression, nor did it synchronize initiation of disease as expected (Figure5.2).

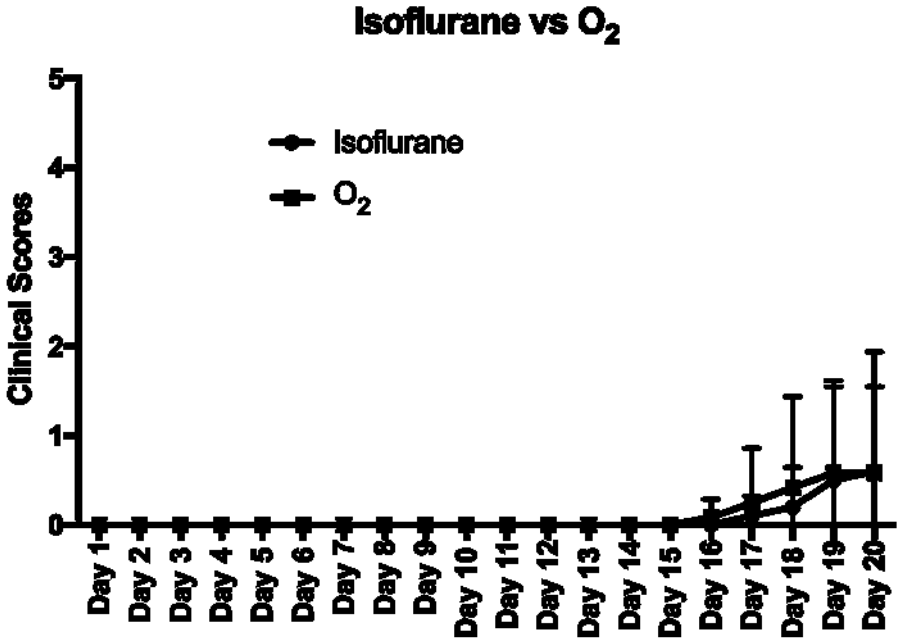

Figure 5.2 Clinical EAE after exposure to isoflurane

Clinical progression was monitored over an 18 day time period and mice were exposed to either 3% isoflurane or oxygen for 15 mins on day 11. No significant difference was seen between these two groups.

5.1.3 Discussion

In this set experiments we sought to use isoflurane as a method of increasing the BBB permeability in EAE model. However, we were unable to achieve an increase in disease incidence or severity by administering isoflurane to EAE mice 11 days after the

induction of disease. Furthermore, we were unable to show increases in BBB permeability with isoflurane treatment. This was surprising considering that Tetrault et al. reported increases in BBB permeability in the cortex and thalamus of cats at 3% isoflurane, and permeability in the thalamus of cats at 1% isoflurane [87]. In our experiments, mice exposed to 3% isoflurane did not show any increases in Evans blue extravasation in the spinal cord as compared to mice treated with oxygen. One possible explanation for the difference found in our study as compared to theirs is that we are using mice instead of cats. However it is unlikely that higher levels of isoflurane would be needed in mice as compared to cats. This is because the Minimum Alveolar Concentration (MAC), which is the concentration at 1 atmosphere that produces immobility in 50% of animals exposed to a noxious stimulus, is 1.63±0.06 in cats and 1.41±0.03 in mice [88]. This means that mice are actually anesthetized at slightly lower concentration than cats on average, and thus the effects of the anesthetic on the BBB should be similar if not a little more pronounced in mice given the same concentration of isoflurane. Additionally, since less than 0.2% of the inspired dose of isoflurane is metabolized by the animal, it is unlikely that the higher metabolism of mice would have any significant impact on blood concentrations of isoflurane [88].

In addition to examining BBB permeability with Evans blue dye, we also decided to try to enhance our EAE model with isoflurane. For this experiment, day 11 was chosen for the administration of isoflurane based on increases in peripheral immune responses seen in our previous studies. For example, in our EAE/CBD study we clearly saw an increase in the MOG specific IFN-γ responses at day 10. Thus, we hypothesized that by day 11 a population of MOG specific T cells should be present and

able to cross the BBB if it was sufficiently disrupted. The results from this experiment seem to reinforce the results found in the previous experiment using Evans blue dye, in that we saw no change in disease, which suggests that the BBB was not disrupted. The combined results from these two experiments suggest that isoflurane does not cause sufficient disruption of the BBB to enhance the EAE model. However, it should be noted that to fully explore isoflurane as a method of enhancing this model, more time points for isoflurane administration should be added to future studies.

5.2 Passive transfer model development

In addition to our attempts to increase BBB permeability with isoflurane, our lab has recently been exploring the use of the P-EAE model as a method of examining the later stages of the MOG_{35-55} specific immune response, and as a more robust form of disease. This model is a useful tool for exploring immune responses of EAE mice independently from the non-specific responses to CFA and HKMT that are present in the active EAE model that has been used in our previous studies. In our initial work with CBD in the active EAE model, we found that CBD was capable of reducing clinical disease and modestly reducing neuroinflammation, which is similar to results found by other labs [4, 5]. Thus we hypothesized that CBD would have similar effects on the P-EAE model. Here we will discuss a couple of experiments in which we utilized 2D2 transgenic mice to initiate P-EAE, and how the development of this model has led to some important age dependent discoveries. More specifically, in some of our early CBD studies with this model we observed that older mice initiated EAE more effectively than

younger mice, which led us to wonder if there were differences in the cell populations obtained from older mice as compared to younger mice.

Based on previous studies from other labs, we chose to examine several cell populations including central memory T cells, effector memory T cells, Th1 cells, Th17 cells, and $CD4^{-}CD8^{-}$ T cells (double negative T cells). The choice to include memory T cells, Th1, and Th17 cells was inspired by a study that examined the ability of memory T cells and naïve T cells from 2D2 mice to induce disease in WT mice [89]. Based on this study we hypothesized that older mice have more robust memory T cell responses as compared to younger mice, and thus generate higher clinical disease. We also decided to look for changes in the double negative T cells recovered from 2D2 mice, since a previous study by Grishkan et al. found that repeated stimulations of T helper cells by anti-CD3/anti-CD28 coated Dynal beads to simulate the chronic stimulation generated a double negative population of T cells similar to those found in autoimmune lymphoproliferative syndrome (ALPS) and systemic lupus erythematosus (SLE) [90]. In the context of the present study, we examined transgenic T cells for any shift in the double negative population to see if a similar type of chronic stimulation was occurring in the transgenic T cells of older mice 2D2 mice.

5.2.1 Materials and Methods

5.2.1.1 P-EAE induction

Experiments were approved by Mississippi State University Institutional Animal Care and Use Committee (IACUC). Active EAE was induced in 2D2 transgenic C57BL/6 female mice as described in Chapter 2 using 100 µl of CFA containing 100 µg of

MOG_{35-55} peptide with 0.5 mg of HKMT. These mice were obtained from Jackson Laboratories at 8 weeks of age, and were either rested for two weeks before EAE induction or kept until approximately 6 months of age before active EAE induction. Cells were then harvested from the spleen, axial lymph nodes, and inguinal lymph nodes for culture. 20×10^6 cells from lymph nodes and spleens were cultured separately in 4mls of 1x RPMI/5%BCS/1% Pen-Strep/50 μM 2-ME for 72 hr in a 6 well plate in the presence of 50μg/ml of MOG_{35-55} peptide. All of the cells were then harvested, combined into a single suspension, and concentrated in PBS so that each WT recipient mouse was injected i.p. with approximately $30\text{-}40 \times 10^6$ cells in 200μl of PBS. In later experiments cells were set aside before culture to stain for central memory and effector memory T cells, and cells were set aside after culture to stain for central memory T cells, effector memory T cells, $CD3^+CD4^-CD8^-$ T cells, IFN-γ producing T cells, and IL-17A producing T cells. After P-EAE induction, the mice were monitored over the next 15 days for clinical disease using the same scoring system outlined in Chapter 2.

Two sets of experiments were performed using this method of P-EAE induction. The aim of the first set of experiments was to determine the effects of prolonged CBD treatment on P-EAE. To this end, P-EAE mice were treated with either 75mg/kg of CBD in 100μl of CO, 150mg/kg of CBD in 100μl of CO, or 100μl of CO for the entire 15 day time course of P-EAE. Due to some inconsistencies that were discovered during these experiments a second set of experiments was then designed to test the age dependent immune response of 2D2 transgenic mice, and no CBD was used during this set of experiments.

5.2.1.2 Staining for flow cytometry

Before culture, cells from the lymph nodes and spleen of each mouse were stained for central and effector memory T cells, and after the 72hr restimulation culture with MOG_{35-55} the cells were stained for central and effector memory T cells, $CD3^+CD4^-CD8^-$ T cells, and IFN-γ/IL-17A producing T cells. For the IFN-γ and IL-17A staining cells were treated with Brefeldin A for 4 hr before extracellular staining. Extracellular staining was performed in a similar fashion to that described in Chapter 2. Briefly, the cells were rinsed twice with 1x PBS and stained with 0.1µl of NIR FVD in 50µl of PBS for 30mins at 4°C. The cells were then rinsed twice more with PBS, and incubated at RT for 15 min in 50 µl of FC buffer containing 0.5 µl of Fc Block. 50 µl of FC buffer containing 0.3 µl extracellular antibodies was added to each well and allowed to incubate at RT for 30 min. To stain for central/effector memory T cells, extracellular antibodies included CD3-Pacific Blue (BioLegend Clone 17A2), CD4-APC (BioLegend Clone GK1.5) CD8-PE-Cy7 (BioLegend Clone 53-6.7), CD62L-PE-Cy5 (eBioscience Clone MEL-14), CD44-BV785 (BioLegend Clone IM7), Vβ11-PE (BioLegend Clone RR3-15), and Vα3.2-FITC (BioLegend Clone RR3-16). Extracellular antibodies for the $CD3^+CD4^-CD8^-$ T cell stain included CD3-Pacific Blue (BioLegend Clone 17A2), CD4-APC (BioLegend Clone GK1.5) CD8-PE-Cy7 (BioLegend Clone 53-6.7), Vβ11-PE (BioLegend Clone RR3-15), NK1.1-PerCP/CY5.5 (BioLegend Clone PK136), γδTCR-FITC (BioLegend Clone GL3) and B220-BV785 (BioLegend Clone RA3-6B2). Extracellular antibodies for the IFN-γ and IL-17A stain included CD3-Pacific Blue (BioLegend Clone 17A2), CD4-APC (BioLegend Clone GK1.5) CD8-PE-Cy7 (BioLegend Clone 53-6.7), and Vα3.2-FITC (BioLegend Clone RR3-16). After extracellular staining cells that underwent the memory

T cell stain and $CD3^+CD4^-CD8^-$ T cell stain were then rinsed twice with FC buffer, fixed for 15 mins with BD Cytofix, and resuspended in 300µl of FC buffer for flow cytometry. Cells for the IFN-γ and IL-17A stain were rinsed twice FC buffer, fixed with BD Cytofix for 15mins, and rinsed once with FC buffer and once with BD Permwash buffer (BD Bioscience).Then the cells were resuspended in BD Permwash buffer containing 0.5 µl of IFN-γ-PE (BioLegend Clone XMG1.2) and 0.5 µl of IL-17A-BV650 (BioLegend Clone TC11-18H10) and allowed to incubate overnight at 4°C. The cells were rinsed with FC buffer and resuspended in 300 µl of FC buffer for flow cytometry.

5.2.1.3 Flow cytometry

Cells stained with intracellular and extracellular florescent antibodies were analyzed using an ACEA Novocyte flow cytometer (ACEA Biosciences, San Diego, CA).

5.2.1.3.1 *Memory T cells*

Live lymphocytes from the MOG_{35-55} restimulated cells were selected by gating on cells that did not stain with NIR FVD and then passing them through singlet gate and a lymphocyte gate based on their SCC and FSC characteristics. Transgenic T cells were then selected based on their expression of CD3 Vβ11 and Vα3.2. Cells from this population were then divided based on their expression of CD62L and CD44. Naïve cells, central memory cells, and effector memory cells were identified as $CD62L^+CD44^-$, $CD62L^+CD44^+$, and $CD62L^-CD44^+$ respectively (Figure 5.3) as previously described by Williams et al. [89].

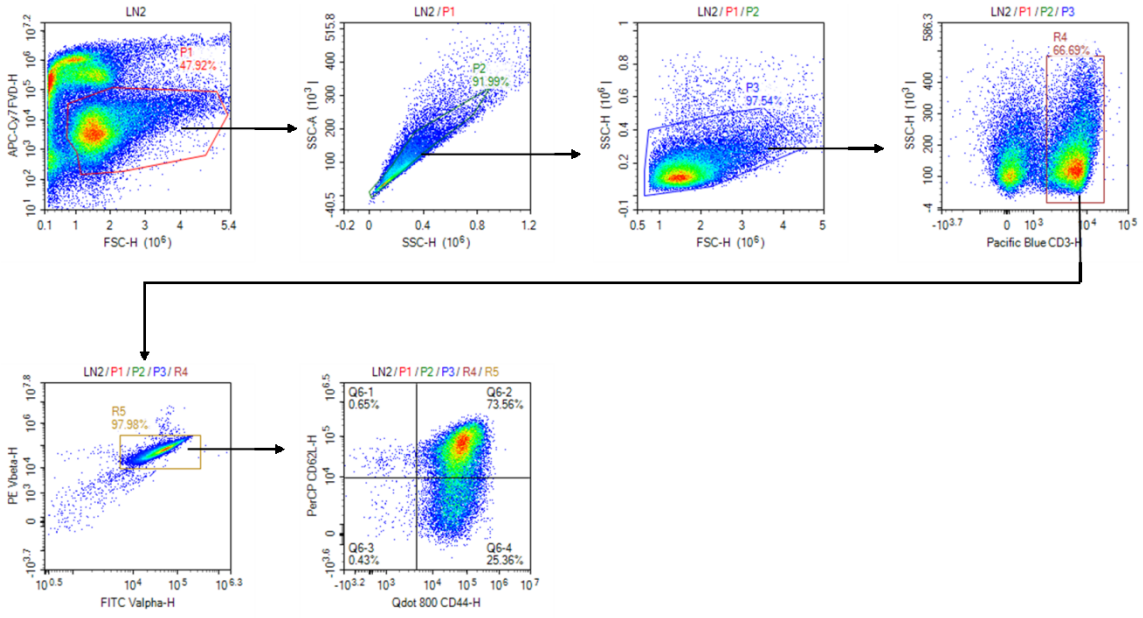

Figure 5.3 Memory and effector transgenic T cells gating strategy

Cells were first passed through a live cell gate based on NIR FVD staining and then through a doublet exclusion gate and a lymphocyte gate. From this population Transgenic T cells were identified as $CD3^{+}V\beta11^{+}V\alpha3.2^{+}$ cells, which were then further divided into naïve, memory, and effector cells based on expression of CD44 and CD62L. Memory cells were identified as $CD44^{+}CD62L^{+}$, naïve cells were identified as $CD44^{-}CD62L^{+}$, and effector cells were identified as $CD44^{+}CD62L^{-}$.

5.2.1.3.2 *Double negative T cells*

Similar to the gating for memory T cells, we first identified live lymphocytes from the MOG_{35-55} restimulated cells based on staining with NIR FVD and their SSC and FSC characteristics. Then, we identified transgenic T cells base on their expression of CD3 and Vβ11. Vα3.2 was excluded from this analysis because we determined in the memory cell stains that Vβ11 and Vα3.2 are almost exclusively expressed together. Thus we were able to stain for more markers by excluding Vα3.2 here. Once we

isolated the transgenic cell population we identified the CD4/CD8 double negative population as the $CD4^{-}$ $CD8^{-}$ γδTCR^{-} $NK1.1^{-}$ $B220^{-}$ population (Figure 5.4).

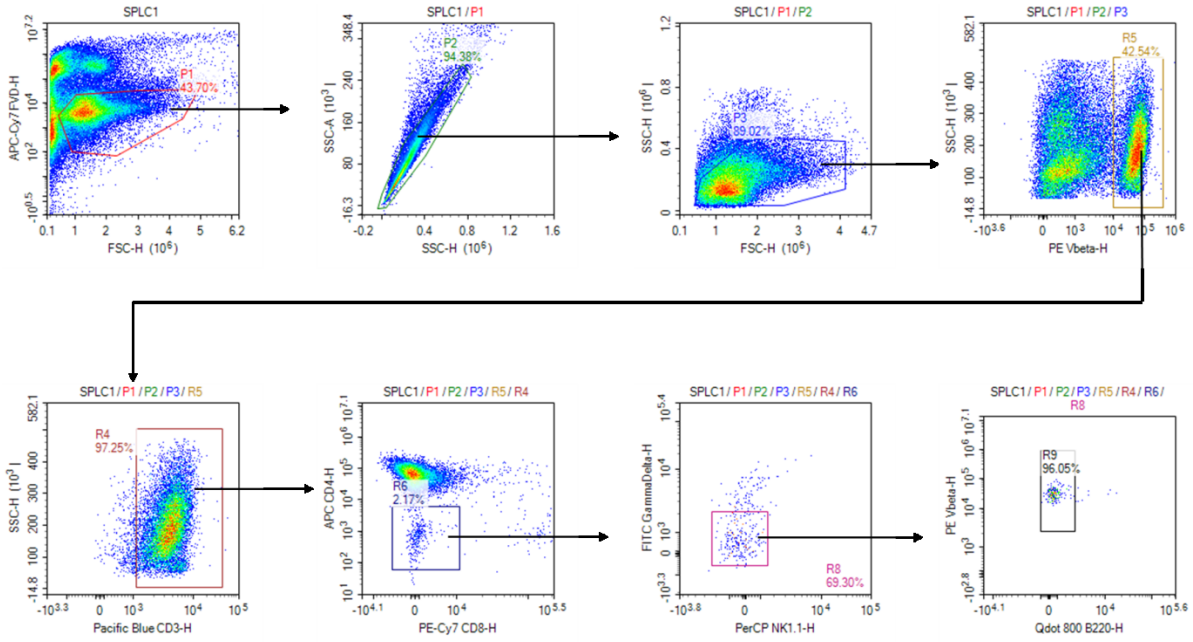

Figure 5.4 Double negative transgenic T cells gating strategy

Cells were first passed through a live cell gate based on NIR FVD staining and then through a doublet exclusion gate and a lymphocyte gate. From this population Transgenic T cells were identified as $CD3^{+}V\beta11^{+}$ cells. Double negative cells were then identified $CD4^{-}CD8^{-}$ cells that were also $NK1.1^{-}$γδ$TCR^{-}B220^{-}$.

5.2.1.3.3 *IL-17A and IFN-γ producing T cells*

Lymphocytes were selected as before, and this time expression of CD3 and Vα3.2 was used to identify transgenic T cells. From this population, we then identified the $CD4^{+}$ cells that expressed IFN-γ and IL-17A (Figure 5.5).

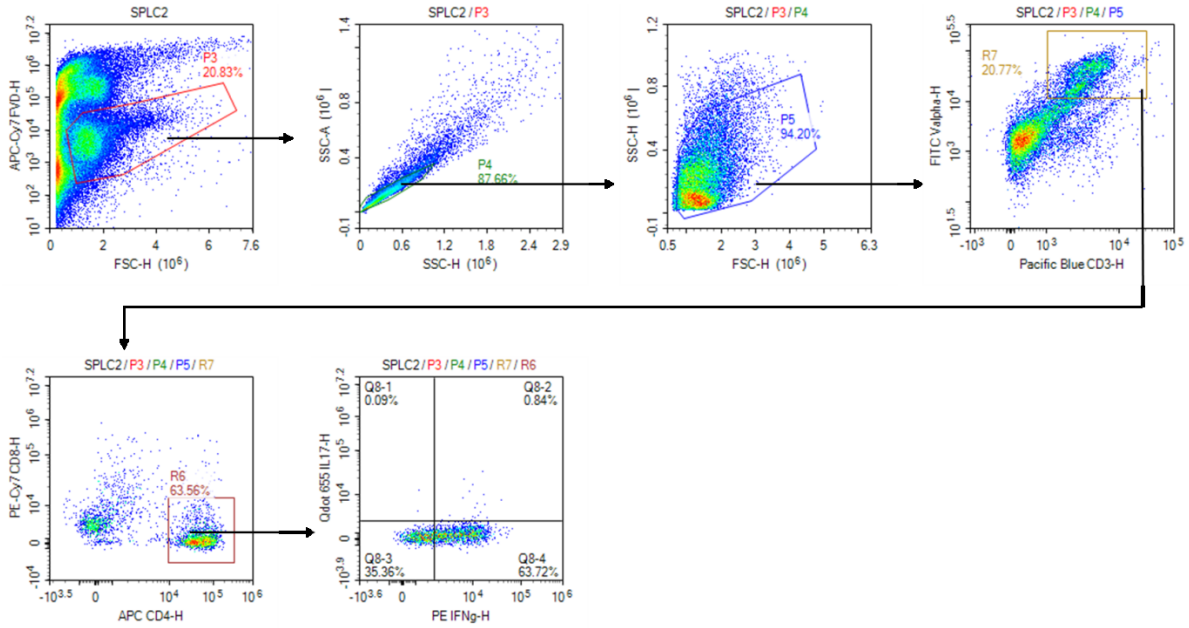

Figure 5.5 Th1 and Th17 transgenic T cells gating strategy

Cells were first passed through a live cell gate based on NIR FVD staining and then through a doublet exclusion gate and a lymphocyte gate. From this population Transgenic T cells were identified as $CD3^{+}V\alpha3.2^{+}$ cells. This population was then further divided into $CD4^{+}IFN\text{-}\gamma^{+}$ cells and $CD4^{+}IL\text{-}17A^{+}$ cells which represented the Th1 and Th17 populations respectively.

5.2.1.3.4 *B cells*

For identification of B cells, we used the sample of cells that were stained for examination of double negative T cells. However, instead of using the other markers used to identify T cells, we simply changed the analysis to look for cells within the lymphocyte population that expressed B220 (Figure 5.6)

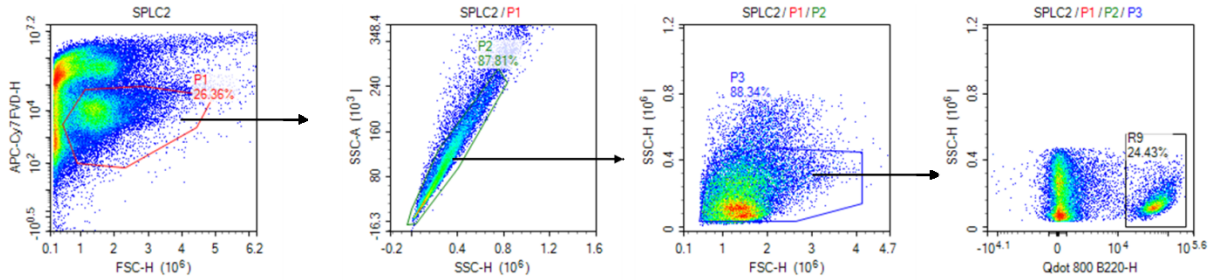

Figure 5.6 B cell gating strategy

Cells were first passed through a live cell gate based on NIR FVD staining and then through a doublet exclusion gate and a lymphocyte gate. From this population B cells were identified as cells that expressed B220.

5.2.1.4 Histologic staining

Spinal cords were taken for each set of experiments that were performed and decalcified and placed in paraffin blocks as described in Chapter 2. 5µm sections from the P-EAE CBD studies were then cut to perform H&E and Iba-1 staining. Sections for the Iba-1 staining were first deparafinized and rehydrated by placing them through xylene, 100% ethanol, 95% ethanol, DI water at 2 mins each. Antigen retrieval was performed by placing the slides in TRS for 30mins in a steamer. The slides were then allowed to cool for 10mins and rinsed in PBS. Non-specific binding was blocked by placing the sections in PBS containing 1% BSA and 4% goat serum for 1hr at RT. The blocking solution was then removed and polyclonal rabbit Iba-1 antibodies were placed on the sections in PBS/1% BSA/0.1% Tx. The slides were placed at 4°C and allowed to incubate overnight. The next day the slides were rinsed in distilled water to remove excess antibodies, and incubated for 2 hr in PBS/1% BSA/0.1% Tx containing Alexa

Fluor 488 conjugated goat anti-rabbit IgG antibody (1:200). Slides were rinsed and coverslipped with Vectashield. Images were captured using a Lumenera Digital Camera equipped with Infinity Analyze Software.

5.2.1.5 Statistical analysis

Statistical analysis performed on clinical scores utilized the Mann-Whitney U test, while statistical analysis performed on flow cytometry results was done using one-way ANOVA after transformation of the raw percentages. All statistical analysis was performed with GraphPad Prism 6 or GraphPad Prism 7 software.

5.2.2 Results

5.2.2.1 Effects of CBD on the P-EAE clinical scores

In our initial examination of the P-EAE model, 6 month old 2D2 mice were used in two studies to induce P-EAE, and young mice of approximately 10 weeks of age were used in one final study using CBD. In the first two studies the incidence for P-EAE was 100% in both the P-EAE/CO group and P-EAE/CBD group, and CBD had no effect on P-EAE (Figure 5.7A). Conversely, when P-EAE was induced using young 2D2 mice with the same protocol, no clinical disease was found in any treatment group (Figure 5.7B)

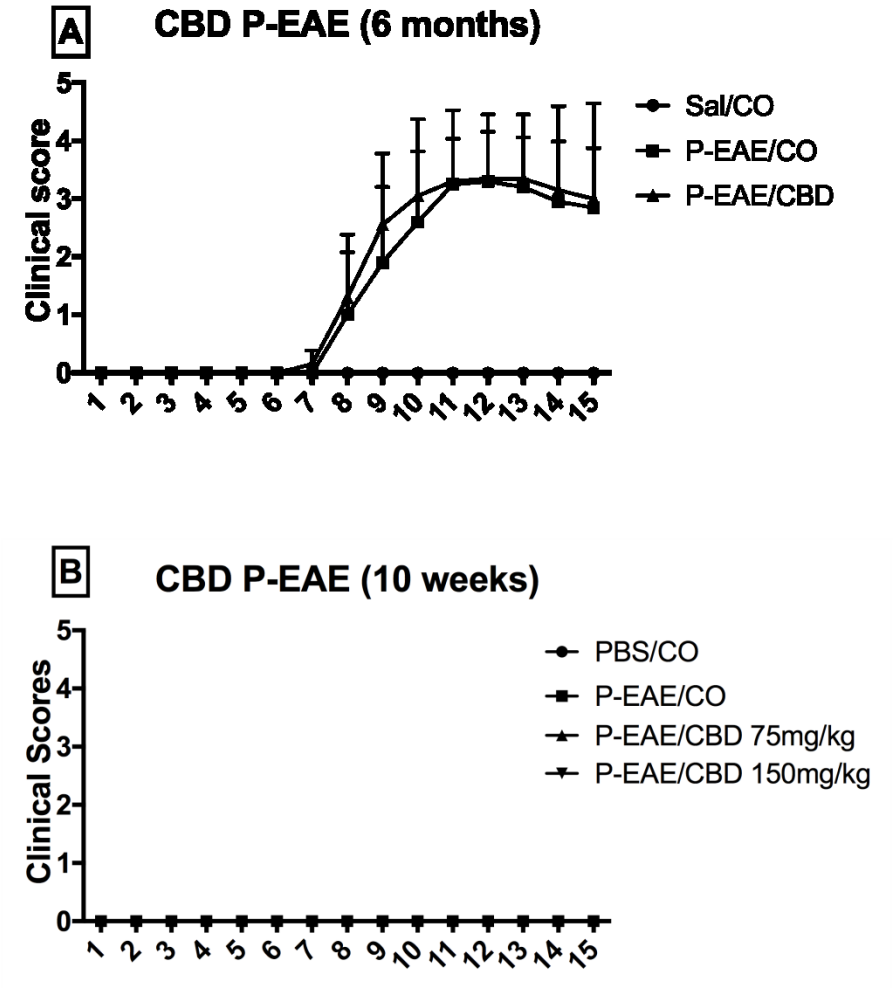

Figure 5.7 Clinical scores for P-EAE CBD studies

P-EAE was induced in WT C57BL/6 mice using restimulated cells from 6 month old 2D2 mice, and recipient mice were treated with either 75mg/kg of CBD in CO or treated with CO. No difference was seen between the clinical scores of the P-EAE/CBD group and the P-EAE/CO group (A). The experiment was repeated again with 10 week old 2D2 mice and treatments of 150mg/kg of CBD in CO, 75mg/kg of CBD in CO, or CO were given to the recipient mice. No clinical disease was seen in any group (B).

5.2.2.2 H&E and Iba-1

Iba-1 and H&E stains were performed on mice from the first two studies exploring CBD's effects on the P-EAE model to examine microglial activation and cellular infiltration respectively. Examination of histologic stains revealed no difference between the P-EAE/CO and P-EAE/CBD groups with regards to cellular infiltration or microglial activation (Figure 5.8).

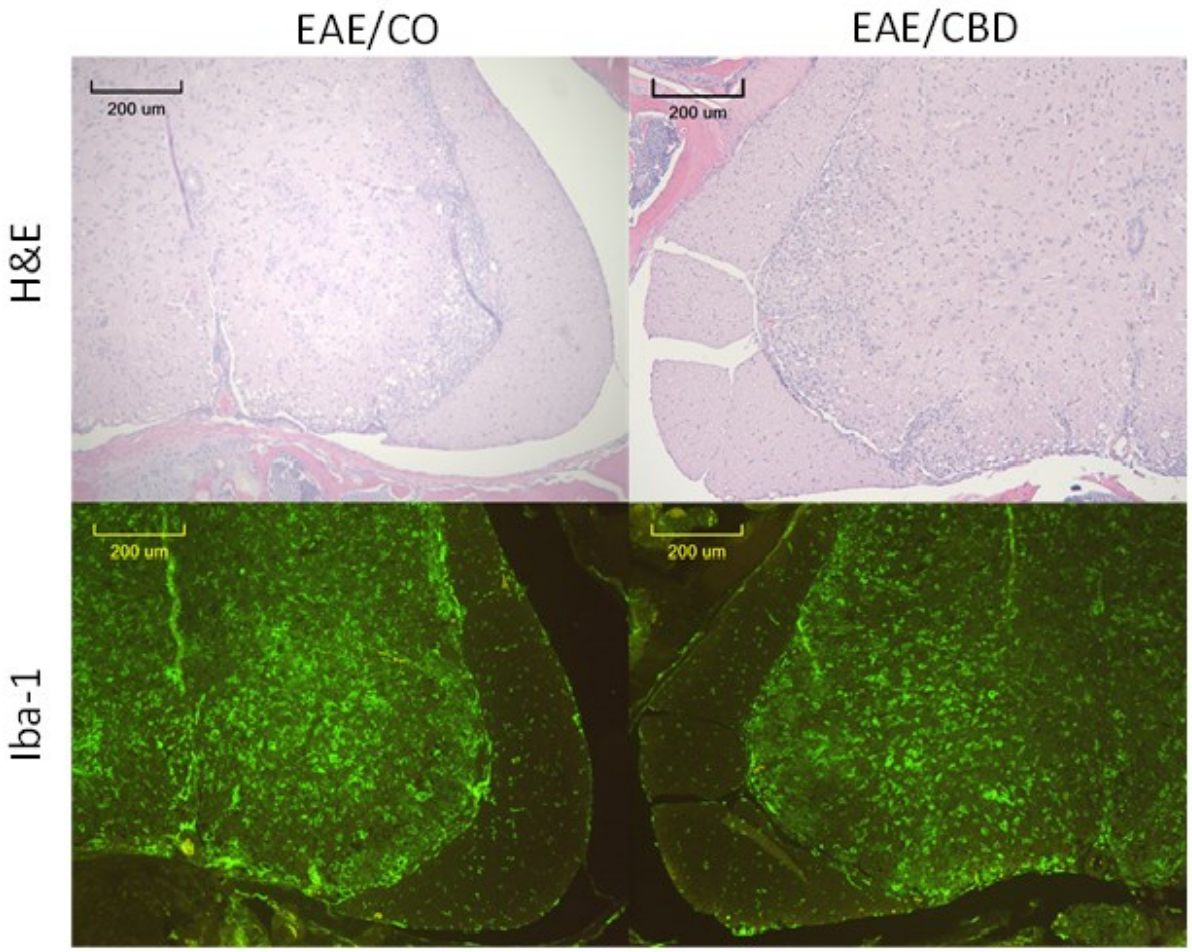

Figure 5.8 H&E and Iba-1 staining of mice from P-EAE CBD studies

H&E stains from the two studies in which clinical disease was not abrogated by CBD showed that there were similar levels of cellular infiltration in CO and CBD treated mice, and Iba-1 staining revealed similar levels of microglial/macrophage activity within the spinal cords of CO and CBD treated mice.

5.2.2.3 Induction of P-EAE using old and young mice

Based on the discrepancy seen between P-EAE induced with mice that were 6 months of age vs 10 weeks of age in our initial studies examining the effects of CBD on

P-EAE, we conducted a set of experiments to determine whether older 2D2 mice were more capable of inducing clinical disease in the P-EAE model. Clinical scores from these studies show that by 15 days after the induction of P-EAE, older 2D2 transgenic mice were able to confer a higher level of clinical disease as compared to younger 2D2 transgenic mice, which confirms our previous observations from the P-EAE CBD study.

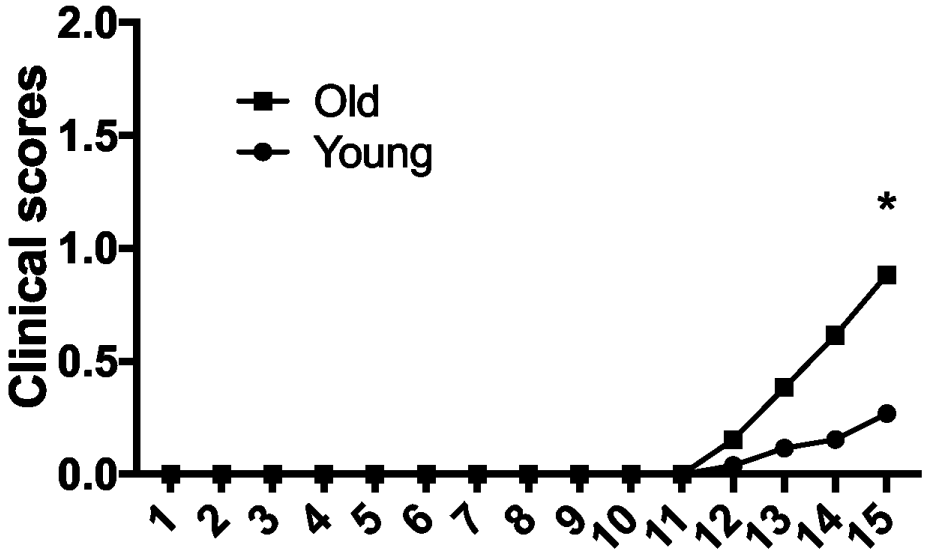

Figure 5.9 Clinical scores from P-EAE old vs young studies

P-EAE was induced in WT C57BL/6 mice using restimulated cells from mice 6 months and 10 weeks of age. Clinical disease began around day 12 for both sets of mice, and by day 15 the P-EAE mice which were induced using cells from older mice (n=13) had a significantly higher average clinical score as compared to P-EAE mice which were induced using younger mice (n=13). * $p < 0.05$

5.2.2.4 Memory cells and effector cells

Analysis of memory and effector T cell populations was performed on both spleen and lymph node isolates before and after the 72 hr restimulation with MOG_{35-55} peptide. This analysis revealed a significantly higher number of MOG_{35-55} specific transgenic central memory T cells before culture in the spleens of young mice as compared to those of older mice (Figure 5.10A). Conversely, the lymph nodes and spleens of 6 month old mice had much higher percentages of MOG_{35-55} specific transgenic effector memory T cells before culture as compared to younger mice (Figure 5.10C). However, after these cells were cultured for 72 hr in the presence of MOG_{35-55} peptide, the differences in effector and central memory T cells were eliminated (Figure 5.10 B&D). When we analyzed the percentage of transgenic T cells in the secondary lymphoid organs we found that younger mice had much higher percentages of the transgenic T cells as compare to older mice, but this difference was lessened after culture as well (Figure 5.10 E&F). The number of transgenic central memory and effector memory T cells is represented as percentages of total transgenic T cells, whereas transgenic T cells are represented as a percentage of the total lymphocytes.

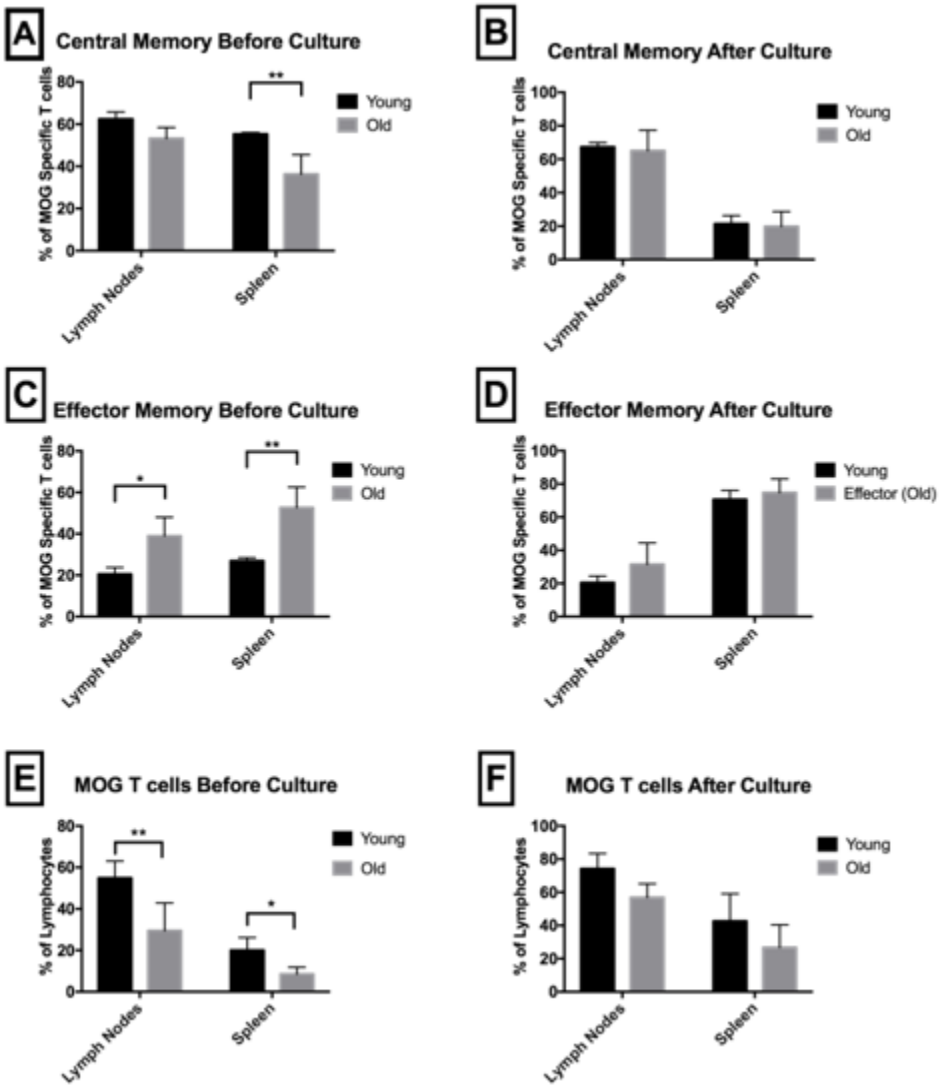

Figure 5.10 Transgenic memory T cells before and after culture

EAE was induced in 2D2 mice 6 months and 10 weeks of age. 11 days after induction, single cell isolates were obtained from the spleens and lymph nodes of these mice, and analyzed before and after restimulation for percentages of transgenic central memory T cells (A & B), transgenic effector memory T cells (C & D), and total percentage of transgenic T cells (E & F) using flow cytometry. The number of transgenic central memory T cells and effector memory T cells are represented as percentages of total transgenic T cells, whereas the number of transgenic T cells is represented as a percentage of the total lymphocytes. For central and effector memory T cells, (n=5) for 6 month old mice before and after culture. For central and effector memory T cells in 10 week old mice, (n=3) before culture and (n=6) after culture. For total transgenic T cells, (n=6) for 10 week old mice before and after culture, and (n=5) for 6 month old mice before and after culture. * $p<0.05$, ** $p<0.01$.

5.2.2.5 $CD4^-CD8^-$ double negative and B cell populations after culture

Double negative T cells were defined as $CD3^+CD4^-CD8^-$ cells that were also $NK1.1^-$, γδ TCR^-, and $B220^-$. Based on these parameters we were not able to detect any significant differences between mice that were 6 months and 10 weeks of age in the double negative T cell populations measured after 72 hr of culture with MOG_{35-55} peptide (Figure 5.11A). Since this stain required that we stain for the B cell marker B220, we also analyzed the percentage B cells that were present after restimulation and it was determined that there was a modestly higher number of B cells in the cultures from older 2D2 mice as compared to the 10 week old 2D2 mice (Figure 5.11B). The number of transgenic double negative T cells is represented as a percentage of total transgenic T cells, whereas the number of B cells is represented as a percentage of total lymphocytes.

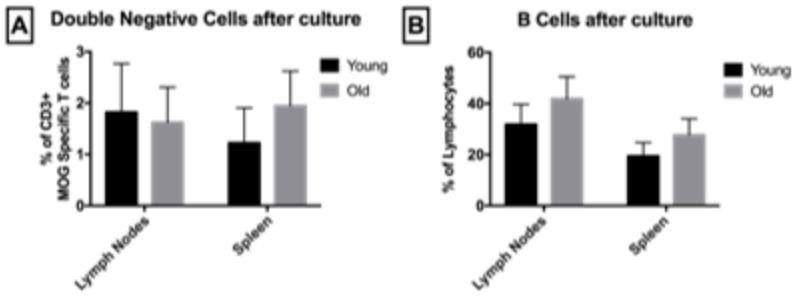

Figure 5.11 Double negative transgenic T cells and B cells after culture

EAE was induced in 2D2 mice 6 months (n=5) and 10 weeks (n=6) of age. 11 days after induction, single cell isolates were obtained from the spleens and lymph nodes of these mice, and analyzed after restimulation for percentages of transgenic $CD4^-CD8^-$ T cells (A) and B cells (B) using flow cytometry. The number of double negative transgenic T cells is represented as a percentage of total transgenic T cells, whereas the number of B cells is represented as a percentage of total lymphocytes.

5.2.2.6 IFN-γ and IL-17A production in T cells after culture

Upon analysis of cells from the ex vivo restimulated cultures for IFN-γ production, it was determined that the percentage of transgenic Th1 cells present in these cultures was significantly higher in the splenocytes of older mice as compared to that of younger mice. Conversely when cells were analyzed for IL-17A production, we found that the percentage of Th17 cells present in the restimulated lymph node and spleen isolates were significantly higher in cells restimulated from young mice as compared to older mice, although the percentage of cells represented by the Th17 population was less than 1% of all transgenic T helper cells. The number of Th1 and Th17 cell are represented as the percentage of transgenic $CD4^+$ cells which express either IFN-γ or IL-17A respectively.

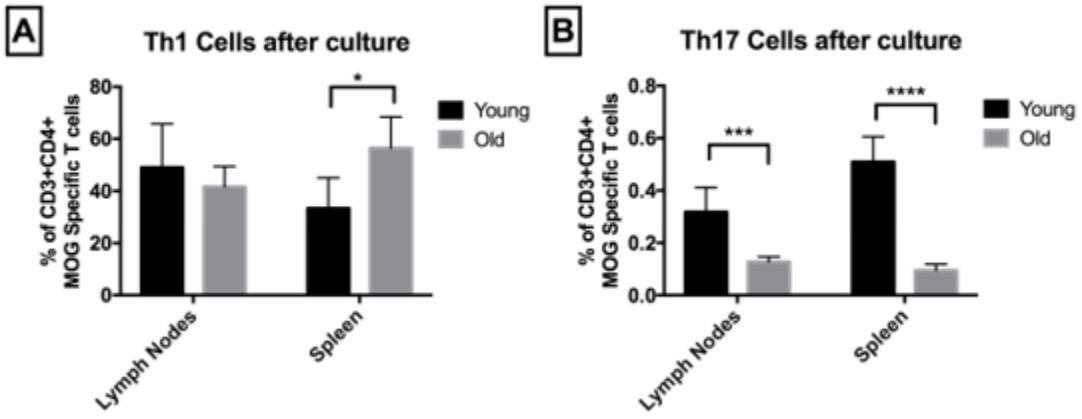

Figure 5.12 Transgenic Th1 and Th17 cells after culture

EAE was induced in 2D2 mice 6 months (n=5) and 10 weeks (n=6) of age. 11 days after induction, single cell isolates were obtained from the spleens and lymph nodes of these mice, and analyzed after restimulation for percentages of transgenic Th1 cells (A) and transgenic Th17 cells (B). The number of Th1 and Th17 cell are represented as the percentage of Transgenic $CD4^+$ cells which express either IFN-γ or IL-17A respectively.
* $p<0.05$, ** $p<0.01$, *** $p<0.01$, **** $p<0.01$

5.2.3 Discussion

The goal of our initial study utilizing the P-EAE model was to explore the effects of CBD on neuroinflammation during the later stages of the T cell response. However, we were surprised to find that in contrast to our work with CBD in the active EAE model CBD did not reduce clinical disease or neuroinflammation in the P-EAE model despite dosing the mice for the entire 15 day time course of the study. One explanation for this difference might be due to robustness of disease seen in the P-EAE. In the two studies in which we were able to induced P-EAE we observed higher clinical scores and more consistent clinical progression as compared to our active EAE model, and so we must consider the possibility that CBD is not able to reduce neuroinflammation past a certain threshold of disease. Another possible explanation for the differences seen between our two models is that there is a fundamental difference between the cell types involved, and CBD's reduced effectiveness in the P-EAE model may be due to certain cell types playing a lesser role in disease. More specifically, in the P-EAE model the primary source of inflammation is a memory response from the cells that were injected into the WT mice, and one of the major cell types that are responsible for this are the 2D2 transgenic T cells. This is in contrast to active EAE, which is driven by HKMT and CFA, and causes a massive innate immune response. These differences in type of immune response may play a key role in determining CBD's effectiveness in reducing neuroinflammation in EAE. This is similar to the work done by our lab in *Cnr1*$^{-/-}$ mice which showed differential IFN-γ production in splenocytes depending on which cell populations were activated. Like in the previous study, if CBD is capable of reducing inflammation when the response is predominated by the innate immune response, but

has no effect on T cells, or more specifically memory T cells, then it may explain why we did not observe a reduction in clinical disease when P-EAE mice were treated with CBD. In an attempt to address the first question involving disease robustness, we decided to increase the dose of CBD to 150mg/kg to see if higher levels of CBD would be more effective in the P-EAE model. Unfortunately, during these experiments, which were conducted with the younger mice, we were unable to induce disease in the WT mice. This led us to wonder why we had 100% incidence of disease during the first two studies and had 0% incidence in a third study.

After reviewing our methodology for all three experiments, it was determined that one of the major differences between the first two experiments and the third was the age of the 2D2 mice. The 2D2 mice from the first two experiments had been allowed to age for approximately 6 months before they were used to induce P-EAE, and in the third set of experiments the mice were only 10 weeks of age when they were used. With this in mind, additional experiments were performed to confirm whether or not 6 month old mice induced more severe P-EAE as compared to 10 week old mice, and to identify potential differences in the transgenic T cell population after 2D2 mice are injected with MOG_{35-55} peptide. An additional four rounds of P-EAE were performed for this set of experiments, with two rounds using mice 10 weeks of age and two rounds using mice 6 month of age. Interestingly, while the clinical scores from these studies did show significantly higher disease in P-EAE induced with older 2D2 mice, the time of onset for the latter experiments did not match the time of onset for the experiments performed with CBD. One possible explanation for this discrepancy is that the treatments given to the mice in the first studies expedited disease progression in the mice which received

cells from the 6 month old 2D2 mice, and suppressed disease in mice which received cells from the 10 week old mice. Moreover, since this observation occurred in both the CO and CBD groups we suspect CO to be the cause of the discrepancy. However, despite these differences, the significantly higher clinical scores observed in older mice in the later rounds of experiments did confirm that 6 month old mice were more capable of inducing clinical disease as compared to 10 week old mice.

To examine differences between the transgenic T cells in these mice 11 days after the initiation of active EAE, we chose to include central memory T cells, effector memory T cells, and IFN-γ producing T cells in our analyses based on a previous study by Williams et al. which used 2D2 mice to show effector memory Th1 cells played an important role in the induction of P-EAE [89]. The results from the present study strongly suggest a difference between the memory T cell response of younger 2D2 mice and older 2D2 mice to MOG_{35-55} peptide. More specifically, we found that there was an initial memory response in the older mice which shifted the balance of central and effector memory T cells to favor the effector memory phenotype in both the spleens and lymph nodes. However, once these cell populations were cultured, the effector memory T cell population did increase in younger mice. Additionally, we found that splenocytes from older mice had higher percentages of IFN-γ producing T cells after culture as compared to 10 week old mice. While we did not actually stain for IFN-γ production in memory T cells, considering the extremely high percentage of effector memory T cells in the transgenic T cell pool, the data suggests that the higher percentage of IFN-γ producing T cells in the transgenic T cell population of 6 month old mice likely represents an increase in the functional abilities of the effector memory T cells derived from the

spleens of these mice as compared to younger mice. Taken together, these results show a higher percentage of transgenic effector memory T cells isolated from older mice, which appear to show higher functional capabilities as measured by IFN-γ production. Based on the results from previous studies it is likely that this population is responsible for the increased clinical scores produced when P-EAE is induced with older mice [89]. It should also be noted that a significantly higher number of Th17 cells were found in the spleens and lymph nodes of younger mice as compared to older mice. However, considering the low numbers of Th17 cells that were recovered after the 72hr culture, and that Williams et al. found transgenic Th17 cells to be less capable of transferring disease than Th1 cells, we do not think the increase in Th17 cells found in young mice contributed significantly to disease progression in the present study [89].

In addition to the differences observed in memory T cells, we also found that fewer cells were recovered from spleens and lymph nodes of older 2D2 mice (results not shown) and that the percentage of transgenic T cells was lower in older mice as compared to younger mice. Initially this seemed counterintuitive, since we expected to see a more robust response from the transgenic T cells of older mice. However, when we considered these results in light of the results of the B cell stain, we realized that the lower percentage of transgenic T cells found in the spleens and lymph nodes of older mice likely represents a more balanced immune response in these mice. However, since the primary focus of this study was on the functional response of transgenic T cells in 2D2 mice, we did not stain for B cell prior to culture, which is when the greatest difference was seen between young and old mice with respect to transgenic T cell percentages. It would be interesting to explore this further in future studies to see if the

B cell response of 2D2 mice was enhanced in older mice before culture, which would suggest that the immune response in older mice develops beyond the initial T cell responsiveness that is inherited as part of the transgenic nature of these mice.

One final population of cells we chose to look at was the double negative T cells. Initially we suspected that we would find a population of transgenic T cells that were under chronic stimulation in vivo, and thus would have adopted the double negative phenotype similar to those found in a previous study [90]. However, we found no such population within either set of mice. The results from the double negative stain performed after restimulation of transgenic T cells concluded that double negative cells were not responsible for the increased clinical disease seen when P-EAE was initiated with cells from older 2D2 mice.

5.2.4 Conclusion

This study represents an important advancement in our understanding of how the immune system ages. Here we show a functional difference in the memory response of T cells between mice of different ages in the context of the P-EAE model. This model is commonly used to study MS, a disease in which patients gradually accumulate neurologic dysfunction with age and which does not show clinical symptoms until 20-30 years of age [14, 19, 89, 91]. The difference shown in this study suggests that even when 2D2 mice have not manifested clinical disease prior to administration of MOG_{35-55} peptide, there are fundamental changes occurring in their responsiveness to MOG_{35-55} peptide. We believe this represent an important model that can be used to understand how the immune system evolves in MS patients even prior to the initial onset of clinical symptoms, and as the patient ages.

REFERENCES

1. Dobson, R. and G. Giovannoni, *Multiple sclerosis - a review.* Eur J Neurol, 2019. **26**(1): p. 27-40.

2. Tintore, M., A. Vidal-Jordana, and J. Sastre-Garriga, *Treatment of multiple sclerosis - success from bench to bedside.* Nat Rev Neurol, 2019. **15**(1): p. 53-58.

3. Burstein, S., *Cannabidiol (CBD) and its analogs: a review of their effects on inflammation.* Bioorg Med Chem, 2015. **23**(7): p. 1377-85.

4. Mecha, M., et al., *Cannabidiol provides long-lasting protection against the deleterious effects of inflammation in a viral model of multiple sclerosis: a role for A2A receptors.* Neurobiol Dis, 2013. **59**: p. 141-50.

5. Kozela, E., et al., *Cannabidiol inhibits pathogenic T cells, decreases spinal microglial activation and ameliorates multiple sclerosis-like disease in C57BL/6 mice.* Br J Pharmacol, 2011. **163**(7): p. 1507-19.

6. Taylor, A.L. and M.J. Llewelyn, *Superantigen-induced proliferation of human CD4+CD25- T cells is followed by a switch to a functional regulatory phenotype.* J Immunol, 2010. **185**(11): p. 6591-8.

7. Park, Y.H., et al., *Suppression of proliferative response of BoCD4+ T lymphocytes by activated BoCD8+ T lymphocytes in the mammary gland of cows with Staphylococcus aureus mastitis.* Vet Immunol Immunopathol, 1993. **36**(2): p. 137-51.

8. Park, Y.H., et al., *Unique features of bovine lymphocytes exposed to a staphylococcal enterotoxin.* J Vet Sci, 2006. **7**(3): p. 233-9.

9. Maresz, K., et al., *Direct suppression of CNS autoimmune inflammation via the cannabinoid receptor CB1 on neurons and CB2 on autoreactive T cells.* Nat Med, 2007. **13**(4): p. 492-7.

10. Pryce, G., et al., *Cannabinoids inhibit neurodegeneration in models of multiple sclerosis.* Brain, 2003. **126**(Pt 10): p. 2191-202.

11. Browne, P., et al., *Atlas of Multiple Sclerosis 2013: A growing global problem with widespread inequity.* Neurology, 2014. **83**(11): p. 1022-4.

12. Ramagopalan, S.V., et al., *Sex ratio of multiple sclerosis and clinical phenotype.* Eur J Neurol, 2010. **17**(4): p. 634-7.

13. Alonso, A., et al., *Incidence of multiple sclerosis in the United Kingdom : findings from a population-based cohort.* J Neurol, 2007. **254**(12): p. 1736-41.

14. Mallucci, G., et al., *The role of immune cells, glia and neurons in white and gray matter pathology in multiple sclerosis.* Prog Neurobiol, 2015. **127-128**: p. 1-22.

15. Compston, A. and A. Coles, *Multiple sclerosis.* Lancet, 2008. **372**(9648): p. 1502-17.

16. Martyn, C.N., M. Cruddas, and D.A. Compston, *Symptomatic Epstein-Barr virus infection and multiple sclerosis.* J Neurol Neurosurg Psychiatry, 1993. **56**(2): p. 167-8.

17. Belbasis, L., et al., *Environmental risk factors and multiple sclerosis: an umbrella review of systematic reviews and meta-analyses.* Lancet Neurol, 2015. **14**(3): p. 263-73.

18. International Multiple Sclerosis Genetics, C., et al., *Genetic risk and a primary role for cell-mediated immune mechanisms in multiple sclerosis.* Nature, 2011. **476**(7359): p. 214-9.

19. Dendrou, C.A., L. Fugger, and M.A. Friese, *Immunopathology of multiple sclerosis.* Nat Rev Immunol, 2015. **15**(9): p. 545-58.

20. Langrish, C.L., et al., *IL-23 drives a pathogenic T cell population that induces autoimmune inflammation.* J Exp Med, 2005. **201**(2): p. 233-40.

21. Brucklacher-Waldert, V., et al., *Phenotypical and functional characterization of T helper 17 cells in multiple sclerosis.* Brain, 2009. **132**(Pt 12): p. 3329-41.

22. Tzartos, J.S., et al., *Interleukin-17 production in central nervous system-infiltrating T cells and glial cells is associated with active disease in multiple sclerosis.* Am J Pathol, 2008. **172**(1): p. 146-55.

23. Babbe, H., et al., *Clonal expansions of CD8(+) T cells dominate the T cell infiltrate in active multiple sclerosis lesions as shown by micromanipulation and single cell polymerase chain reaction.* J Exp Med, 2000. **192**(3): p. 393-404.

24. Constantinescu, C.S., et al., *Experimental autoimmune encephalomyelitis (EAE) as a model for multiple sclerosis (MS).* Br J Pharmacol, 2011. **164**(4): p. 1079-106.

25. Boven, L.A., et al., *Myelin-laden macrophages are anti-inflammatory, consistent with foam cells in multiple sclerosis.* Brain, 2006. **129**(Pt 2): p. 517-26.

26. Bogie, J.F., P. Stinissen, and J.J. Hendriks, *Macrophage subsets and microglia in multiple sclerosis.* Acta Neuropathol, 2014. **128**(2): p. 191-213.

27. Howell, O.W., et al., *Meningeal inflammation is widespread and linked to cortical pathology in multiple sclerosis.* Brain, 2011. **134**(Pt 9): p. 2755-71.

28. Li, R., et al., *Cytokine-Defined B Cell Responses as Therapeutic Targets in Multiple Sclerosis.* Front Immunol, 2015. **6**: p. 626.

29. Feger, U., et al., *Increased frequency of CD4+ CD25+ regulatory T cells in the cerebrospinal fluid but not in the blood of multiple sclerosis patients.* Clin Exp Immunol, 2007. **147**(3): p. 412-8.

30. Haas, J., et al., *Reduced suppressive effect of CD4+CD25high regulatory T cells on the T cell immune response against myelin oligodendrocyte glycoprotein in patients with multiple sclerosis.* Eur J Immunol, 2005. **35**(11): p. 3343-52.

31. Vos, C.M., et al., *Blood-brain barrier alterations in both focal and diffuse abnormalities on postmortem MRI in multiple sclerosis.* Neurobiol Dis, 2005. **20**(3): p. 953-60.

32. Sallusto, F., et al., *T-cell trafficking in the central nervous system.* Immunol Rev, 2012. **248**(1): p. 216-27.

33. Crook, K.R. and P. Liu, *Role of myeloid-derived suppressor cells in autoimmune disease.* World J Immunol, 2014. **4**(1): p. 26-33.

34. McGeachy, M.J., L.A. Stephens, and S.M. Anderton, *Natural recovery and protection from autoimmune encephalomyelitis: contribution of CD4+CD25+ regulatory cells within the central nervous system.* J Immunol, 2005. **175**(5): p. 3025-32.

35. Lotfi, N., et al., *Roles of GM-CSF in the Pathogenesis of Autoimmune Diseases: An Update.* Front Immunol, 2019. **10**: p. 1265.

36. Ta, T.T., et al., *Priming of microglia with IFN-gamma slows neuronal gamma oscillations in situ.* Proc Natl Acad Sci U S A, 2019. **116**(10): p. 4637-4642.

37. M. Mecha, A.F., F.J. Carrillo-Salinas, C. Guaza, *Chapter 93: Cannabidiol and Multiple Sclerosis*, in *Handbook of Cannabis and Related Pathologies*, V.R. Preedy, Editor. 2017, Academic Press: S.l. p. 1 online resource.

38. Pertwee, R.G., *The diverse CB1 and CB2 receptor pharmacology of three plant cannabinoids: delta9-tetrahydrocannabinol, cannabidiol and delta9-tetrahydrocannabivarin.* Br J Pharmacol, 2008. **153**(2): p. 199-215.

39. Deiana, S., et al., *Plasma and brain pharmacokinetic profile of cannabidiol (CBD), cannabidivarine (CBDV), Delta(9)-tetrahydrocannabivarin (THCV) and cannabigerol (CBG) in rats and mice following oral and intraperitoneal administration and CBD action on obsessive-compulsive behaviour.* Psychopharmacology (Berl), 2012. **219**(3): p. 859-73.

40. Chen, W., et al., *Magnitude of stimulation dictates the cannabinoid-mediated differential T cell response to HIVgp120.* J Leukoc Biol, 2012. **92**(5): p. 1093-102.

41. Karmaus, P.W., et al., *Cannabidiol (CBD) enhances lipopolysaccharide (LPS)-induced pulmonary inflammation in C57BL/6 mice.* J Immunotoxicol, 2013. **10**(3): p. 321-8.

42. Kaplan, B.L., A.E. Springs, and N.E. Kaminski, *The profile of immune modulation by cannabidiol (CBD) involves deregulation of nuclear factor of activated T cells (NFAT).* Biochem Pharmacol, 2008. **76**(6): p. 726-37.

43. Kaplan, B.L., C.E. Rockwell, and N.E. Kaminski, *Evidence for cannabinoid receptor-dependent and -independent mechanisms of action in leukocytes.* J Pharmacol Exp Ther, 2003. **306**(3): p. 1077-85.

44. Howlett, A.C., Shim, J.Y. , *Cannabinoid Receptors and Signal Transduction*, in *Madame Curie Bioscience Database [Internet]*. 2000-2013, Landes Bioscience: Austin, TX.

45. Turcotte, C., et al., *The CB2 receptor and its role as a regulator of inflammation.* Cell Mol Life Sci, 2016. **73**(23): p. 4449-4470.

46. Pryce, G. and D. Baker, *Control of spasticity in a multiple sclerosis model is mediated by CB1, not CB2, cannabinoid receptors.* Br J Pharmacol, 2007. **150**(4): p. 519-25.

47. Ameri, A., *The effects of cannabinoids on the brain.* Prog Neurobiol, 1999. **58**(4): p. 315-48.

48. Svizenska, I., P. Dubovy, and A. Sulcova, *Cannabinoid receptors 1 and 2 (CB1 and CB2), their distribution, ligands and functional involvement in nervous system structures--a short review.* Pharmacol Biochem Behav, 2008. **90**(4): p. 501-11.

49. Kaminski, N.E., et al., *Identification of a functionally relevant cannabinoid receptor on mouse spleen cells that is involved in cannabinoid-mediated immune modulation.* Mol Pharmacol, 1992. **42**(5): p. 736-42.

50. Galiegue, S., et al., *Expression of central and peripheral cannabinoid receptors in human immune tissues and leukocyte subpopulations.* Eur J Biochem, 1995. **232**(1): p. 54-61.

51. Vaney, C., et al., *Efficacy, safety and tolerability of an orally administered cannabis extract in the treatment of spasticity in patients with multiple sclerosis: a randomized, double-blind, placebo-controlled, crossover study.* Mult Scler, 2004. **10**(4): p. 417-24.

52. Zajicek, J., et al., *Cannabinoids for treatment of spasticity and other symptoms related to multiple sclerosis (CAMS study): multicentre randomised placebo-controlled trial.* Lancet, 2003. **362**(9395): p. 1517-26.

53. Wade, D.T., et al., *Do cannabis-based medicinal extracts have general or specific effects on symptoms in multiple sclerosis? A double-blind, randomized, placebo-controlled study on 160 patients.* Mult Scler, 2004. **10**(4): p. 434-41.

54. Collin, C., et al., *Randomized controlled trial of cannabis-based medicine in spasticity caused by multiple sclerosis.* Eur J Neurol, 2007. **14**(3): p. 290-6.

55. Lorente Fernandez, L., et al., *Clinical experiences with cannabinoids in spasticity management in multiple sclerosis.* Neurologia, 2014. **29**(5): p. 257-60.

56. Spaulding, A.R., et al., *Staphylococcal and streptococcal superantigen exotoxins.* Clin Microbiol Rev, 2013. **26**(3): p. 422-47.

57. Sundberg, E.J., Y. Li, and R.A. Mariuzza, *So many ways of getting in the way: diversity in the molecular architecture of superantigen-dependent T-cell signaling complexes.* Curr Opin Immunol, 2002. **14**(1): p. 36-44.

58. Faulkner, L., et al., *The mechanism of superantigen-mediated toxic shock: not a simple Th1 cytokine storm.* J Immunol, 2005. **175**(10): p. 6870-7.

59. Moza, B., et al., *Structural basis of T-cell specificity and activation by the bacterial superantigen TSST-1.* EMBO J, 2007. **26**(4): p. 1187-97.

60. Ferens, W.A., et al., *Activation of bovine lymphocyte subpopulations by staphylococcal enterotoxin C.* Infect Immun, 1998. **66**(2): p. 573-80.

61. Lee, S.U., et al., *Identity of activation molecule 3 on superantigen-stimulated bovine cells is CD26.* Infect Immun, 2001. **69**(11): p. 7190-3.

62. Tebartz, C., et al., *A major role for myeloid-derived suppressor cells and a minor role for regulatory T cells in immunosuppression during Staphylococcus aureus infection.* J Immunol, 2015. **194**(3): p. 1100-11.

63. Rao, P. and B.M. Segal, *Experimental autoimmune encephalomyelitis.* Methods Mol Biol, 2012. **900**: p. 363-80.

64. Moline-Velazquez, V., et al., *Myeloid-derived suppressor cells limit the inflammation by promoting T lymphocyte apoptosis in the spinal cord of a murine model of multiple sclerosis.* Brain Pathol, 2011. **21**(6): p. 678-91.

65. Ioannou, M., et al., *Crucial role of granulocytic myeloid-derived suppressor cells in the regulation of central nervous system autoimmune disease.* J Immunol, 2012. **188**(3): p. 1136-46.

66. Hegde, V.L., et al., *Critical Role of Mast Cells and Peroxisome Proliferator-Activated Receptor gamma in the Induction of Myeloid-Derived Suppressor Cells by Marijuana Cannabidiol In Vivo.* J Immunol, 2015. **194**(11): p. 5211-22.

67. Hegde, V.L., P.S. Nagarkatti, and M. Nagarkatti, *Role of myeloid-derived suppressor cells in amelioration of experimental autoimmune hepatitis following activation of TRPV1 receptors by cannabidiol.* PLoS One, 2011. **6**(4): p. e18281.

68. Dhital, S., et al., *Cannabidiol (CBD) induces functional Tregs in response to low-level T cell activation.* Cell Immunol, 2017. **312**: p. 25-34.

69. Elliott, D.M., et al., *Cannabidiol Attenuates Experimental Autoimmune Encephalomyelitis Model of Multiple Sclerosis Through Induction of Myeloid-Derived Suppressor Cells.* Front Immunol, 2018. **9**: p. 1782.

70. Malfait, A.M., et al., *The nonpsychoactive cannabis constituent cannabidiol is an oral anti-arthritic therapeutic in murine collagen-induced arthritis.* Proc Natl Acad Sci U S A, 2000. **97**(17): p. 9561-6.

71. Giacoppo, S., et al., *Target regulation of PI3K/Akt/mTOR pathway by cannabidiol in treatment of experimental multiple sclerosis.* Fitoterapia, 2017. **116**: p. 77-84.

72. Huseby, E.S., et al., *A pathogenic role for myelin-specific CD8(+) T cells in a model for multiple sclerosis.* J Exp Med, 2001. **194**(5): p. 669-76.

73. Kozela, E., et al., *Cannabinoids decrease the th17 inflammatory autoimmune phenotype.* J Neuroimmune Pharmacol, 2013. **8**(5): p. 1265-76.

74. Pagany, M., et al., *Myelin oligodendrocyte glycoprotein is expressed in the peripheral nervous system of rodents and primates.* Neurosci Lett, 2003. **350**(3): p. 165-8.

75. Leweke, F.M., et al., *Cannabidiol enhances anandamide signaling and alleviates psychotic symptoms of schizophrenia.* Transl Psychiatry, 2012. **2**: p. e94.

76. Bisogno, T., et al., *Molecular targets for cannabidiol and its synthetic analogues: effect on vanilloid VR1 receptors and on the cellular uptake and enzymatic hydrolysis of anandamide.* Br J Pharmacol, 2001. **134**(4): p. 845-52.

77. Elmes, M.W., et al., *Fatty acid-binding proteins (FABPs) are intracellular carriers for Delta9-tetrahydrocannabinol (THC) and cannabidiol (CBD).* J Biol Chem, 2015. **290**(14): p. 8711-21.

78. Lou, Z.Y., et al., *The inhibition of CB1 receptor accelerates the onset and development of EAE possibly by regulating microglia/macrophages polarization.* J Neuroimmunol, 2018. **317**: p. 37-44.

79. Li, Y.H., et al., *Mdivi-1, a mitochondrial fission inhibitor, modulates T helper cells and suppresses the development of experimental autoimmune encephalomyelitis.* J Neuroinflammation, 2019. **16**(1): p. 149.

80. Zhou, S., et al., *Pro-inflammatory Effect of Downregulated CD73 Expression in EAE Astrocytes.* Front Cell Neurosci, 2019. **13**: p. 233.

81. Fletcher, J.M., et al., *T cells in multiple sclerosis and experimental autoimmune encephalomyelitis.* Clin Exp Immunol, 2010. **162**(1): p. 1-11.

82. Lou, Z.Y., C.B. Zhao, and B.G. Xiao, *Immunoregulation of experimental autoimmune encephalomyelitis by the selective CB1 receptor antagonist.* J Neurosci Res, 2012. **90**(1): p. 84-95.

83. Dinges, M.M., P.M. Orwin, and P.M. Schlievert, *Exotoxins of Staphylococcus aureus.* Clin Microbiol Rev, 2000. **13**(1): p. 16-34, table of contents.

84. Mangmool, S. and H. Kurose, *G(i/o) protein-dependent and -independent actions of Pertussis Toxin (PTX).* Toxins (Basel), 2011. **3**(7): p. 884-99.

85. Giacoppo, S., et al., *Purified Cannabidiol, the main non-psychotropic component of Cannabis sativa, alone, counteracts neuronal apoptosis in experimental multiple sclerosis.* Eur Rev Med Pharmacol Sci, 2015. **19**(24): p. 4906-19.

86. Savarin, C., et al., *Astrocyte response to IFN-gamma limits IL-6-mediated microglia activation and progressive autoimmune encephalomyelitis.* J Neuroinflammation, 2015. **12**: p. 79.

87. Tetrault, S., et al., *Opening of the blood-brain barrier during isoflurane anaesthesia.* Eur J Neurosci, 2008. **28**(7): p. 1330-41.

88. Kohn, D.F., et al., *Anesthesia and Analgesia in Laboratory Animals*. 1997, New York: Academic Press.

89. Williams, J.L., et al., *Memory cells specific for myelin oligodendrocyte glycoprotein (MOG) govern the transfer of experimental autoimmune encephalomyelitis.* J Neuroimmunol, 2011. **234**(1-2): p. 84-92.

90. Grishkan, I.V., et al., *Helper T cells down-regulate CD4 expression upon chronic stimulation giving rise to double-negative T cells.* Cell Immunol, 2013. **284**(1-2): p. 68-74.

91. Mannara, F., et al., *Passive experimental autoimmune encephalomyelitis in C57BL/6 with MOG: evidence of involvement of B cells.* PLoS One, 2012. **7**(12): p. e52361.

APPENDIX A

LIST OF PUBLICATIONS

A.1 Publications and contributions

Nichols, J.M., Kaplan, B.L.F. *Immune Responses Regulated by Cannabidiol*. Cannabis and Cannabinoid Research, 2019. http://doi.org/10.1089/can.2018.0073

This review article examines recent advancements in our understanding of how cannabidiol regulates the immune response. My contribution to the review consisted of a section on cannabidiol in the EAE model and MS, and the organization of the table which corresponds to this section.

Kummari, E., Nichols, J.M., Yang, E.J., Kaplan, B.L.F. Neuroinflammation and B-Cell Phenotypes in Cervical and Lumbosacral Regions of the Spinal Cord in Experimental Autoimmune Encephalomyelitis in the Absence of Pertussis Toxin. Neuroimmunomodulation. 2019. 26(4):198-207. doi: 10.1159/000501765.

My contributions to this publication consisted of H&E staining and immunohistochemical staining for CCL2 and VCAM-1 in the spinal cords of normal and EAE mice. Through these stains we were able to show increased levels of infiltration, CCL2, and VCAM-1 in the spinal cords of EAE mice without the use of PTX. Additionally, we used these stains to examine differences between the cervical and lumbosacral spinal cord segments for each mouse.